UNIVERSITÀ DEGLI STUDI
DI GENOVA

XXXIII Cycle

PhD Program
Biotechnologies in Translational Medicine

Curriculum: Tissue Engineering and Regenerative Medicine

Functional Characterization of Mesenchymal Stromal Cell- Derived Extracellular Vesicles

Candidate: Cansu Gorgun

Tutor: Dr. Roberta Tasso
Coordinator: Prof. Rodolfo Quarto

April, 2021, Genova,Italy

SUMMARY

Mesenchymal Stromal Cells (MSCs) are currently considered a powerful tool for the treatment of multiple diseases. Indeed, the original hypothesis underlying MSC based regenerative therapies was based on functional recovery as a consequence of stem cell differentiation. But it is now clear that other mechanisms of action are involved. The recent emerging paradigm shift suggests that the paracrine effects of MSCs may be as important as cell differentiation in eliciting functional tissue repair. Among the factors responsible for the paracrine effects, extracellular vesicles (EVs) have been recently described as new players in cell-cell communication, as mediators of proteins, lipids, and genetic information. MSCs derived-EVs showed to be involved in a wide spread of processes, including angiogenesis, senescence, proliferation, and differentiation, beside strong immunomodulatory properties, and a key role in tissue homeostasis. The aim of this thesis is to characterize EVs released by MSCs to investigate their involvement as modulators of MSC paracrine effects. Exploiting this natural intercellular signaling mechanism could be beneficial to overcome some important limitations of cell therapies and, in this scenario, they could represent an efficient therapeutic vehicle for regenerative medicine.

CHAPTER 1 5

INTRODUCTION 5

1.1 General Introduction 6

1.2 State of Art and Objectives 13

CHAPTER 2 15

A Method for the Isolation and Flow Cytometry Characterization of Extracellular-Vesicle Subpopulations Derived from Human Mesenchymal Stromal Cells 13

2.1 Introduction 16

2.2 Methodology for the Isolation of Different Subsets of Mesenchymal Stromal Cell–Derived Extracellular Vesicles 17

2.2.1 Methodology for the Flow Cytometry Setup, Acquisition, and Analysis 18

2.2.1.1 Flow cytometer preparation 19

2.2.1.2 Adjustment of instrument settings 19

2.2.1.3 Sample preparation and acquisition 21

2.3 Discussion 24

2.4 Conclusion 26

CHAPTER 3 27

Dissecting the effects of preconditioning with inflammatory cytokines and hypoxia on the angiogenic potential of Mesenchymal Stromal Cell (MSC)-derived soluble proteins and Extracellular Vesicles (EVs) 27

3.1 Introduction 28

3.2 Materials and Methods 29

3.2.1 Isolation and culture of human adipose tissue-derived Mesenchymal Stromal Cells (MSCs) 29

3.2.2 MSC pre-conditioning and collection of MSC Conditioned Media (CM) 30

3.2.3 Extracellular Vesicles (EVs) isolation and generation of Depleted-Medium (DM) 31

3.2.4 Flow cytometry characterization of EVs 31

3.2.5 Nanoparticle Tracking Analysis (NTA) on MSC-derived EVs 32

3.2.6 Transmission Electron Microscopy (TEM) 32

3.2.7 Western Blot Analysis 33

3.2.8 Human Umbilical Vein Endothelial Cell (HUVEC) culture 33

3.2.9 HUVEC Proliferation Assay 33

3.2.10 HUVEC Migration Assay 34

3.2.11 Tube Formation Assay 34

3.2.12 *Ex vivo* Metatarsal Sprouting Assay 34

3.2.13 Bioinformatic approach to Proteome Profiler™ Human Angiogenesis Antibody Array 35
3.2.14 RNA Preparation and Next Generation Sequencing of EVs 36
3.2.15 miRNAseq Data Analysis 36
3.2.16 Statistical analysis 37

3.3 Results 38
3.3.1 Pre-conditioning with pro-inflammatory cytokines and hypoxia does not alter MSC properties 38
3.3.2 Preconditioned MSCs secrete EVs of different sizes 39
3.3.3 EVs are less sensitive than soluble proteins to the environmental variations in the context of angiogenesis 44
3.3.4 The soluble factors released by inflammation-activated MSCs possess a distinctive secretome profile 50
3.3.5 The microRNA (miRNA) landscape of MSC-derived EVs is not majorly affected by cell preconditioning 53

3.4 Discussion 56

3.5 Conclusion 59

3.6 Supplementary Information 60

CHAPTER 4 67

Extracellular Vesicles from adipose tissue- and bone marrow-mesenchymal stromal cells play different roles in the endochondral ossification process 67

4.1 Introduction 68

4.2 Materials and Methods 69
4.2.1 Isolation and culture of Mesenchymal Stromal Cells (MSCs) 69
4.2.2 Extracellular Vesicles (EVs) separation and characterization 70
4.2.3 Tunable Resistive Pulse Sensing (TRPS) 70
4.2.4 Transmission Electron Microscopy (TEM) 70
4.2.5 Western Blot Analysis 71
4.2.6 Flow cytometry characterization of EVs 71
4.2.7 Proteome profiling of EVs 72
4.2.8 *Ex vivo* metatarsal sprouting assay 72
4.2.9 *Ex vivo* metatarsal bone growth assay 73
4.2.10 Histological and immunohistochemical analysis 73
4.2.11 Statistical analysis 73

4.3 Results 74
4.3.1 ADSCs and BMSCs release EVs with similar characteristics 74
4.3.2 Differentially expressed proteins in BMSC- and ADSC-EVs 78
4.3.3 ADSC-sEVs promote vessel outgrowth from fetal metatarsal explants more efficiently than BMSC-sEVs 82
4.3.4 Metatarsal bone explants exposed to BMSC-sEVs exhibit more organized growth plate areas compared to ADSC-sEVs 83

4.4 Discussion 88

4.5 Conclusion 92

4.6 Supplementary Information 93

CHAPTER 5 95

General Discussion 95

References 99

PhD Portfolio 117

CHAPTER

1

INTRODUCTION

1.1 General Introduction

Adult Mesenchymal Stromal Cells

Stem cells are undifferentiated cells which have self-renewal and differentiation potential to produce mature progeny cells, including both non-renewing progenitors and terminally differentiated effectors. Among all other stem cell types, such as hematopoietic stem cells and neural stem cells, mesenchymal stem cells (MSCs) are currently among the best characterized adult stem cells isolated from various tissue sources such as bone marrow, adipose tissue, dental tissues, amniotic membrane and fluid, placenta and fetal membrane, endometrium, menstrual blood, peripheral blood, synovial fluid, salivary gland, limb bud, skin and foreskin, sub-amniotic umbilical cord lining membrane and Wharton's jelly[1]. The ability of these cells to self-renew and differentiate into multiple cells, makes them an attractive candidate for regenerative medicine applications[2]. The first concept of mesenchymal stem cells was introduced by Alexander Friedenstein who isolated them from the bone marrow as fibroblastic precursors [3,4]. Following, the current popular term "Mesenchymal Stem Cells - MSC" has been proposed by Arnold Caplan [5] in 1991, emphasizing the self-renewal and differentiation potential of these cells. In 1999, James Dennis and his colleagues acknowledged the existence of a mesenchymal stem cell. However, they strongly suggested that, on a functional level, these cells would be identified by the term "progenitors" [6] rather than "stem cells". In early 2000, Paolo Bianco and his colleagues recognized MSC as skeletal stem cells [7]. Meantime, in 2001 and 2002, Patricia Zuk and her colleagues identified that adipose tissue stromal compartment contained cells with differentiation potential and therewith, adipose tissue derived mesenchymal stromal cells had started to gain attention [8]. Within the discovery of human amniotic stem cells and other MSC types, in 2006, the International Society for Cellular Therapy proposed the term *"multipotent mesenchymal stromal cells"* with predefined criteria such as cluster differentiation (CD) markers which can be applied only to human MSC [9]. Even through, a new definition and minimal criteria has been set to define MSCs, more recently in 2017 Arnold Caplan suggested that MSC acronym should define the term of "Medicinal Signaling Cells" due to their secretion capacity of bioactive factors with immunomodulatory and trophic effects (Fig.1.1) [10].

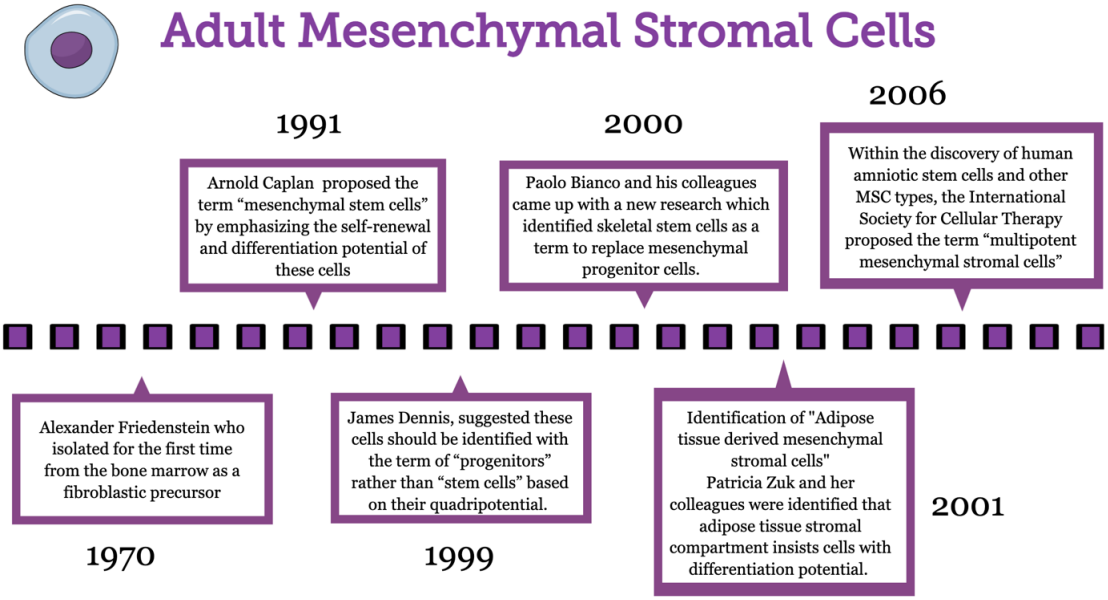

Figure 1.1: The timeline of major scientific advances during the history of adult mesenchymal stromal cell research.

Mesenchymal Stromal Cell Paracrine Activity

With the identification of MSCs, a huge body of research had been focused on their therapeutic benefits in regenerative medicine applications [11–14]. While most of the research had attempted to transplant MSCs to the damaged tissues as engrafts, other works had benefited from the differentiation potential of these cells [15]. Many are the issues related to the use of MSCs in classical cell-based therapies. Among them, the requirement of a huge number of cells that have to maintain their properties in terms of differentiation and immunomodulation. Indeed, it has been reported that human MSCs become senescent during long-term culture, manifested by decline in differentiation potential, shortening of the telomere length and morphological alterations. Moreover, it has been reported in many preclinical settings that less than 5% of infused MSCs reached the injured site, while most of them remained entrapped in filter organs [16]. The beneficial effect exerted by the few engrafted cells have been explained by their paracrine activity, modulating the surrounding damaged environment. These observations led the scientific community to change the paradigm regarding MSCs, from just "reparative" cells that can engraft in injured tissues and directly differentiate to replace damaged organs to "factories" of biologically active molecules. In this new paradigm, MSCs act cross-talking with

injured cells to limit tissue destruction or enhance repair by a variety of paracrine mechanisms. Since MSCs have a regulatory phenotype and respond actively to the environmental signals, their secretory activity can be deeply modulated. In this context, the MSC secretome has emerged as a new cell-free therapy approach.

Mesenchymal Stromal Cell-Derived Secretomes

The term "secretome" was introduced in 2000 by Tjalsma and colleagues referring to a protein export from the cytoplasm to destinations outside the cell [17,18]. The secretome includes growth factors, chemokines, cytokines in soluble-free form, but recent studies have demonstrated that also non-protein components, such as lipid, micro-RNAs and messenger-RNA, are secreted by cells inside spherical nanometer-scale bi-layered proteolipids which are called "Extracellular Vesicles" (Fig.1.2)

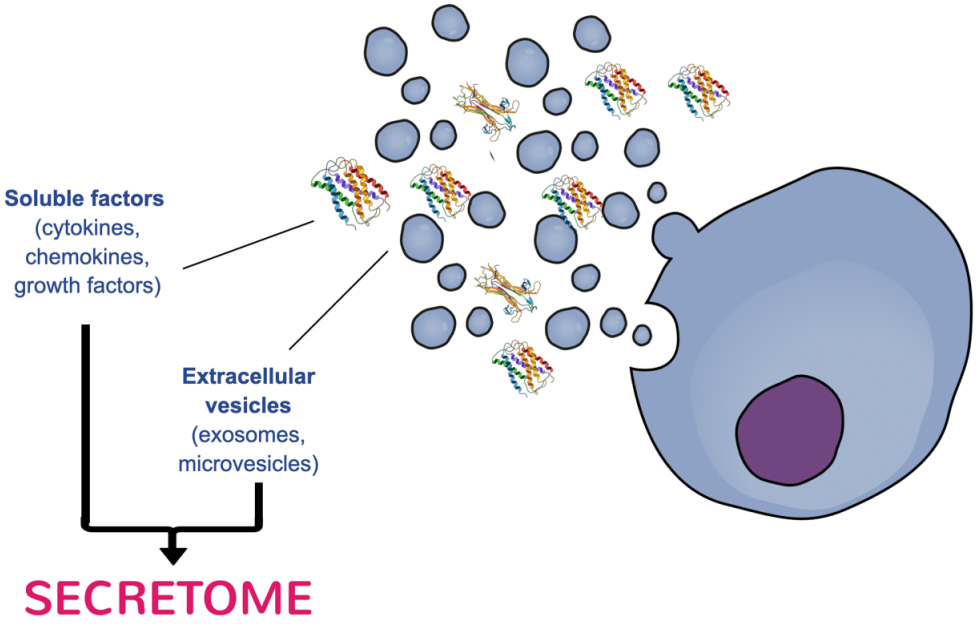

Figure 1.2: Overview of the secretome. The secretome comprises of soluble proteins and secreted extracellular vesicles. The proteins include biologically active factors such as cytokines, chemokines and growth factors. The extracellular vesicles include exosomes and microvesicles.

In order to overcome the limitations associated with cell-based therapies, secretome-based approaches have emerged in the field of regenerative medicine. Some studies have reported that the utilization of stem cell-conditioned medium, corresponding to the cell secretome, possess the same regenerative

effect obtained by cell transplantation [19,20]. Preconditioning and optimization of MSC culture conditions are key strategies to improve MSC function *in vitro* and *in vivo*. All of these procedures contribute to improving MSC transplantation efficacy in tissue engineering and regenerative medicine [21]. Recently, studies have demonstrated that pretreated MSCs showed better cell survival, increased differentiation efficacy, enhanced paracrine effects and an improved homing ability into injury sites [22]. Different are the pre-conditioning strategies, such as hypoxia [23,24], inflammation [22,25], three-dimensional culture systems [26,27] and pharmacological compounds [28,29]. Although a great majority of the research were focused on the evaluation of the changes in the released soluble factors upon pre-conditioning, recent data indicated that "Extracellular Vesicle" cargo content, which consist also mRNA, miRNA, and protein could be altered by preconditioning, playing a crucial role in mediating cell-communication and therapeutic effects.

Extracellular Vesicles

Extracellular vesicles (EVs) are spherical nanometer-scale bi-layered proteolipids secreted by cells that can be engulfed by neighboring cells in order to facilitate cell-cell communication. In the field of bone research, the EV term was firstly mentioned in 1969 as "matrix vesicles" [30]. In the different fields, researchers invented various names to identify EVs [31].

Indeed, cells release heterogeneous vesicles of different sizes and intracellular origins, including small EVs generated in the endosomal compartments (i.e., exosomes) and EVs of various sizes budding from the plasma membrane, generally referred to as microvesicles. While microvesicles mainly bud from the membrane and have the size range of 100-900 nm, exosomes are released by microvesicular bodies and they have narrow size range such as < 150 nm [32]. EVs transfer genetic material (proteins, miRNA, mRNA) from one cell to another, thereby influencing the recipient cell function and have emerged as critical components of human physiology with enormous therapeutic potential [33,34]. To prevent any confusion about the nomenclature the International Society for Extracellular Vesicles (ISEV) community suggested in the recently updated position paper on the Minimal Information for Studies of Extracellular Vesicles (MISEV2018), to use the term "extracellular vesicle (EV)" unless the subcellular origin of the vesicle is demonstrated [35]. According to these guidelines, authors are encouraged to include information on the physical characteristics of the EVs (e.g., size and/or density ranges), biochemical composition of EVs) and/or descriptions of conditions or cell of origin (e.g., oncosomes, hypoxic EVs) to define EV subtypes [36,37] .

Moreover, EV-Track database system has been developed to allow sharing of protocols and help EV-researchers to compare the methods and separation techniques [38].

In the term of separation methods, currently differential centrifugation (ultracentrifugation) is the one of the most used approach. Except of ultracentrifugation, various EV separation techniques such as size chromatography, density-gradient separation, immunoaffinity, polymer-based precipitation, ultrafiltration and commercial kits can be used individually or combined for the separation of EVs [39] (Fig.1.3) .

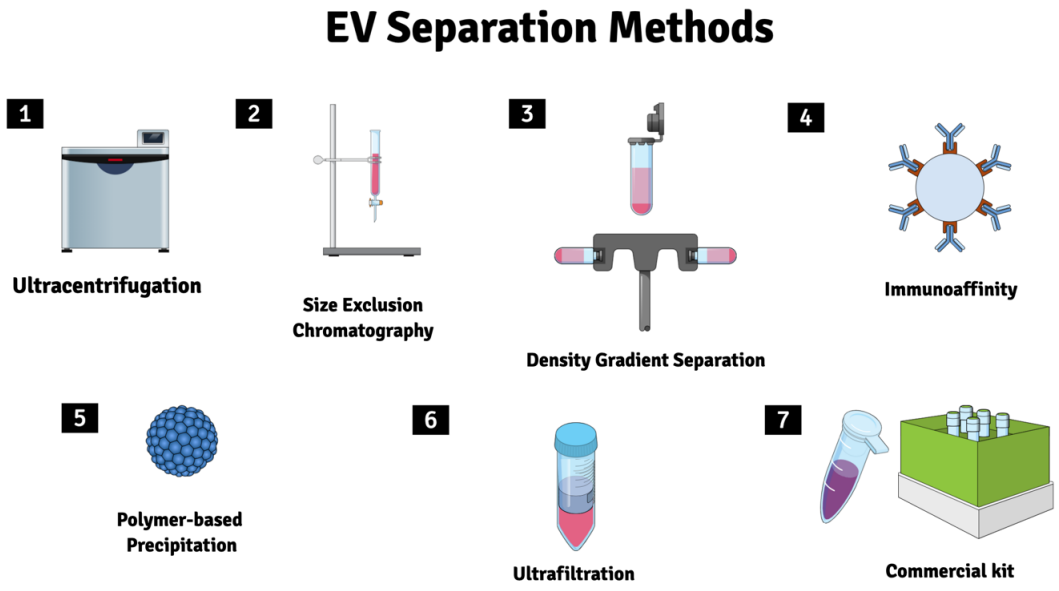

Figure 1.3: Graphical summary of the most used EV separation methods.

However, each method has its own advantages and limitations. Ultracentrifugation is an easy technique based on the separation of components other than EVs from a solution in a stepwise manner. However, one of the limitations in using ultracentrifugation for isolation of EVs is coprecipitation of protein aggregates and nucleosome fragments which can lead to decreased sample purity and may affect downstream analysis. The density-gradient separation, which employs ultracentrifugation combined with a sucrose gradient, can lead to increased sample purity as protein and protein-RNA aggregates can be efficiently separated from the exosomes. This method allows the separation of EVs based on their densities from low density exosomes to higher density microvesicles.

Size exclusion chromatography provides a selection of EVs based on their size and quite compatible with various types of fluids, and an extra pre-treatment step is generally not required. In recent years' SEC-based separation has becoming increasingly popular for EV-based experimental and clinical investigations [40], especially in the context of biofluids, such as plasma and serum, enriched in contaminants, such as plasma proteins and lipoproteins, with sizes similar to those of exosomes [41].
Immuno-selection techniques allow a selection based on surface markers such as tetraspanins (CD9, CD63, CD81) or immune-regulator molecules (HLA class I and II) expressed by vesicles. However, since this method is quite expensive, it is not suitable for large sample volumes. On the other hand, polymer-based separation can be used on a wide range of sample volumes, but overall disadvantages of this method rely on the contamination issues with non-EV proteins, retention of chemicals or polymers, and long processing time. Ultrafiltration is usually done in successive steps to isolate EVs of precisely desired size [42]. The simplicity of the procedure, the ability for concurrent processing of many samples, and the lack of limitations on sample volume are all notable advantages associated with this method. The disadvantages include: filter plugging which results in loss of sample, and sample contamination by proteins [42]. Commercial kits are relatively fast in comparison with other methods and they have easy protocols to follow. However, these kits are generally costly and there is a high concentration of impurities following separation [43].
Considering the variable sources of EVs and different separation methods, researchers need to optimize the methods and find a balance between purity, efficiency, and downstream applications of the isolated vesicles within the research question of the work.

Mesenchymal Stromal Cell-derived Extracellular Vesicles

MSC-derived EVs carry a complex cargo of lipids, proteins, and RNAs like the EVs derived from other cells. The importance of MSC-EVs in regenerative medicine is based on their therapeutic effects. MSC-derived EVs also have been shown to deliver an immunosuppressive phenotype and to possess therapeutic benefits [44]. The mechanisms underlying the EV packaging process require further study and it is important to analyze the sub-types of MSC-derived EVs with functions that mirror those of their parent cells [45].
The diversity of MSC-based therapeutic intervention implies the applicability of MSC-derived EVs to the treatment of various disorders. Their therapeutic effects have been observed in several different types of diseases, including bone defects, cardiac injury, and brain injury [46]. Overall, these results

indicated that MSC-derived EVs mediate the therapeutic effects in various diseases through multiple mechanistic pathways and provide a novel approach for the treatment of degenerative and acute injury-related diseases [47].

Pre-conditioning strategies **applied on** MSCs may induce phenotypic changes on cells that may impair/improve the therapeutic efficacy of any produced EV. As mentioned above, MSCs can respond to pathological stimuli and secrete various trophic factors required for tissue repair. Considering that EVs can contain many molecules that play certain biological roles, it is possible that in response to a pathological stimulus, MSCs can release EVs loaded with a set of molecules required for tissue repair and regeneration [48]. Furthermore, the exposure of MSCs to injury stimuli [49] or hypoxia [50] can trigger the enrichment of a global set of trophic molecules in the released EVs. This suggests that appropriate preconditioning of parent MSCs may allow the tailoring of EV contents to efficiently support repair of specific diseases. Apart from the different culture conditions, also the tissue-specific origin of MSCs can influence the cargo content of EVs [51–53].

1.2 State of Art and Objectives

Mesenchymal stromal cells (MSCs) are characterized by a regulatory phenotype and respond promptly to the environmental signals modulating their secretory activity. An appropriate preconditioning may induce MSCs to release secretomes with an enhanced regenerative potential. Secretomes are composed by both soluble factors and heterogeneous populations of extracellular vesicles (EVs). However, with proper isolation methods and characterization strategies, it is possible to distinguish the various EV subpopulations, potentially exerting specific effects. Several methods have been adopted to count and characterize EVs (e.g., nanoparticle tracking analysis, electron microscopy, resistive pulse sensing), but there is still considerable confusion about the definition of EV phenotype and the standardization of protocols for analysis. All the methodologies present difficulties and limitations, ranging from low sensitivity to very high cost to poor statistical validation. In this context, last-generation flow cytometry (FCM) could become a methodology of choice, characterized by crucial advantages: relatively low cost, multiparameter phenotyping, and good statistical robustness of the data due to a large number of events being analyzed at the same time. This thesis aimed, in **Chapter 2**, to generate a protocol for isolating subpopulations of EVs purified from human adipose tissue derived MSCs by density gradient centrifugation and characterizing them by flow cytometry. The procedures described here can be easily reproduced and can be employed regardless of the cell type used to obtain EVs. The developed technique for characterization of EV subpopulations by FCM has been used also in the following chapters.

The EV subtypes, as well as the soluble component of the cell secretome, can be modulated by adopting different preconditioning approaches. In this context, MSCs are versatile progenitors able to sense the surrounding environment and actively respond to changes of the milieu modulating the secretion of specific mediators. This indicates that with the appropriate preconditioning it would be possible to improve their therapeutic paracrine efficacy, harnessing the regulatory immunogenic, angiogenic, and osteogenic properties. In **Chapter 3**, it has been evaluated how the environmental variations affected the functional characteristics of the different MSC secretome fractions. Specifically, this chapter shows for the first time the effects of a simultaneous stimulation with pro-inflammatory cytokines (TNF-α and IL-1α) and hypoxia (1% O_2) on the angiogenic potential of the different components of the MSC secretome.

The secretome of MSCs derived from different tissue sources is considered an innovative therapeutic tool for regenerative medicine. Although adipose tissue-and bone marrow-derived MSCs (ADSCs and BMSCs, respectively) share many biological features, the different tissue origins can be mirrored by variations in their secretory profile, and in particular in the secreted extracellular vesicles (EVs). **Chapter 4** is aimed to characterize both middle-size and small-size EVs released by AD-MSCs and BM-MSCs for investigating their different in different phases of the endochondral ossification process. Their involvement in an endochondral ossification setting was investigated using *ex vivo* metatarsal culture models that allowed to explore both blood vessel sprouting and bone growth plate dynamics.

This thesis ends with a general discussion, conclusion and future perspectives of the work presented in **Chapter 5**.

CHAPTER

2

A Method for the Isolation and Flow Cytometry Characterization of Extracellular-Vesicle Subpopulations Derived from Human Mesenchymal Stromal Cells

Gorgun C, Reverberi D, Rotta G, Villa F, Quarto R, Tasso R. Isolation and Flow Cytometry Characterization of Extracellular-Vesicle Subpopulations Derived from Human Mesenchymal Stromal Cells. Curr Protoc Stem Cell Biol. 2019 Feb;48(1):e76. doi: 10.1002/cpsc.76. Epub 2019 Jan 9. PMID: 30624011.

2.1 Introduction

For many years, mesenchymal stromal cells (MSCs) have been considered a central cell source for regenerative-medicine applications due to these cells' multipotent properties. In the last decade, MSCs have also received great attention for their marked paracrine activity [54] (exerted via both soluble factors and extracellular vesicles (EVs). In particular, given the array of signals carried by vesicles through horizontal transfer of molecules, EVs have assumed an emerging role [55,56].

EVs comprise a heterogeneous mixture of membrane-surrounded structures that consists of different subpopulations. The main vesicular types include exosomes (50 to 160 nm in diameter), microvesicles (160 to 900 nm), and apoptotic bodies (>900 nm)[57]. It has been demonstrated that the EV subpopulations possess different densities and that their cargo and functional properties can vary, thus drawing attention to the importance of considering all the subtypes released by a specific cell source [34,58,59]. Differential centrifugation is one of the most commonly used methods for EV isolation in laboratory practice. However, it is generally used to isolate smaller EVs, whereas larger vesicles, such as shedding microvesicles, are partially eliminated during this experimental procedure, causing loss of heterogeneity[58]. Therefore, many attempts have been made to ameliorate both isolation techniques and characterization methods. Advanced flow cytometry (FCM) is one of the most promising approaches, as it can be used to analyze a large range of particle diameters <1 μm; in contrast, conventional FCM is useful for appropriately discriminating only larger particles (e.g., platelets)[60,61].

In this chapter, a methodology for isolation of human MSC–derived EV subpopulations by density gradient centrifugation (Methodology 1.2) is optimized for applications beyond those detailed in previously published paper[62], where the intent was to isolate a mixed population of EVs without taking into consideration the different subtypes. Vesicular characterization by FCM is explained in Materials and Methods 1.3, taking advantage of recently developed technologies. Compared to previously published paper[62] here, it is proposed a more accurate FCM characterization that allows proper discrimination between different-sized vesicular subpopulations.

2.2 Methodology for the Isolation of Different Subsets of Mesenchymal Stromal Cell–Derived Extracellular Vesicles

Cells release different types of EVs: exosomes, microvesicles, and apoptotic bodies. Each EV subset is characterized by a defined molecular composition and specific biological functions. Understanding whether the heterogeneous ensemble or a single EV subpopulation is responsible for the properties exerted by EVs is a topic of widespread interest [58]. In this unit, it is described a useful method for dissecting EV heterogeneity based on density gradient ultracentrifugation (Fig. 2.1). Compared to previously published paper [62], where a mixed population of vesicles was considered, here, it is proposed an advanced isolation protocol, useful for isolating microvesicles from exosomes.

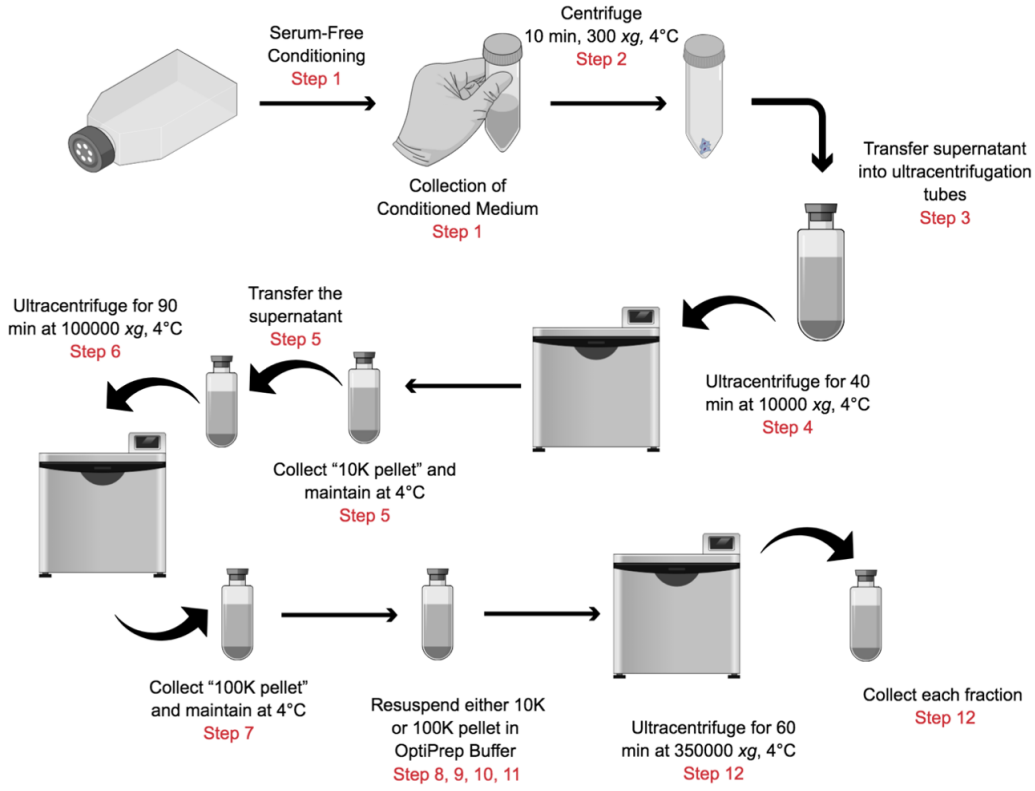

Figure 2.1: Schematic depicting the experimental steps for isolating different subsets of extracellular vesicles.

MSC-conditioned serum-free medium (MSC-CM) was harvested as previously described[62] and transferred to 50-ml conical centrifuge tubes. While it is recommended to prolong serum-free incubation from 24 hours to 48, 72, or 96 hours if using primary cell cultures to obtain a sufficient

number of vesicles for further analysis, in here a serum-free conditioning timeframe of 96 hours was used. MSC-CM was centrifuged 10 min at 300 × g, 4°C, to remove cell debris and supernatants were transferred into SW28 open-top polypropylene ultracentrifugation tubes. Another ultracentrifugation step (40 min at 10,000 × *g*, 4°C, using SW28 rotor) was performed and at the end of the centrifugation, supernatants were carefully transferred into new SW28 tubes and pellets were reserved pellets ("10K pellets"). Transferred supernatants were ultracentrifuged for 90 min at 100,000 × *g*, 4°C, using SW28 rotor. Following, new supernatants were discarded and any pellets that have formed were reserved ("100K pellets"). In order to isolate the EV-subpopulations, 10K or 100K pellets were resuspended in 1.4 ml OptiPrep buffer (0.25 M sucrose,1 mM EDTA,10 mM Tris, pH 7.4). Each resuspended pellet was carefully transferred into an SW55Ti open-top polypropylene ultracentrifugation tube. Following, 1.4 ml OptiPrep Density Gradient Medium (60% (w/v) stock solution, Sigma-Aldrich, D1556) were added to both 10K and 100K resuspended pellets and mixed carefully by pipetting up and down (30% final concentration). In order to create the density gradient, 1.2 ml of 20% OptiPrep solution was carefully added on top of 30% solution, without disturbing the bottom layer. As last step, 1.1 ml of 10% OptiPrep solution was added on top of 20% solution, again without disturbing the bottom layer. Without shaking the tubes during the placement in the rotor, tubes were ultracentrifuged for 60 min at 350,000 × *g*, 4°C, by using SW55Ti rotor. At the end of the centrifugation, tubes were carefully removed from the rotor and ten fractions (455 µl/fraction) were collected starting from top of the tube. In order to remove any trace of OptiPrep, each fraction waw transferred into a new SW55Ti tube and washed by adding 3.5 ml filtered 1× D-PBS and ultracentrifuged for 90 min at 100,000 × g, 4°C, using SW55Ti rotor. Obtained pellets derived from each fraction was resuspended in a small volume (50 to 100 µl) of an appropriate buffer (e.g., D-PBS or serum-free medium) to allow maximal vesicle retrieval and transfer solution into a low-binding collection tube.

2.2.1 Methodology for the Flow Cytometry Setup, Acquisition, and Analysis

In recent years, the progress attained in the field of EV research has drastically changed methodological approaches based on multiparameter FCM. Despite being one of the most promising techniques for EV characterization, its successful use implies accurate setup of the instrument[61].

Several technical precautions have to be considered to standardize the protocol, limit nonspecific background, and avoid possible artifacts. Setting the trigger parameter on fluorescent signals and optimizing the sheath-fluid pressure and the sample injection pressure are just some of the precautions

that must be considered before starting EV analysis. As a whole, these technical expedients are useful when analyzing events falling in areas close to the sensitivity limit of the instrument and are normally referred to as "non-conventional FCM", "high-resolution FCM", or "next-generation FCM"[63]. Given increasing interest in discriminating different-sized EVs, the appropriate setup of "last-generation" flow cytometers, together with the use of a mixture of fluorescent beads of varying diameters, is critical for correct analysis[64]. Here, it is described a useful protocol for characterization of MSC-derived EV subtypes, taking advantage of a non-conventional FCM modality and the latest published technical indications[65]. Compared to previously published article[62] here, it is proposed an updated and advanced method to accurately identify and characterize vesicles with diameters <1 μm.

2.2.1.1 Flow cytometer preparation

Twenty-four hours before acquisition, fluidic levels of the BD FACSAria II instrument and replenish fluids (FACS Flow Sheath solution, FACS Clean Solution, sterile distilled water, and 70% ethanol) were checked. Thirty minutes before acquisition, workstation and FACSDiva software was started-up and switched-on instrument for laser warmup. Since *the presence of air bubbles could induce acquisition of artifacts*, after starting up the fluidics, both instrument cleanliness and absence of bubbles were tested by sequentially acquiring sterile distilled water and EV suspension buffer (PBS/EDTA) in sterile disposable 5-ml FACS tubes. After removal of the closed-loop nozzle, a 130-μm nozzle tip was used to minimize sheath flow pressure in the flow cell chamber and to reduce speed of particles interacting with the laser beam. Flow cytometer's performance was tested according to the manufacturer's instructions using CS&T beads (BD Biosciences) with flow cytometer in "CST mode". And following and cleanliness of the flow chamber was tested by acquiring sterile distilled water.

2.2.1.2 Adjustment of instrument settings

The fluorescence channels (i.e., FITC for CFSE, PE-Cy7 for blue laser at 488 nm, APC for red laser at 633 nm, and BV-421 for violet laser at 405 nm) was checked and tested. Due to Rayleigh scattering[66] , smaller particles have a size similar to the wavelength of the blue laser (488 nm), which defines physical characteristics. Within this reason, scatter on SSC was selected, which is preferential to FSC. Since the fluorescent intensity of small particles is very low, electronic "Height" (-H) parameter rather than the "Area" (-A) parameter was used to allow optimal signal detection. Following, starting

dot plot (FITC-H vs. SSC-H) was drawn and threshold on the fluorescence channel instead of physical scatter was selected. The threshold on the fluorescence channel is not widely used, but it allows one to avoid background noise in the analysis and, consequently, to set a more targeted dimensional gate[67]. On the other hand, the clusters corresponding to the different-sized beads (100, 160, 200, 240, 300, 500, and 900 nm) have to be visualized over the threshold triggering. In this way, it is possible to draw a correct "dimensional gate", excluding both background signal (smaller than the 100-nm cloud) and particles >900 nm. In this unit, both types of Megamix-Plus beads [(FSC and SSC), Biocytex] was prepared as a mixture of fluorescent beads of varying diameters in EV suspension buffer following the beads' manufacturer's instructions. Following the loading of FACS tube, FL1 gain voltage was adjusted until visualization of the small cloud corresponding to 900-nm beads in the upper right part of the dot plot. Also, a histogram reporting SSC-H channel to clearly visualize the peaks generated by the fluorescent beads was drawn. This will allow delineation of the gate(s) of interest in the desired size range (Fig. 2.2).

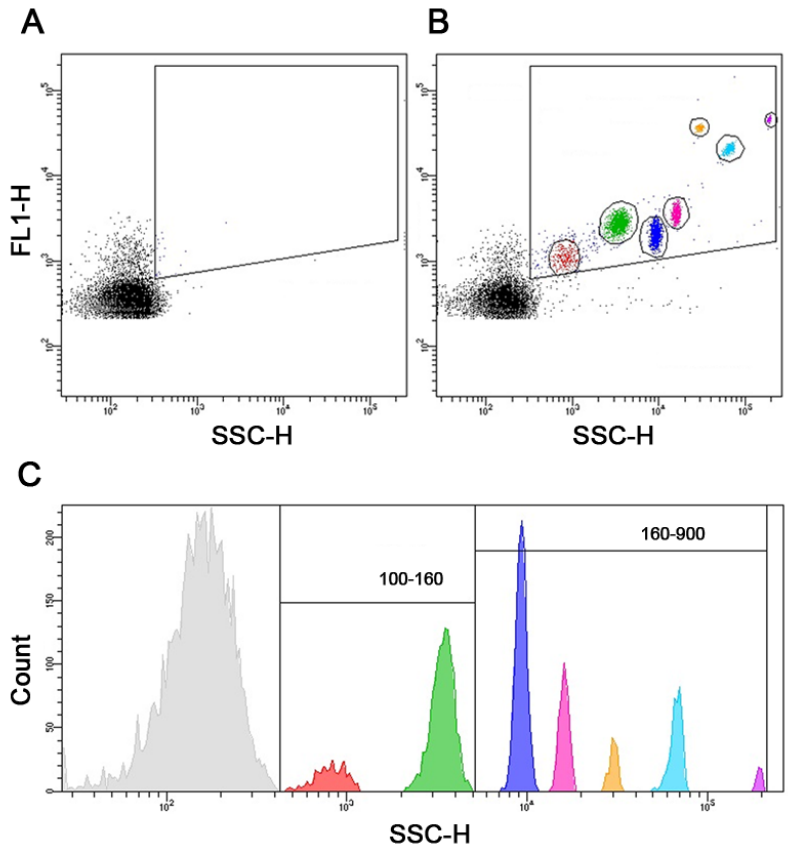

Figure 2.2: Representative bidimensional dot plots (FL1-H vs. SSC-H, in logarithmic scale) rep- resenting (**A**) the extracellular-vesicle suspension buffer (PBS/EDTA; blank control), useful to delineate a dimensional gate excluding background (black) and (**B**) the fluorescent suspension and relative sub-gating in the dimensional gate (red: 100 nm, green: 160 nm, blue: 200 nm, pink: 240 nm, light orange: 300 nm, cyan: 500 nm, and purple: 900 nm). (**C**) Visualization as SSC-H histogram peaks of the various dimensions of Megamix beads (gray: background).

2.2.1.3 Sample preparation and acquisition

Selected EV fraction suspensions were transferred into FACS tubes. CFSE (Invitrogen, V12883) stock solution was prepared following manufacturer's instructions and a final concentration (1 µM) was used by diluting stock solution in EV suspension buffer. Firstly, a control tube containing a selected EV fraction suspension stained with CFSE (e.g., 1 µl intermediate solution in 100 µl; 1 µM final CFSE concentration) at 4°C was loaded. Following, a tube containing a selected EV fraction suspension stained with CFSE at room temperature was loaded to set correct dimensional gate (Fig. 2.3).

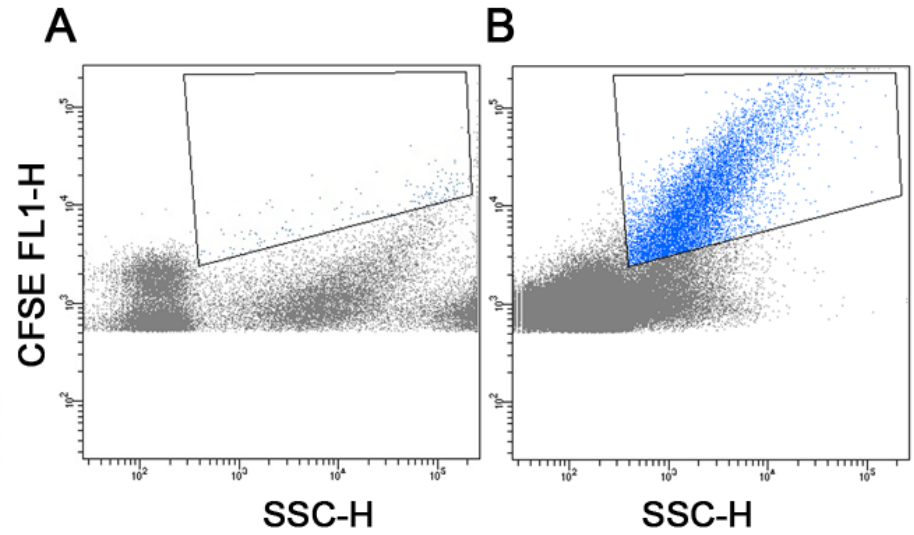

Figure 2.3: Control for CFSE specificity. (**A**) Dot plot for vesicles stained with CFSE at 4°C. (**B**) Dot plot for vesicles stained with CFSE at room temperature (25°C).

After setting the correct dimensional gate, in order to obtain an accurate visualization of EVs by labeling the samples with CFSE, specific fluorochrome-conjugated antibodies, PE-Cy™7 Mouse Anti-Human CD63 (BD Biosciences, 561982), PE Mouse Anti-Human CD9 (BD Biosciences, 555372), BV421 Mouse Anti-Human CD81 (BD Biosciences, 740079) were used to determine tetraspanin family marker expressions with their corresponding isotype-control antibodies BV421 Mouse Anti-Human CD3 Clone UCHT1 (BD Biosciences, 562426), PE-Cy™7 Mouse IgG1 κ Isotype Control (BD Biosciences, 557872) PE Mouse IgG1, Clone 40 Isotype Control (BD Biosciences, 345816). All stained samples were acquired recording ~ 50,000 events (Fig. 2.4).

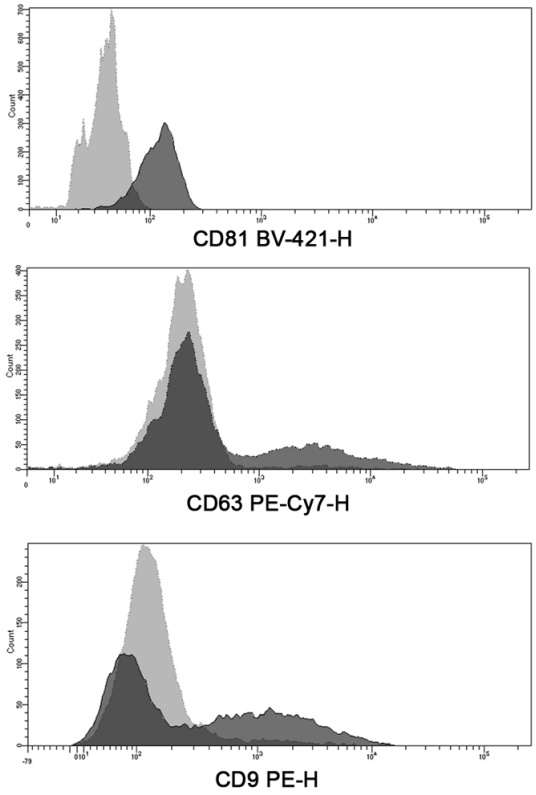

Figure 2.4: Flow cytometry analysis of mesenchymal stromal cell–derived extracellular vesicles. The presented data are from one representative experiment analyzing the vesicles present in a 100K pellet. The areas under the black lines identify cells reacting with CD81 (upper panel), CD63 (middle panel), and CD9 (bottom panel). The areas under the gray lines indicate the interactions of cells with corresponding nonreactive immunoglobulin of the same isotype.

Fluorescent spillover by compensation was checked and removed by compensation, acquiring a single-color tube for each channel, creating a compensation matrix using program application tools, and later applying the matrix to each sample tube. Following an absolute count of labeled EVs contained in each tube was obtained by using TruCount tubes (BD Biosciences) (Fig. 2.5). By FCM analysis, absolute number of EVs/µl by comparing vesicular events to bead events (as a reference number, it is recommended to record 10,000 events included in the gate of the beads) was determined and the number of positive EV events were divided by the number of bead events and multiplied by the TruCount bead concentration.

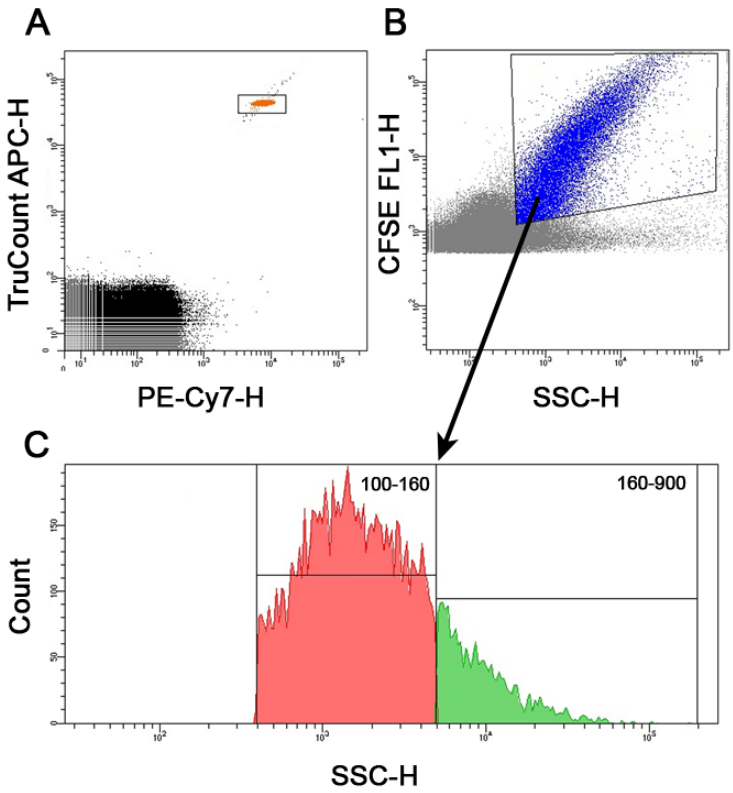

Figure 2.5: (**A**) A known number of TruCount beads (orange) is gated to obtain an absolute count of other subpopulations. (**B**) After exclusion of TruCount beads (gray), extracellular vesicles can be counted in a dimensional gate (blue) in FL1-H vs. SSC-H. (**C**) Using the reference of a mixture of fluorescent beads of varying diameters, we can visualize extracellular-vesicle sub-gates within CFSE-positive events (red: from 100 nm up to 160 nm; green: from 160 nm up to 900 nm) in an SSC-H histogram.

2.3 Discussion

For many years, MSCs have been considered a remarkable cell source for regenerative- medicine applications. More recently, a paradigm shift has emerged, suggesting that these cells' beneficial effects are often due to the cells' paracrine activity[68]. Given that MSCs have a regulatory pheno- type and respond actively to environmental signals, their secretory activity can be deeply modulated[69,70]. In this context, EVs are recognized as important components of the MSC secretome, and a growing body of literature has examined the regenerative potential of MSC- derived EVs using different approaches[71].

The term “extracellular vesicle” defines a heterogeneous population of exosomes, microvesicles, and apoptotic bodies. During traditional EV isolation, discarding the pellet after 10K centrifugation or filtering the supernatant with a 0.22-μm filter could in part exclude larger vesicles, such as shedding microvesicles, from further analysis. However, recent papers have highlighted the importance of considering different subtypes, which may have different functional properties[34,59,72]. For this reason, it is becoming increasingly important to develop and optimize useful protocols to isolate the different subpopulations, avoiding the possibility of losing subtypes.

Several methods have been adopted to count and characterize EVs (e.g., nanoparticle tracking analysis, electron microscopy, resistive pulse sensing), but there is still considerable confusion about the definition of EV phenotype and the standardization of protocols for analysis[73]. All the methodologies present difficulties and limitations, ranging from low sensitivity to very high cost to poor statistical validation. Last generation FCM could become a methodology of choice, characterized by crucial advantages: relatively low cost, multiparameter phenotyping, and good statistical robustness of the data due to a large number of events being analyzed at the same time.

On the other hand, some critical issues may affect different aspects of the protocols presented in this chapter. One of these is the starting amount of vesicles which is necessary to perform downstream analysis. Indeed, while the optimization of this protocol, it has been observed that primary cultures release fewer vesicles than cell lines do. Given that excessive expansion of primary cultures could lead to cellular senescence and permanent phenotypic and functional changes, it is not recommended to increase the cells’ passage number in order to obtain more secreting cells. A possible approach to augment the amount of secreted EVs is to prolong the serum-free conditioning timeframe. However, it is strongly recommended checking both cell viability and early/late apoptotic markers when optimizing this timeframe.

Another crucial aspect that should be taken into account is the selection of fractions based on density gradient separation. It is highly recommended to use “wet- table” ultracentrifuge tubes when preparing OptiPrep density gradients. The use of non- wettable tubes could in fact cause disruption of the density layers[74]. Within this reason, experimental procedure was performed with polypropylene tubes instead of the widely used polyallomer tubes.

Moreover, sample preparation for FCM must be systematic: the choice and purity of buffers, the concentrations of particles, the fluorescent dyes used to discriminate intact vesicles, and the titration of the antibodies as well as the isotype controls have to be considered with great care. The final concentration of EVs is in fact a crucial factor in avoiding the "swarming effect": when the concentration of nano-sized particles is too high, the cytometer is no longer able to discriminate single events, thus generating artifacts. The opposite can also happen: when the particles are too diluted or are stained with an improper concentration of antibody, they can remain "embedded" in the background signal. On the other hand, it is also very important to check the injection pressure of the sample in the chamber (sample flow rate) and the pressure of the transport liquid (sheath flow pressure), which creates the laminar flow. Both pressures must be as low as possible in order to slow down the flow of the vesicles.

2.4 Conclusion

This chapter described a methodology for isolating subpopulations of extracellular vesicles (EVs) purified from human adipose tissue–derived mesenchymal stromal cells by density gradient centrifugation and characterizing them by flow cytometry (FCM). Determining the optimal strategy for isolating EVs is a critical step toward retrieving the maximal amount while ensuring the recovery of different vesicular subtypes. Moreover, the characterization of EV subpopulations by FCM is depicted by taking the advantage of non-conventional modalities, in accordance with the latest technical indications. If the protocols are followed as indicated, optimal results are warranted. These protocols can be adapted to isolate and characterize EV sub-populations from cell types other than MSCs.

CHAPTER

3

Dissecting the effects of preconditioning with inflammatory cytokines and hypoxia on the angiogenic potential of Mesenchymal Stromal Cell (MSC)-derived soluble proteins and Extracellular Vesicles (EVs)

Gorgun C, Ceresa D, Lesage R, Villa F, Reverberi D, Balbi C, Santamaria S, Cortese K, Malatesta P, Geris L, Quarto R, Tasso R. Dissecting the effects of preconditioning with inflammatory cytokines and hypoxia on the angiogenic potential of mesenchymal stromal cell (MSC)-derived soluble proteins and extracellular vesicles (EVs). Biomaterials. 2021 Feb;269:120633. doi: 10.1016/j.biomaterials.2020.120633. Epub 2020 Dec 28. PMID: 33453634.

3.1 Introduction

Mesenchymal Stromal Cells (MSCs) are versatile progenitors able to sense the surrounding environment and actively respond to changes or requirements of the milieu modulating the secretion of specific mediators [75]. It's widely accepted that in many experimental and clinical settings the MSC potency and therapeutic efficacy do not depend on the physical closeness of the transplanted cells to the damaged tissue, but rather on their paracrine activity [76,77]. The array of trophic factors and extracellular vesicles (EVs) secreted by MSCs is broadly defined as the cell secretome. When MSCs are injected *in vivo* and encounter the harsh environment typical of a damaged tissue, they face a decline in their biological performances [21]. Preconditioning represents an adaptive strategy to improve MSC therapeutic efficacy, preparing cells to survive in hostile conditions and enhancing their regulatory activities [78,79]. In this context, one of the major challenges in MSC-based therapies is to develop *in vitro* culture methods that mimic the injury environment, without compromising cell quality and function. Strong inflammation and hypoxia are two simultaneous and related conditions during the early phases of the tissue healing process [80,81]. Indeed, in the context of the wound microenvironment, the activation of innate immune cells, mainly neutrophils and monocytes, results in an enhanced release of chemokines and cytokines, such as Tumor Necrosis Factor-α (TNF-α) and Interleukin-1α and -1β (IL-1α and IL-1β), that act as mediators of the host defense [82]. In these phases, wound sites are also characterized by low oxygen tension due to disruption of the vasculature surrounding the injury [80]. This is the complex milieu that transplanted MSCs encounter and that mitigate their function and survival; treating cells with the same stimuli before transplantation could overcome these limitations and enhance their paracrine activity [21,83].

The control of blood vessel growth plays a key role to restore blood supply and ensure rapid vascularization of damaged tissues [84]. Several literature reports indicate that MSC secretome can exert different effects in the context of angiogenesis, and many of these differences largely depends upon the various culture conditions [85,86]. It has been described that MSCs respond positively to hypoxic preconditioning, showing a decreased apoptosis even in severe microenvironmental conditions and an increased expression of angiogenic factors [87,88]. Although various cytokines and chemical compounds have been proven to have cell-protective effects [89], contrasting results have been published regarding the angiogenic potential of MSCs licensed by a pro-inflammatory microenvironment [90–92].

In the present study we evaluated the influence of a short-term preconditioning with both hypoxia (1% O2) and inflammatory stimuli (TNF-α and IL-1α) on the angiogenic potential of human adipose tissue-derived MSC secretome. In particular, we compared the effect of the total conditioned medium (CM) with that exerted by the corresponding fractions composed by either small- or medium-sized extracellular vesicles (sEVs and mEVs), and with the vesicle-depleted medium, enriched only in soluble factors. Extensive *in vitro* and *ex vivo* data demonstrated that the synergistic action of hypoxia and inflammation affected the MSC secretome fractions at different extents. In response to inflammatory cytokines, MSCs released soluble factors with a strong anti-angiogenic effect on endothelial cell proliferation, migration and tubulogenesis. On the contrary, and depending on the specific aspect of the angiogenic process, the corresponding EV fractions were less sensitive to the influence of external stimuli. Our findings suggest that a deep investigation into how preconditioning can specifically influence the different cell paracrine activities is fundamental to provide new insights for the therapeutic use of the MSC secretome.

3.2 Materials and Methods

3.2.1 Isolation and culture of human adipose tissue-derived Mesenchymal Stromal Cells (MSCs)

MSCs were obtained from subcutaneous adipose tissue, as previously described [93] and in compliance to Regione Liguria Ethical Committee authorization (P.R. 23571). Briefly, subcutaneous adipose tissue in the form of liposuction aspirates was obtained from human healthy donors during routine lipoaspiration after informed consent. Adipose tissue was extensively washed with cold phosphate-buffered saline (PBS) and digested in 0.1% type I Collagenase (Gibco, MI, Italy) in PBS at 37°C for 60 minutes. The resulting stromal vascular fraction (SVF) pellet was extensively rinsed and plated at a density equivalent to 2 ml of liposuction tissue aspirate/54cm^2 of surface area and cultured in Dulbecco's MEM (D-MEM) (Biochrom GmbH, Berlin, Germany) supplemented with 10% fetal bovine serum (FBS) (Gibco, Milan, Italy), 2mM of l-glutamine, and 50 mg/ml penicillin/streptomycin. The cultures were performed in the presence of 1 ng/ml of fibroblast growth factor-2 (FGF-2; Peprotech, Milan, Italy) (standard condition). Medium was changed every 3 days and cells expanded after reaching about 85% confluence using 0.05% trypsin-EDTA (Gibco, MI, Italy). All cultures were maintained in a humidified incubator at 37°C with 5% CO_2. The

immunophenotype was evaluated by flow cytometry on MSC cultured in standard condition using the following monoclonal antibodies to: CD31-FITC (390), CD34-FITC (4H11), CD45-PE (2D1), CD73-FITC (AD2), mouse IgG1 kappa Isotype Control-FITC (P3.6.2.8.1), mouse IgG1 kappa Isotype Control-PE (P3.6.2.8.1) (eBioscience), and monoclonal antibodies to: CD90-PE (5E10), CD29-PE (MAR4), CD105-PE (266), CD44-FITC (L178), mouse IgG1 kappa Isotype Control-FITC (MOPC-21), mouse IgG1 kappa Isotype Control-PE (MOPC-21) (BD Biosciences). Cells were analyzed using a flow cytometer (FACSCanto, BD Biosciences).

The MSC differentiation potential into osteogenic and adipogenic lineages was verified *in vitro*. Briefly, cells cultured in standard condition were detached from cultures reaching 90% confluence, washed, and plated at a concentration of $5x10^4$ cells/cm^2 in 24-well culture plates. Osteogenic differentiation was induced by stimulating cultures with 50 mg/ml ascorbic acid, 1.5mg/mL β-glycerophosphate, and 10^{-7}M dexamethasone in D-MEM for 14 days. The presence of calcium deposits was revealed using Alizarin Red- S staining. To check the adipogenic differentiation potential, MSCs were stimulated for 21 days in D-MEM supplemented with 1% FBS, 10^{-7}M dexamethasone, and 6 ng/ml insulin. Lipid droplets were revealed by staining with Oil Red staining. Only cells that were in passage 2 or 3 were used for extracellular vesicle separation.

3.2.2 MSC pre-conditioning and collection of MSC Conditioned Media (CM)

When MSCs reached around 70% confluence, cells were rinsed twice with PBS and maintained for 20 minutes in D-MEM supplemented with 2mM l-glutamine and 50 mg/ml penicillin/streptomycin (serum-free medium) to remove FBS residue. Medium was then removed and replaced with fresh serum-free medium and cultures split into four subcultures maintained for 24 hours under normoxia (20% O_2) (Nor), hypoxia (1% O_2) (Hyp), normoxia supplemented with 50 ng/ml Tumor Necrosis Factor-α (TNF-α) (PeproTech, London, UK) and 50 ng/ml Interleukin 1-α (IL1-α) (PeproTech, London, UK) (Nor^{INF}), and hypoxia supplemented with 50 ng/ml TNF-α and 50 ng/ml IL1-α (Hyp^{INF}). The immunophenotype of MSCs cultured in Nor, Hyp, Nor^{INF} and Hyp^{INF} conditions was evaluated by flow cytometry exploiting the same anti-human antibodies above described. Cell viability of MSCs cultured for 24 hours in Nor, Hyp, Nor^{INF} and Hyp^{INF} conditions was detected by FITC Annexin V Apoptosis Detection Kit (BD Biosciences), according to manufacturer's instructions. Cells were analyzed using a flow cytometer (FACSCanto; BD Biosciences). Conditioned media (CM) from

Nor, Hyp, Nor^{INF} and Hyp^{INF} were collected. Half of each CM preparation was used to isolate extracellular vesicles and generate the corresponding amount of depleted medium, as described in the next paragraph, and the other half of CM was concentrated with Amicon®-Ultra-15, 3 kDa centrifugal filter tubes (Merck, Massachusetts, USA). In order to quantify the protein amount, BCA (BicinChoninic Acid) Protein Assay Kit (Thermo Fisher Scientific, Massachusetts, USA) was used.

3.2.3 Extracellular Vesicles (EVs) isolation and generation of Depleted-Medium (DM)

We have submitted all relevant data of our experiments to the EV-TRACK knowledgebase (EV-TRACK ID: EV200171) [38]. EVs were separated from Nor-, Hyp-, NorINF-, and HypINF- CM by differential ultracentrifugation using a Beckman Coulter ultracentrifuge (Optima L-90K), according to an already published protocol [94]. After collecting the CM, cells/cell debris and apoptotic bodies were removed centrifuging the CM for 10 min at 300 *x*g and for 20 min at 2000 *x*g, respectively. The resulting supernatant was transferred into ultracentrifugation tubes (Beckman-Coulter, USA) and subjected to a first centrifugation for 40 min at 10.000 *x*g (10K pellet) to obtain an EV pellet (10K pellet) enriched with medium sized-vesicles (mEVs). Supernatants were then centrifuged for 120 min at 100.000 *x*g in order to obtain a pellet (100K pellet) enriched with small sized-vesicles (sEVs). Supernatants derived from 100K centrifugation were collected as depleted media (DM) and concentrated to reach the same volume of their corresponding CM. All EV pellets were washed in PBS and centrifuged at the same speed before being resuspended in sterile filtered (0.22 μm) PBS or serum-free medium, in the same volume of their corresponding CM and DM. A SW28 swinging bucket rotor (Beckman Coulter) has been used during the ultracentrifugation steps.

3.2.4 Flow cytometry characterization of EVs

EV characterization by flow cytometry was performed as previously described [95]. Briefly, each EV preparation was suspended in filtered PBS and distributed in flow cytometry tubes (100 μl/tube). For each preparation, one tube has been stained with 1 μM CFDA-SE at 4°C (Vybrant™ CFDA SE Cell Tracer Kit, Thermo Fisher Scientific), that represents the control to verify CFDA-SE specificity, and one tube containing EVs was stained with the same amount of CFDA-SE at room temperature (RT) to visualize intact vesicles and set the correct dimensional gate. A mixture of fluorescent beads of varying diameters (Megamix-Plus FSC and Megamix-Plus SSC, Biocytex) suspended in filtered PBS

was used following the manufacturer's instructions to discriminate EV size. Expression of typical vesicle markers CD9 (APC Mouse Anti-Human CD9, Biolegend, 312108), CD63 (PE-CyTM7 Mouse Anti-Human CD63, BD Biosciences, 561982) and CD81 (BV421 Mouse Anti-Human CD81, BD Biosciences, 740079) was evaluated within the CFDA-SE-positive events using the BD FACSAria II (BD Biosciences).

3.2.5 Nanoparticle Tracking Analysis (NTA) on MSC-derived EVs

EV concentrations and sizes were determined using a NanoSight LM10 instrument (Malvern Instruments Ltd, Malvern, UK) equipped with 405 nm laser and CCD camera. Readings were done as triplicates of 60 s at 30 frames per second, at a camera level set to 10 and monitoring of temperature.

3.2.6 Transmission Electron Microscopy (TEM)

MSCs were washed out in 0.1 M cacodylate buffer and immediately fixed in 0.1 M cacodylate buffer containing 2.5% glutaraldehyde (Electron Microscopy Science, Hatfield, PA, USA) for 1 h at room temperature. Cell pellets were post-fixed in osmium tetroxide for 2 h and 1% uranyl acetate for 1 h. Subsequently, samples were dehydrated through a graded ethanol series and embedded in epoxy resin (Poly-Bed; Polysciences, Inc., Warrington, PA) for 24 h at 60°C. Ultrathin sections (50 nm) were cut and stained with 5% uranyl acetate in 50% ethanol and observed with Hitachi TEM microscope (HT7800 series, Tokyo, Japan). Electron microscopic analysis on separated vesicle preparations was performed as follows. The extracellular vesicle (EV) preparations were resuspended in 20 µl PBS (pH 7.4) and fixed by adding an equal volume of 2% paraformaldehyde in 0.1 mol/l phosphate buffer (pH 7.4). EVs were then adsorbed for 10 minutes to formvar-carbon coated copper grids by floating the grids on 5 µl drops on parafilm. Subsequently, grids with adhered vesicles were rinsed in PBS and negatively stained with 2% uranyl acetate for 5 minutes at room temperature. Stained grids were embedded in 2.5% methylcellulose for improved preservation and air dried before examination. Electron micrographs were taken at Hitachi TEM microscope (HT7800 series, Tokyo, Japan) equipped with Megaview 3 digital camera and Radius software (EMSIS, Germany). To visualize EV size distribution, the results were plotted as colorblind safe scatter dot plot in which each size measured is represented as a point along with lines for the median value and the range.

3.2.7 Western Blot Analysis

For western blot analysis, the pre-conditioned MSCs and their corresponding separated mEVs and sEVs were resuspended in RIPA buffer (1% NONIDET p-40, 0.1% SDS, 0.1% Sodium deoxycholate, protease inhibitor cocktail 1x, in PBS pH 7.5) and protein content was quantified by BCA assay. Afterwards, 10 μg of proteins for each sample was loaded on 4–20% Mini-PROTEAN®TGX™ Precast Gel for electrophoresis, and proteins were blotted onto a PVDF membrane with a semi-dry transfer system (all from Bio-Rad Europe, Basel, Switzerland). Blot membrane was incubated overnight at 4°C with the following specific primary antibodies: anti-syntenin (1:1000 dilution, ab133267 Abcam, USA), anti-mitofilin (1:1000 dilution, PA5 89627, Invitrogen, USA) and anti-Grp94 (1:1000 dilution, ab238126, Abcam, USA), and anti-lamin A (1:1000 dilution, ab26300, Abcam, USA) prepared in odyssey blocking buffer (LI-COR, USA) at the dilution as recommended by the manufacturer. Following, membranes were incubated with appropriate secondary antibodies such as IRDye® 680RD or 800CW goat anti-mouse or goat anti-rabbit secondary Ab (LI-COR Biosciences, Lincoln, Nebraska, USA). Infrared signal was detected using Odyssey CLx Detection System (LI-COR Biosciences).

3.2.8 Human Umbilical Vein Endothelial Cell (HUVEC) culture

HUVECs were plated on 1.5% (v/v) gelatin (Sigma-Aldrich, MO, USA) coated 10 cm Petri dishes and cultured in Medium 199 (Euroclone, Milan, Italy) supplemented with 10% FBS (Gibco, Milan, Italy), 2mM l-glutamine, 50 mg/ml penicillin/streptomycin, 100 mg/ml heparin (PharmaTex, Milan, Italy), 10 μg/ml FGF-acidic, 10 μg/ml FGF-basic, 10 μg/ml EGF (Peprotech, London, UK), 1 mg/ml hydrocortisone (Sigma-Aldrich, MO, USA) (complete medium). For the described experiments, positive controls were set up with complete HUVEC medium while negative controls were set up with serum-free Medium 199 (SF). HUVECs were used at maximum passage number 5.

3.2.9 HUVEC Proliferation Assay

HUVECs were seeded at the density of 1x104 cells per well on gelatin-coated 96-well plates and incubated in complete medium for 24 hours to allow cell adhesion. In order to synchronize the cells before starting treatments, complete medium was replaced with SF medium for 24 hours. Following, HUVECs were treated for 24 hours with secretome fractions (CM, DM, mEVs and sEVs) derived

from the 4 different MSC culture conditions (Nor, Hyp, NorINF, HypINF). Cell proliferation was measured with the use of the Cell Proliferation Enzyme-linked immunosorbent assay (ELISA), Bromodeoxyuridine (BrdU) (Roche Mannheim, Germany), according to the manufacturer's instructions. Three independent experiments were performed.

3.2.10 HUVEC Migration Assay

HUVEC migration was examined using a modified Boyden chamber technique. A 24-well Transwell apparatus (Costar) was used, with each well containing a 6.5-mm polycarbonate membrane with 8 μm pores and coated with 100 μL of 1.5 % (v/v) gelatin (Sigma-Aldrich, MO, USA). HUVECs (5×10^4) were placed on the membrane, and the chambers were immersed in a 24-well plate that was filled with the secretome fractions (CM, DM, mEVs and sEVs) derived from Nor, Hyp, Nor^{INF}, Hyp^{INF} conditions. After 9 h incubation, the membranes were washed briefly with PBS and the upper side of each membrane was then wiped gently with a cotton ball. Cells were fixed with methanol and the ones migrated in the lower part of the inserts were stained with Giemsa's Azur eosin methylene blue solution (10% v/v). Images were taken by Axiovert 200M microscope (Carl Zeiss Microscopy GmbH, Jena, Germany). Images were analyzed by ImageJ with Cell Counter plug-in. Three independent experiments were performed.

3.2.11 Tube Formation Assay

Tube formation capacity by HUVECs was analyzed by using an Angiogenesis μ-slide system (Ibidi GmbH, Planegg/Martinsried, Germany). μ-slide wells were coated with growth factor reduced (GFR) Matrigel (Corning, NY, USA). After matrigel polymerization, HUVECs ($1x10^4$) were plated and incubated at 37°C for 7 hours in presence of the different secretome fractions. After incubation, cells were stained with Calcein-AM (Corning, NY, USA) and images of complete wells were taken with fluorescence microscope (Nikon Eclipse 80i, Tokyo, Japan). Images were analyzed by using Image J Software with Angiogenesis-Analyzer plug-in. Three independent experiments were performed.

3.2.12 *Ex vivo* Metatarsal Sprouting Assay

Mice were bred and maintained at the Animal Facility of "IRCCS Ospedale Policlinico San Martino". All animal procedures were approved by the Italian Ministry of Health and by the Institutional (IRCCS

Ospedale Policlinico San Martino) Ethical Committee (Authorization n. 55/2020-PR) and performed in accordance with the national current regulations regarding the protection of animals used for scientific purpose (D. Lgs. 4 Marzo 2014, n. 26, legislative transposition of Directive 2010/63/EU of the European Parliament and of the Council of 22 September 2010 on the protection of animals used for scientific purposes). The metatarsal angiogenesis assay was performed as previously described[96]. Briefly, E17.5 wild-type mice embryos (C57BL/6) were used, and metatarsal bones were isolated under stereomicroscope. Each bone was placed into 24-well plate and incubated for 96 hours for bone attachment in α-MEM-GlutaMAX medium (GiBCo, Waltham, MA, United States), supplemented with 10% FBS (Gibco, Milan, Italy) and 50 mg/ml penicillin/streptomycin (complete medium). Complete medium was replaced with experimental secretome fractions in α-MEM-GlutaMAX medium supplemented with 2% FBS. While positive control was set up with complete medium, negative control was set up with 2% FBS for maintaining the fibroblast viability around the bones. After 7 days, bones were fixed and stained with rat anti-Mouse CD31 (clone SZ31) (Dianova, Hamburg, Germany). Images were captured by transmitted light microscopy using a Zeiss Axiovert 200M microscope. CD31-positive pixels were analyzed with Image J software with vessel density plugin. Three independent experiments were performed.

3.2.13 Bioinformatic approach to Proteome Profiler™ Human Angiogenesis Antibody Array

The relative expression of 55 angiogenesis-related proteins were determined in CM derived from the 4 different culture conditions (Nor, Hyp, Nor^{INF}, Hyp^{INF}) by using a Proteome Profiler™ Human Angiogenesis Antibody Array (R&D Systems, Minnesota, USA) according to the manufacturer's instructions. Briefly, 30 μg of each CM f derived from three independent experimental replicates were pre-incubated with the cocktail of antibodies and added onto membranes overnight at 4°C. After several washing steps, streptavidin-horseradish peroxidase was added for 30 minutes and chemiluminescence of membranes was detected. Image J software with protein array analyzer plugin was used to determine the pixel density of each spot. Among 55 proteins, only the ones that were expressed at least in two independent primaries/experimental group were considered.

Statistical analyses were performed with R, under version R-3.5.1. Multivariate analysis was first carried on by dimensionality reduction on batch corrected data. Batch correction was done by considering the 3 primary donors as different batches thanks to the limma package in R. In effect, a linear model was

fitted to the data, including both batches and regular treatments, then the component due to batch effects was removed. Principal components were identified by singular value decomposition as implemented in the R built-in function prcomp. To assess differentially expressed proteins between treatment conditions, MANOVA with Pillai–Bartlett statistic was applied on log10 transformed and centered scaled data without batch effect correction since the donor effect was accounted for the linear model as a blocking variable. In the one-way MANOVA, the explanatory variable was either the inflammatory status regardless of the oxygen level or the oxygen level regardless of the inflammatory status, allowing n=6 observations per level. Values of $p < 0.05$ were considered statistically significant and are reported in figure's legend. Significance was also confirmed by univariate ANOVA with Bonferroni correction for multiple testing. Data distribution was evaluated on the basis of quantile–quantile (QQ) and residuals plots.

3.2.14 RNA Preparation and Next Generation Sequencing of EVs

mEVs and sEVs isolated from MSC cultured in Nor, Hyp, Nor^{INF} and Hyp^{INF} conditions were suspended in 700 µL of Qiazol reagent (Qiagen, Limburg, the Netherlands). EV RNA was extracted with the miRNeasy Micro Kit (Qiagen) according to the manufacturer's instructions and stored at -80°C. miRNA content was assessed by performing the Qubit® microRNA Assay Kit with the Qubit® 2.0 Fluorometer, and RNA quality and sizes were checked with Agilent 2100 Bioanalyzer (Agilent Technologies, Foster City, CA) using the Agilent Small RNA chip according to manufacturer's protocol. For RNASeq, each sequencing library was constructed from 9.2 ng of isolated miRNA. The small RNA libraries were prepared and amplified using QIAseq miRNA Library kit (Qiagen), following manufacturer's instructions. Libraries were pooled after quality check and quantification by TapeStation (Agilent Technologies, Foster City, CA) using Agilent High Sensitivity D1000 ScreenTape. Pooled libraries were quantified by real-time qPCR following "Sequencing Library qPCR Quantification" Guide (Illumina Inc., San Diego, CA) and sequenced by Illumina NextSeq platform using the 75 cycles high output kit (Illumina Inc., San Diego, CA).

3.2.15 miRNAseq Data Analysis

FastQ data files obtained by sequencing were primarily processed by a GeneGlobe pipeline to map reads to human genome and perform Unique Molecular Indices (UMI) Analysis. Following analysis

was performed on UMI-filtered reads. Differential miRNA Expression Analyses was performed using a custom R script based on Limma[97] and EdgeR[98] Bioconductor Packages. To compare the overall enrichment of miRNA species in the total vesicular RNA, miRNA reads of each sample were normalized to the miRNA fraction of total RNA. After normalization, pairwise comparisons were made according to the Limma-Voom workflow[99]. For each comparison, miRNAs emerging as outliers in volcano plots (fold change / p value scatterplots) were selected as differentially expressed, and then used to perform a hierarchical clustering of the compared samples. In case the selected miRNAs were not able to correctly classify the samples, more stringency was used for the outlier selection. Global estimates of intra-class and inter-class heterogeneity were generated analyzing the linear model fitting parameters calculated by lmFit function of Limma package. The median value of the coefficient of variation (calculated using fitting coefficients as mean values) of all miRNAs was used as intra-class heterogeneity estimate. The median absolute deviation of fold change estimates of all miRNAs, restricted to the experimental comparisons, was used as inter-class heterogeneity estimate. Given the nature of the estimates, their statistical analysis was performed by Student's t-test. Correlation matrix of miRNA expression was performed calculating Sperman correlation of the subset of miRNAs showing more variability across all samples (55% of sequenced miRNA species).

3.2.16 Statistical analysis

Differences in EV size revealed by flowcytometry were performed using an unpaired two- tailed Student's t test. PI/Annexin data were analyzed by two-way ANOVA. Statistical analysis of differences between multiple groups such as particle concentration, *in vitro* angiogenesis assays and *ex vivo* metatarsal assay were performed applying One-way ANOVA and Tukey's multiple comparisons test. Data are presented as mean ± SD considering at least three independent replicates for each assay and analyzed by GraphPad Prism (Graph Pad Software, Inc.). For all analyses $p< 0.05$ was considered statistically significant. In all cases: **** $p<0.0001$, *** $p<0.001$, ** $p <0.01$, * $p <0.05$.

3.3 Results

3.3.1 Pre-conditioning with pro-inflammatory cytokines and hypoxia does not alter MSC properties

The main mechanism by which MSCs participate to tissue repair is through a paracrine activity and their interaction with the injured environment is a central part of this process [100]. Here, an approach based on the pre-conditioning of MSCs with pro-inflammatory cytokines and hypoxia, alone or in combination, was explored for mimicking a cellular environment more consistent with that found *in vivo*. In agreement with the guidelines of the International Society for Cell Therapy (ISCT) [9], human adipose tissue-derived MSCs grown in standard condition constitutively expressed CD29, CD44, CD73, CD90 and CD105, considered to be markers of progenitor cells of the mesenchymal lineage (Supplementary Fig. 3.1a). The expression of CD31, CD34 and CD45 was always less than 1%, indicating the absence of contaminating endothelial, myeloid, and hematopoietic cells (Supplementary Fig. 3.1a). Adipose tissue-derived MSCs possessed the ability to differentiate toward the osteogenic and adipogenic lineages (Supplementary Fig. 3.1b). To find out if any of the adopted pre-conditioning approaches might alter cell phenotype, the expression of the same markers was evaluated in MSCs maintained for 24 hours in normoxia (Nor), hypoxia (Hyp), normoxia with inflammatory stimuli (Nor^{INF}), and hypoxia with inflammatory stimuli (Hyp^{INF}). No statistically significant differences were observed between the four treatment groups, and in comparison, with cells grown in standard condition (Supplementary Fig. 3.2a-d), indicating that MSCs preserve a correct immunophenotype after the 24h conditioning. Flow cytometry of Annexin V/PI-stained cells was used to quantify the apoptotic rate of MSCs exposed to serum deprivation for 24h in Nor, Hyp, Nor^{INF} and Hyp^{INF} conditions. The different pre-conditioning treatments did not alter the percentage of apoptotic, necrotic or viable cells. Only the addition of inflammatory cues to normoxic cells significantly increased the percentage of viable cells when compared to normoxia, with a concomitant decrease in the percentage of late apoptotic cells (Supplementary Fig. 3.1c). Taken together, these results indicate that the selected pre-conditioning approaches exerted no significant effects on the phenotype or viability of MSCs.

3.3.2 Preconditioned MSCs secrete EVs of different sizes

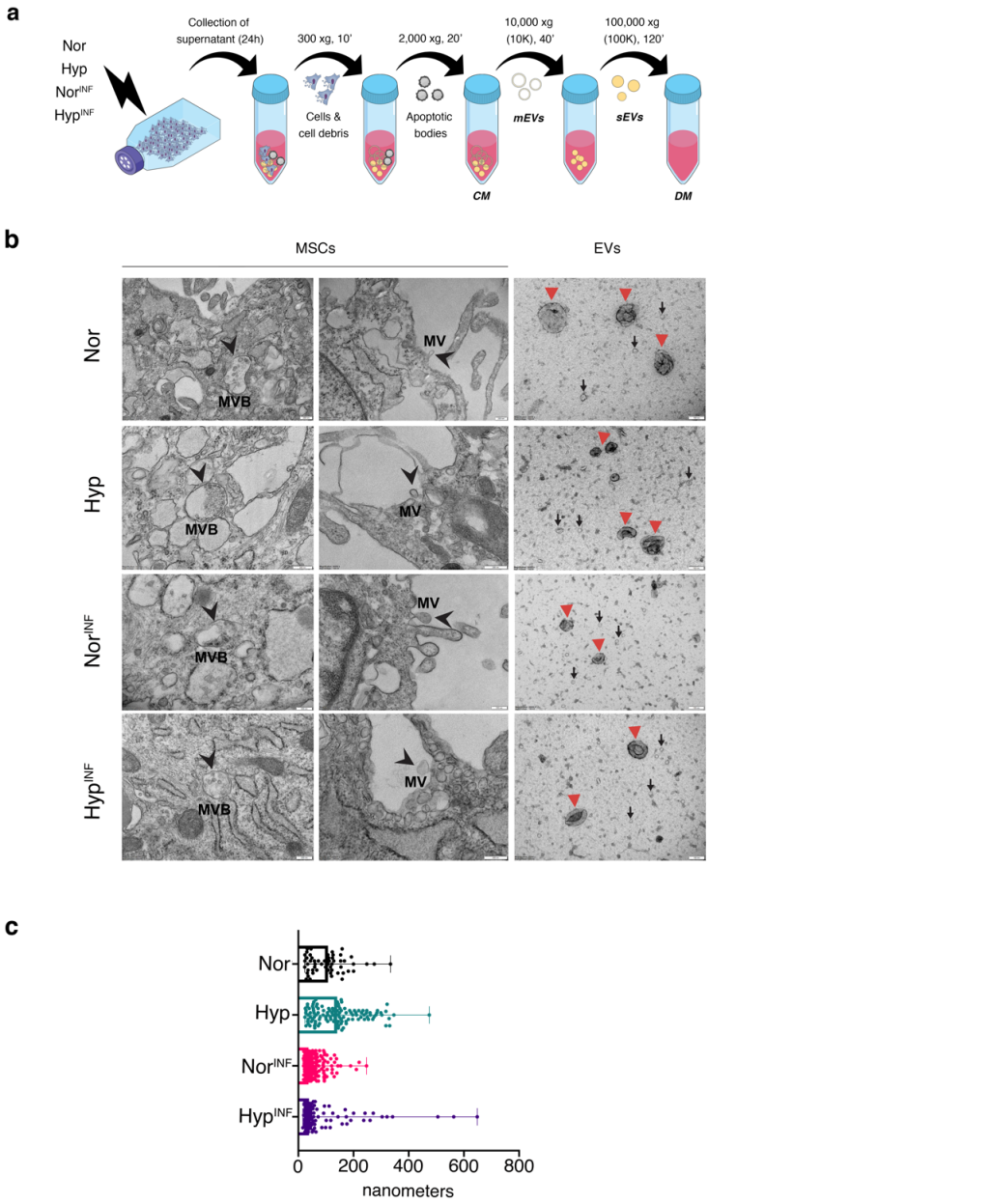

Figure 3.1: Separation and characterization of MSC-derived EVs. (a) Schematic depicting the workflow used to separate the total conditioned medium (CM) and the different secretome fractions (DM, mEVs, and sEVs). (**b**) Representative TEM images of MSCs cultured in Nor, Hyp, Nor^{INF} and Hyp^{INF} conditions containing multivesicular bodies (MVB) (black arrowheads, left panels) and putative microvesicles budding from the plasma membrane (black arrowheads, middle panels). Right panels show representative TEM images of separated EVs indicating the presence of both smaller EVs (arrows) and larger EVs (red arrowheads). (**c**) TEM analysis of EV size. Data are visualized as scatter dot plot showing EV size distribution among different conditions. Each size measurement of EVs is showed as a point, whereas lines represent the median value and the range.

Since the cell secretome comprises a complex mixture of soluble factors and a variety of extracellular vesicles (EVs) [101], the effect of the stimulation under either normoxia or hypoxia in presence or absence of inflammatory cues was investigated on the total conditioned medium (CM), on the corresponding EV fraction, and on the so-called depleted medium (DM), that is the CM depleted of EVs (enriched only in soluble factors) (Fig. 3.1a). For EV separation, CM were collected from MSC-Nor, MSC-Hyp, MSC-Nor^{INF}, and MSC-Hyp^{INF} and subjected to differential ultracentrifugation. After initial low-speed centrifugation (300 xg and 2,000 xg) to remove cells and cell debris, pelleted material recovered at medium (10,000 *x*g = 10K) centrifugation speed, enriched in medium-sized vesicles (mEVs), was washed and compared with the material pelleted at high-speed (100,000 *x*g = 100K) centrifugation, considered to be enriched in small-sized EVs (sEVs) (Fig. 3.1a).

Firstly, whole mounts of materials retrieved from MSCs after the 24h preconditioning and from the separated EVs (10K and 100K pellets pooled together) were analyzed by transmission electron microscopy (TEM) to obtain an overview of the heterogeneity of the secreted vesicles. TEM analysis of MSCs revealed the presence in all conditions of both multivesicular bodies (MVBs) containing smaller exosomes (Fig.3.1b, left panels - black arrowheads) and larger microvesicles (MVs) budding from the plasma membrane (Fig.3.1b, middle panels - black arrowheads), indicating the release of a mixed population of EVs. Images of corresponding EV pellets revealed the presence of a heterogeneous population of vesicles of different sizes ranging from 30 nm to 200 nm (Fig. 3.1b, right panels, red arrowheads and Fig. 3.1c) suggesting that the separation procedure selected a mixed population of vesicles enriched mostly, but not only, in sEVs. EVs showed round or cup-shaped morphology and were surrounded by a bilayer membrane. Smaller vesicles (30-50 nm in size) appeared round-shaped and electron-lucent (arrows), whereas larger EVs (50-200 nm) exhibited the cup-shaped morphology and appeared more electron dense (red arrowheads) (Fig.3.1b, right panels).

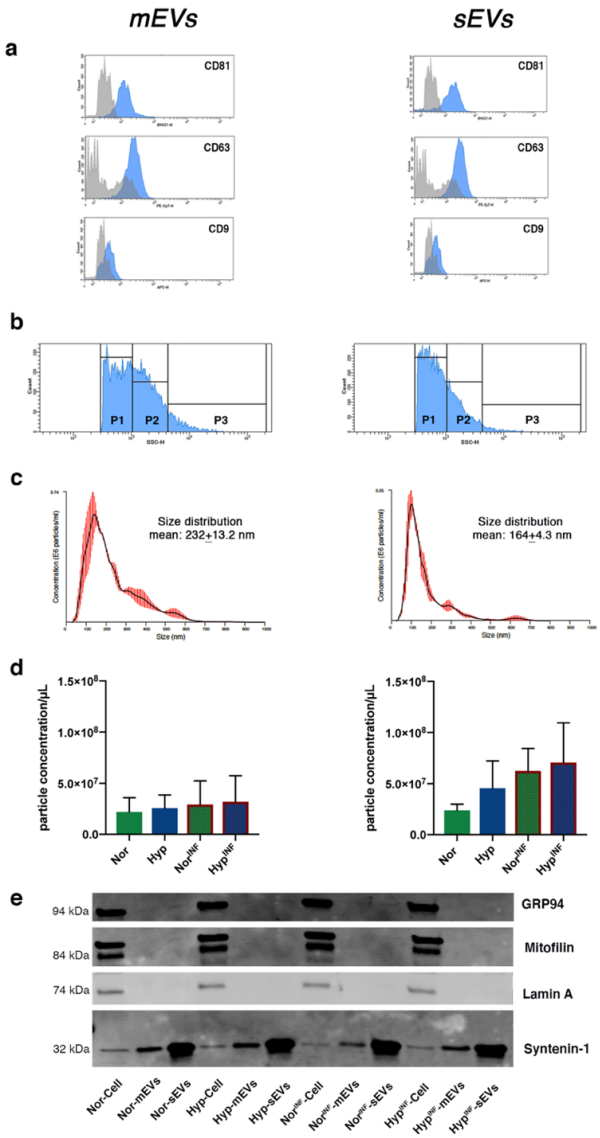

Figure 3.2: Size distribution and particle concentration of EV subtypes. (a) Flow cytometry analysis of MSC-derived mEVs (left panels) and sEVs (right panels). The areas under the blue lines identify vesicles reacting with CD81, CD63, and CD9. The areas under the gray lines indicate the interactions of vesicles with corresponding nonreactive immunoglobulin of the same isotype. **(b)** Using the reference of a mixture of fluorescent beads of varying diameters, three different sub-gates can be visualized within CFSE-positive events (P1: ≤100 nm, P2: from 100 to 160 nm, P3: from 160 to 900 nm) in a SSC-H histogram. (**c**) Representative histograms showing the calculated mean ± SD of size distribution by NTA analysis of purified mEVs and sEVs. (**d**) Histograms representing the concentration/µL of mEVs and sEVs derived from the 4 preconditioning treatments (Nor, Hyp, Nor^{INF}, Hyp^{INF}). These results are based on three replicates of three independent experiments. (**e**) Western blot analysis of mEVs and sEVs and their corresponding cell lysates derived from the different preconditioning approaches (Nor, Hyp, Nor^{INF} and Hyp^{INF}). While Grp94 and Lamin A presence were observed only in cells and confirmed the non-contamination of EVs with cellular components, syntenin was mostly present mEVs and sEVs as a cytosolic EV marker. A large EV marker, Mitofilin, was expressed only in cells but it was absent in both mEVs and sEVs.

It's well known that EVs of different sizes and intracellular origins have different functional properties [94,102]. For this reason, we analyzed separately the vesicles retrieved from the 10K (enriched in mEVs) and from the 100K pellet (enriched in sEVs). To evaluate whether mEVs and sEVs were successfully purified from Nor-CM, Hyp-CM, Nor^{INF}-CM, and Hyp^{INF}-CM, an already described non-conventional flow cytometry analysis [95] was performed. Both mEVs and sEVs were stained with the cell-permeant, fluorescein-based CFDA-SE tracer that is useful to discriminate intact vesicles from debris and membrane fragments, together with a mixture of fluorescent beads of known varying diameters (Supplementary Fig. 3.3a and 3.3b). Since CFDA-SE is able to passively diffuse within vesicles and interact with intra-vesicular enzymes at room temperature (RT) (Supplementary Fig. 3.3a and 3.3b, right panels), we ensured that at 4°C the cloud of particles was under the level of the dimensional gate in the FL1 intensity channel (Supplementary Fig. 3.3a and 3.3b, left panels). After an accurate titration of antibodies and the use of related isotype controls [95], the expression of the typical vesicular markers CD81, CD63, CD9 belonging to the tetraspanin family was evaluated in mEVs and sEVs (Fig. 3.2a). Both types of vesicles expressed at different extent the three tetraspanin markers, and CD81 was the more expressed cell surface antigen in both types of MSC-derived vesicles (Fig. 3.2a). The diverse preconditioning strategies did not induce statistically significant differences between the two EV subpopulations (Supplementary Fig. 3.3c). In order to evaluate whether the material pelleted at 10K was actually enriched in mEVs compared to the 100K-retrieved material, we took advantage of the use of the above mentioned fluorescent dimensional beads (Supplementary Fig. 3.3a and 3.3b). Beads allowed to define the percentage of vesicles falling within the dimensional gate and with diameters: i) smaller than 100 nm, ii) ranging from 100 to 160 nm, and iii) from 160 to 900 nm (Fig. 3.2b). Our data indicate that the percentage of sEVs with a diameter smaller than 100 nm was significantly higher than the corresponding mEVs in the 4 different culture conditions (Table 3.1). On the contrary, the percentage of vesicles with diameters ranging from 100 to 160 nm was significantly higher in the material pelleted at 10K if compared to the 100K counterparts in all the conditions (Table 3.1). No main differences were observed in the few vesicles ranging from 160 to 900 nm. Only in the Hyp^{INF} condition, the percentage of mEVs bigger than 160 nm was significantly higher than the corresponding sEVs (Table 3.1).

Table 3.1: Flow cytometry analysis revealing the average size of both mEVs and sEVs. Statistical analysis was performed with unpaired Student's t test, considering EVs derived from three independent MSC primary cultures for each condition.

	Size Distribution	mEVS (%) (AVG ± SD)	sEVS (%) (AVG ± SD)	P value (unpaired t test)
Hyp	≤100 nm	65.45 ± 0.5710	73.27 ± 2.414	0.0344 (*)
	100-160 nm	34.54 ± 0.5710	23.38 ± 1.436	0.0020 (**)
	160-900 nm	6.213 ± 0.7044	3.143 ± 0.8827	0.0531 (ns)
Nor	≤100 nm	64.42 ± 0.7436	72.40 ± 1.524	0.0093 (**)
	100-160 nm	35.57 ± 0.7436	27.59 ± 1.524	0.0093 (**)
	160-900 nm	6.227 ± 0.7774	3.697 ± 0.6550	0.0676 (ns)
Hyp^{INF}	≤100 nm	59.11 ± 2.042	74.95 ± 2.920	0.0189 (*)
	100-160 nm	40.88 ± 2.042	25.04 ± 2.920	0.0189 (*)
	160-900 nm	7,913 ± 0,2872	2,900 ± 0,5500	0.0028 (**)
Nor^{INF}	≤100 nm	62,42 ± 0,8818	69,23 ± 1,606	0.0205 (*)
	100-160 nm	37,57 ± 0,8818	31,43 ± 2,235	0.0628 (ns)
	160-900 nm	6,997 ± 1,063	4,620 ± 0,5420	0.1172 (ns)

Nanoparticle tracking analysis (NTA) confirmed the higher representation of medium vesicles in the 10K pellet, resulting in a mean size of 225±31 nm for the 10K pellet, and 170±12 nm for the 100K pellet (p=0.0162). Figure 3.2c shows a representative NTA analysis of m- and sEVs separated from one of the three considered MSC primary cultures stimulated in normoxia. NTA showed that the concentration of mEVs and sEVs released by the same amount of MSCs did not vary significantly among the 4 different culture conditions (Fig. 3.2d). NTA analysis has been also performed on DM samples and their corresponding total CM. As indicated in Supplementary Figure 3.3d, the percentage of total particles in DM derived from the different preconditioning strategies was significantly decreased if compared to their corresponding CM, ensuring a low interference of EVs in the later experiments. FACS and NTA analysis revealed that the EV separation procedure here adopted possessed an intermediate specificity, as already stated in the MISEV 2018 guidelines [103], and the EV sub-fractions largely overlapped.

A western blot analysis has been performed on both mEVs and sEVs as well as on their corresponding cell lysates, derived from the different preconditioning approaches (Nor, Hyp, Nor^{INF}, and Hyp^{INF}) (Fig. 3.2e). We have selected Grp94 (HSP90B1) and Lamin A as proteins associated with other intracellular compartments than plasma membrane/endosomes [103]. These proteins were highly expressed by the cell lysates derived from the different preconditioning strategies, and, more importantly, they were not expressed by corresponding mEVs and sEVs, indicating that our vesicle subpopulations were not contaminated by cells. We have also evaluated the expression of Syntenin, a cytosolic protein expressed by EVs, and in particular by sEVs, as previously indicated [94,103]. We have also checked for the expression of Mitofilin, a protein anchored in the inner mitochondrial membrane, described to be expressed by large and medium-sized EVs released by dendritic cells and some tumor cell lines [94]. Mitofilin was not expressed in our MSC-derived EV subpopulations, and this could be potentially due to the different cell source (as pointed out also in the MISEV2018 paper, there could be some differences in some marker expressions due to the different cells of origin) and to the fact that we did not consider larger vesicles (2K) in our study. Taken together, these results indicate that human adipose tissue-derived MSCs release a large range of EVs, which can be partially separated by their pelleting properties.

3.3.3 EVs are less sensitive than soluble proteins to the environmental variations in the context of angiogenesis

The control of blood vessel growth plays a key role to restore blood supply and ensure rapid vascularization of damaged tissues [84]. To evaluate how an injured environment, here mimicked by low oxygen tension and pro-inflammatory cytokines, influences the angiogenic potential of the different MSC secretome fractions, we took in consideration different aspects of the angiogenic process: endothelial cell proliferation, migration and tubulogenesis. In order to comparatively assess the biological activity of the whole MSC secretome over the fractions within it, namely EVs and soluble factors, a known amount (in terms of protein μg) of total CM was administered according to the number of target endothelial cells in a 1:1 (cell to cell) ratio. Target cells were also stimulated by the corresponding amounts of DM, mEVs and sEVs. Firstly, the effect of the preconditioned MSC-derived secretome fractions on human umbilical vein endothelial cell (HUVEC) proliferation was investigated. CM derived from MSCs stimulated by TNF-α and IL-1α in hypoxic condition (Hyp^{INF}-CM) significantly down-regulated the proliferative capacity of responder cells when compared to its non-

inflamed counterpart (Hyp^{INF}-CM vs Hyp-CM, p≤0.001) (Fig. 3.3a). A similar result was obtained comparing the Hyp^{INF}-DM fraction with Hyp-DM (p≤0.01), suggesting that the soluble factors released by MSCs in a hypoxic-inflamed environment inhibit the proliferation of endothelial cells (Fig. 3.3a). Even if BrdU incorporation by HUVECs was consistently lower in the presence of both Hyp-mEVs and Hyp-sEVs compared to the total Hyp-CM (p≤0.01 and p≤0.05, respectively), the addition of inflammatory factors in hypoxia did not affect the function of the EV fractions (Fig. 3.3a). On the other hand, under normoxia, only total CM were negatively affected by the addition of inflammatory stimuli, inducing a significant decrease of HUVEC proliferation (Nor-CM vs Nor^{INF}-CM, p≤0.01), without inducing major differences in DM, mEVs and sEVs (Fig. 3.3b). No significant differences were observed when HUVECs were incubated with the secretome fractions derived from Hyp^{INF} and Nor^{INF} conditions compared to the control medium containing TNF-α and IL-1α (only INF control condition) (Fig. 3.3a and 3.3b).

Since endothelial cells migrate along chemo-attractants secreted in the microenvironment, we used a transwell migration assay to create the chemical gradient by putting secretome fractions in the lower chamber. Even if Hyp-CM and -DM induced a strong HUVEC migration compared to Nor-CM and -DM (p≤0.0001 and p≤0.001, respectively) (Supplementary Fig. 3.3f), none of the hypoxic secretome fractions prevailed in inducing HUVEC migration (Supplementary Fig. 3.3f). Similarly, to the effects observed in the proliferation assay, MSCs activated by the inflammatory cytokines in hypoxic condition produced a total CM and DM that negatively affected the migratory capacity of HUVECs compared to their corresponding non-inflamed counterparts (Hyp-CM vs Hyp^{INF}-CM, p≤0.0001; Hyp-DM vs Hyp^{INF}-DM, p≤0.01) (Fig. 3.3c). The presence of the inflammatory mediators did not affect the migratory capacity induced by the hypoxic EV fractions (Fig. 3.3c). In normoxia, the EV fractions, and in particular sEVs, are the main components responsible for the generation of a gradient to which HUVECs migrate (Nor-DM vs Nor-sEVs, p≤ 0.001) (Fig. 3.3d), but in this case the addition of inflammation did not significantly alter neither the capacity of the total CM nor the ability of DM and mEVs to induce HUVEC migration (Fig. 3.3d). Only sEVs effect was significantly down regulated (Nor-sEVs vs Nor^{INF}-sEVs, p≤0.01). The presence of TNF-α and IL-1α in control medium (only INF control group) did not exert any significant migratory effect on HUVEC (Fig. 3.3c and 3.3d).

Assays that simulate the formation of capillary-like tubules are regarded as representative of the later stages of angiogenesis. A tube formation assay was used as a quick high-throughput screen to evaluate

the role of the secretome fractions on this specific aspect of the angiogenic process. The quantitative analysis of total branch numbers showed that under hypoxia, MSCs released secretomes that induced the formation of vessel like structures (Fig. 3.3e and 3.3f). Interestingly, inflammatory mediators added to hypoxia exerted a significant inhibitory effect on the capacity of total CM and related secretome fractions to induce the formation of tube-like structures by HUVECs (Hyp-CM vs Hyp^{INF}-CM, $p \leq 0.01$; Hyp-DM vs Hyp^{INF}-DM, $p \leq 0.05$; Hyp-mEVs vs Hyp^{INF}-mEVs, $p \leq 0.01$; Hyp-sEVs vs Hyp^{INF}-sEVs, $p \leq 0.0001$) (Fig. 3.3e and 3.3f). A similar trend was observed in the normoxic counterparts, even if a significant difference was observed only when considering the mEVs fraction (Nor-mEVs vs Nor^{INF}-mEVs, $p \leq 0.01$) (Fig. 3.3g). Taken together, these results indicate that the synergistic action of hypoxia and inflammation affects the MSC secretome fractions to different extents. The ability of soluble factors to induce HUVEC proliferation, migration and differentiation is significantly impaired. On the contrary, the ability of the EV fractions to induce endothelial cell proliferation and migration is not affected, while the capacity of promoting the formation of tube-like structures is significantly impaired.

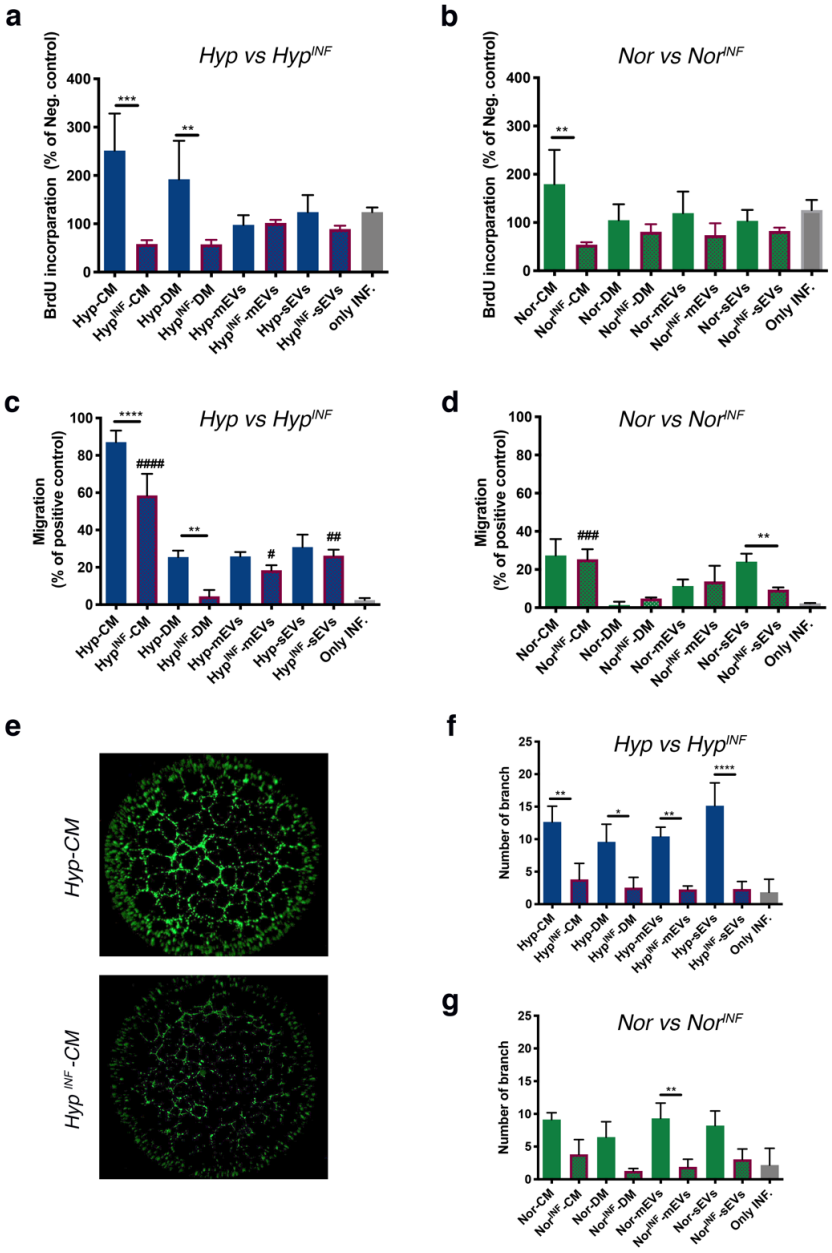

Figure 3.3: The effect of MSC secretome fractions on proliferation, migration and tube formation capacity of HUVECs. (a, b) Proliferation was determined with BrdU incorporation assay. (**c, d**) Cell migration was determined by transwell migration assay. (**e**) Representative images of Calcein AM staining of HUVECs at 7th hour on GFR-Matrigel. (**f, g**) Quantitative analysis of number of branches in tube formation assay. Error bars in the graphs represent mean ± SD. N=3, (*) presents the statistical differences between the groups, while (#) presents the difference from the control "only-INF" experimental group. **** p<0.0001, *** p<0.001, ** p <0.01, * p <0.05, $^{\#\#\#\#}$p<0.0001, $^{\#\#\#}$p<0.001, $^{\#\#}$p<0.01, $^{\#}$p<0.05 (one-way ANOVA and Tukey multiple comparison).

To confirm the *in vitro* results, the mouse fetal metatarsal sprouting assay was selected, since it provides an exceptional tool for studying angiogenesis [96]. In comparison with other commonly used *in vitro* or *ex vivo* angiogenesis assays, vessel outgrowth from mouse fetal metatarsals is more representative of sprouting angiogenesis *in vivo*. It allows the analysis of blood vessel growth with CD31 staining and the mechanisms underpinning this process, in a multicellular microenvironment that drives the formation of a robust and complex vascular network (Fig. 3.4a). The soluble factors released by MSCs stimulated with hypoxia and inflammation inhibited significantly the sprouting of CD31+ vessels, if compared to the hypoxic counterparts (Hyp-CM vs Hyp^{INF}-CM, $p \leq 0.001$; Hyp-DM vs Hyp^{INF}-DM, $p \leq 0.05$) (Fig. 3.4b and 3.4c). The vessel sprouting induced by EV fractions, and in particular by sEVs, were not affected by the inhibitory effect given by the synergistic action of hypoxia and inflammation, but rather they induced a significant increase in vessel sprouting compared to their corresponding soluble factors (Hyp^{INF}-DM vs Hyp^{INF}-sEVs, $p \leq 0.01$) (Fig. 3.4c). In normoxia, the addition of inflammatory cytokines negatively affected only the total CM (Nor-CM vs Nor^{INF}-CM, $p \leq 0.01$), while the effects exerted by the secretome fractions were not significantly affected (Fig. 3.4d). In this assay, the inflammatory cytokines in the control medium (only-INF group) induced a significant increase in vessel density if compared to Hyp^{INF}-CM and Hyp^{INF}-DM ($p \leq 0.01$ and $p \leq 0.05$, respectively) (Fig. 3.4c), as well as to Nor^{INF}-CM and Nor^{INF}-DM ($p \leq 0.05$ and $p \leq 0.01$, respectively) (Fig. 3.4d), suggesting that inflammation-activated MSCs release soluble factors that counteract the angiogenic capacity induced by TNF-α and IL-1α.

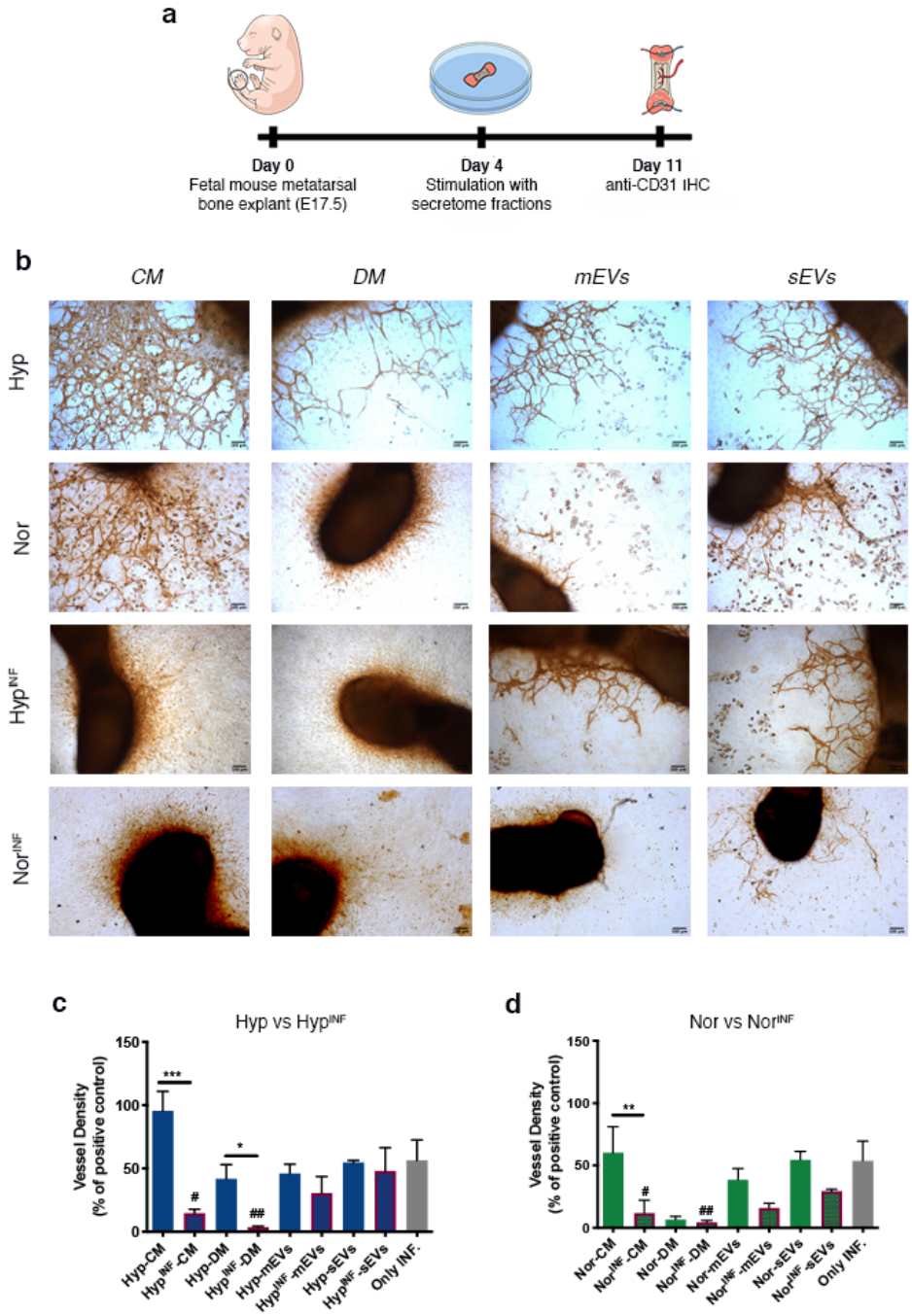

Figure 3.4: Ex vivo metatarsal sprouting assay. (a) Schematic diagram of the experimental plan, illustrating the timeline of the isolation of metatarsals, secretome stimulation and anti-CD31 staining. (**b**) Representative image of CD31+ vessel structures, scale bar:100 µm. (**c, d**) Quantitative analysis of vessel density, CD31-positive cells were considered for the analysis. Error bars in the graphs represent mean ± SD. N=3, (*) presents the statistical differences between the groups, while (#) presents the difference from the control "only-INF" experimental group. **** p<0.0001, *** p<0.001, ** p <0.01, * p <0.05, $^{\#\#}$p<0.01, $^{\#}$p<0.05 (one-way ANOVA and Tukey multiple comparison).

3.3.4 The soluble factors released by inflammation-activated MSCs possess a distinctive secretome profile

The *in vitro* and *ex vivo* analysis above described indicated that inflammation-activated MSCs secreted proteins that inhibited angiogenesis if compared to their non-stimulated counterparts.

To define the profile of the soluble mediators secreted by MSCs, we examined and compared the CM derived from cells stimulated in Nor, Hyp, Nor^{INF} and Hyp^{INF} conditions using a human protein cytokine array. Donor origin of the samples explained most of the variance in the dataset. In order to understand how preconditioning strategies drive the principal components (PC) of the analyzed dataset in the principal component analysis (PCA) and provide the overall structure of the effect of inflammation and hypoxia, donor effect was evaluated and removed with the limma package of R [97] and data distribution has been evaluated (Supplementary Fig. 3.4a and 3.4b).

Based on the amount of secreted proteins, samples that underwent inflammation can be clearly separated from the non-inflamed ones along the first component (PC1) of the PCA, which explained 43.5% of the variance (Fig. 3.5a and 3.5b).

When we analyzed the effects of inflammation, regardless of the oxygen levels, we observed a significant up-regulation in the expression of proteins, such as: i) Granulocyte-Macrophage Colony-Stimulating Factor (GM-CSF) and Monocyte Chemoattractant Protein-1 (MCP-1), involved not only in the recruitment of monocytes/macrophages, but also whose presence is of basic importance in the repair process[104,105]; ii) Heparin-Binding Epidermal growth factor–like Growth Factor (HB-EGF), whose level increases in response to different forms of injuries as well as stimuli, acting as a critical mediator of tissue repair and regeneration[106]; iii) Matrix Metalloproteinase-8 and -9, enzymes implicated in the degradation of most of the extracellular matrix components and therefore actively involved in tissue remodeling associated with pathological situations such as acute injury[107] (Fig. 3.5e). The contribution of each protein to the different components of the PCA further confirmed that the above-mentioned proteins (MMPs, MCP-1, GM-CSF, etc..) were among the main positive drivers of PC1 (Fig. 3.5c). On the other hand, when a similar bioinformatic approach was performed to evidence the effects of hypoxia, regardless of inflammation, the most characterizing and significantly expressed proteins were: i) Endoglin, an auxillary TGF-beta receptor that modulates TGF-beta 1 and beta 3 responses and plays a role in vascular development, angiogenesis and vascular remodeling[108]; ii) Hepatocyte Growth Factor (HGF), a pro-angiogenic factor that exert a striking effect on endothelial cell migration, therefore playing a crucial role in recruiting endothelial cells *in vivo* for the formation

of new blood vessels[109]; iii) Vascular Endothelial Growth Factor (VEGF), a well known signal protein that stimulates the formation of blood vessels[110]; Urokinase-type Plasminogen Activator (uPA), described to be involved in endothelial cell proliferation, migration and tubule formation [111] (Fig 3.5e). Regarding the PCA, samples that underwent hypoxic treatment could separate from the normoxic ones mainly along the second component, which explained 16.7% of the variance (Fig. 3.5d). uPA, VEGF, and Endoglin were also important contributors of PC2 (Fig. 3.5d). Of note, although some proteins, such as DPPIV and Coagulation Factor 3, were main drivers of PC2, they were not differentially expressed due to oxygen levels from the statistical point of view. This is due to the fact that PC1 also explained a small part of the variance between hypoxic and normoxic observations, as shown by the spread of the samples in the PCs space (Fig. 3.5a and 3.5d). The proteins majorly contributing to PC1 and PC2 were also expressed by the corresponding DM derived from the different preconditioning strategies (Supplementary Fig. 3.4c).

Taken together, these results indicate that there is a set of soluble mediators generated by MSCs in a milieu-specific manner, responding to the requirements of the environment.

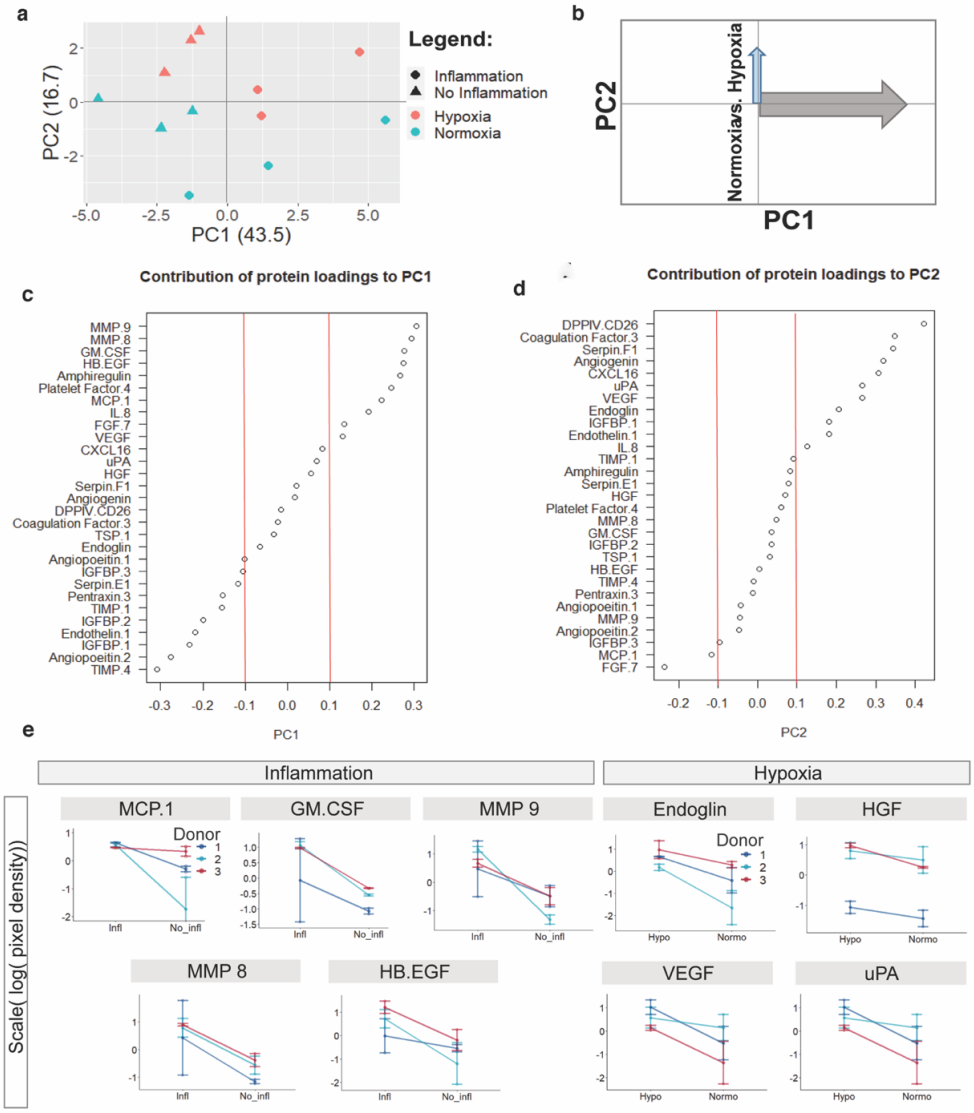

Figure 3.5: Treatment conditions are successfully separated by singular value decomposition and trigger changes in protein expressions. (a) Samples are separated in the principal component analysis with PC1 and PC2 explaining 43.5% and 16.7% of the variance, respectively. (**b**) Schematic summary: based on the response loadings, PC1 is mainly driven by the inflammatory status while PC2 can be defined by the oxygen influence. (**c, d**) Visualization of proteins associated with reduction components and ordered from the most negative contribution to the most positive contribution to PC1 and PC2, respectively. Red dashed lines are arbitrary thresholds (±0.1) set to visualize most important protein contributions. (**e**) Most of the proteins had significantly different levels between donors. Log10 transformed and normalized pixel densities for each protein are represented as a proxy of protein expression on the y-axis. Average and standard error are calculated between normoxia and hypoxia in inflammation (INF) versus conditions without inflammation (No-INF), for each donor. The expression of five proteins was significantly increased (MMP-9: p= 0.005, MMP-8: p= 0.01, GM-CSF: p =0.012, HB-EGF=0.018, MCP-1: p=0.04) for the inflammation influence regardless of oxygen levels in MANOVA. The expression of four proteins was significantly increased (Endoglin: p= 0.009, HGF: p=0.039, VEGF: p=0.031, uPA: p=0.043). for the oxygen level influence regardless of the inflammatory status in MANOVA. Only proteins with p<0.05 are reported.

3.3.5 The microRNA (miRNA) landscape of MSC-derived EVs is not majorly affected by cell preconditioning

Small RNAs within EVs are thought to be major contributors to the molecular events occurring in the recipient cell [112]. We evaluated whether the adopted preconditioning strategies had affected the RNA cargo within both mEVs and sEVs. Capillary electrophoresis profiling on vesicular RNA revealed distinctive peaks around 20 and 70 nucleotides, suggestive of the presence of miRNAs and tRNAs (Supplementary Fig. 3.5a). To better define and compare the small RNA composition of the differently preconditioned MSC-derived EV fractions, we performed RNA sequencing of vesicular RNA. The sequencing yielded a total of 192 million reads, and the technical consistency was validated measuring the correlation between technical replicates, which proved to be higher than the one of biological replicates (Supplementary Fig. 3.5c). The levels of the most variable miRNAs across all samples were used to perform a hierarchical clustering. The two generated main clusters nicely separate mEV and sEV subfractions with only few exceptions (Supplementary Fig. 3.5b).

Cargo RNAs of both mEVs and sEVs include various biotypes that represent a selected portion of the RNA content of the source cell. Indeed, the libraries of both EV fractions were highly enriched in the classes of: i) rRNAs (46.5% in mEVs and 43.5% in sEVs), tRNAs (11.0% in mEVs and 20.1% in sEVs) and mRNAs (1.1% in mEVs and 0.7% in sEVs), that can be considered as possible non-functional degradation products; ii) miRNAs (7.7% in mEVs and 11.7% in sEVs), that have been established to be functional when carried by EVs between cells; iii) piRNAs (1.4% in mEVs and 2.2% in sEVs), that are predicted to be functional but have not been definitively demonstrated to mediate intercellular communication [113] (Fig. 3.6a). Although miRNAs represent a small fraction of all RNA species found in EVs (Fig. 3.6a), an exponentially growing number of new reports indicate that a great part of the EV effects can be attributed to their miRNA content [114–116]. Interestingly, the relative distribution of miRNA species was uneven, with few miRNAs extremely more enriched than others. In particular, 65.5% and 71% of total miRNA reads in mEVs and sEVs respectively was accounted by only 15 highly enriched miRNA species (Fig. 3.6b, 3.6c and Supplementary Fig. 3.6). We therefore focused on the 15 top enriched miRNAs characterizing both m- and sEVs from each culture condition (Nor, Hyp, Nor^{INF} and Hyp^{INF}), unexpectedly identifying a group of only 18 miRNAs. Indeed, 13 out of 18 miRNAs are shared by all the considered experimental groups, indicating that their prevalence is independent of cell preconditioning and EV sub-fractioning (Fig. 3.6d). We also observed that let-7a-

5p and miR-26a-5p are shared by mEVs, while miR-125a-5p is shared by sEVs, suggesting a possible role in discriminating the two MSC-derived EV subsets (Fig. 3.6d).

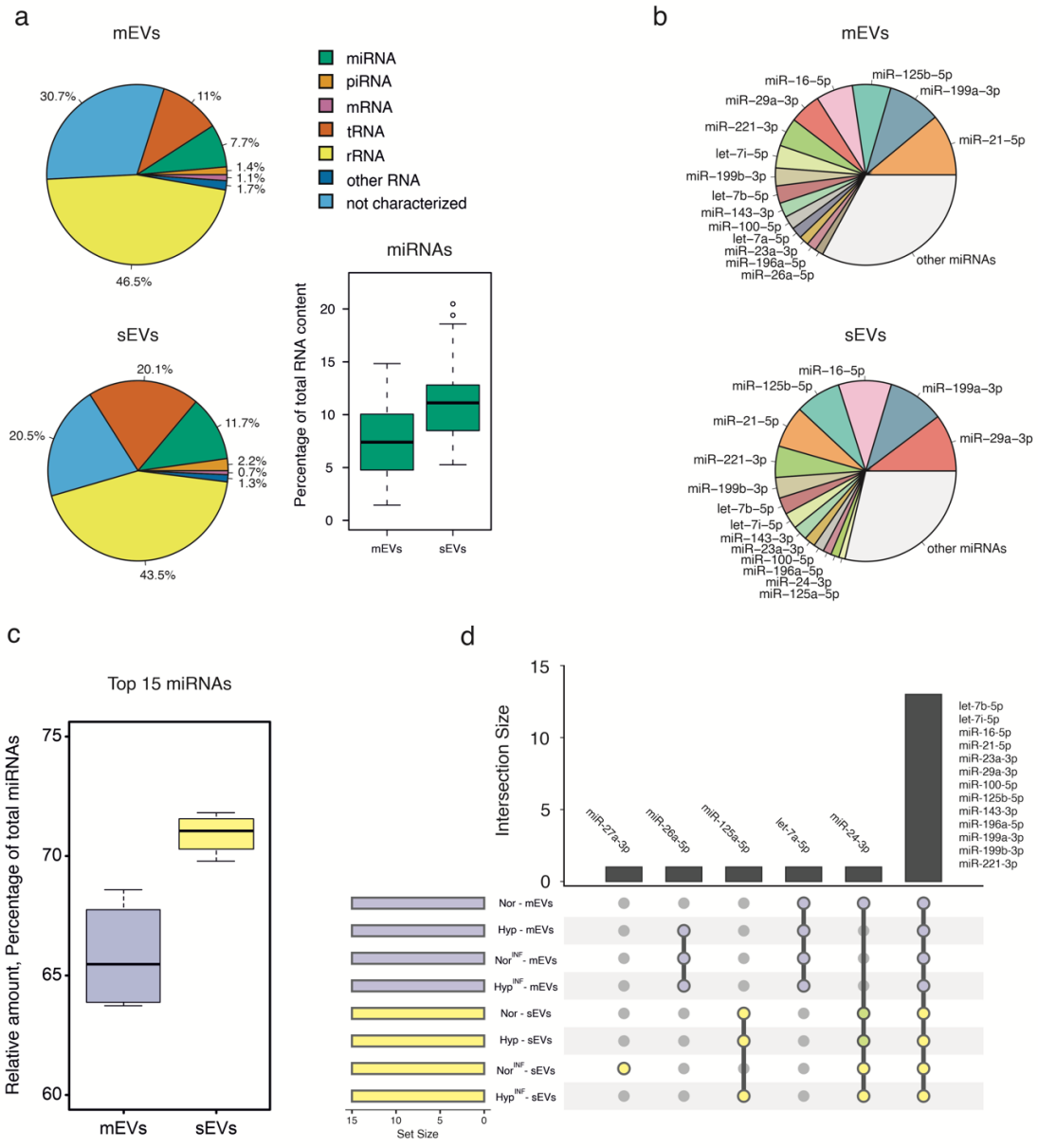

Figure 3.6: Few enriched miRNAs cover the majority of EV miRNA content and are shared by different treatment conditions. (a) Relative distribution of retrieved RNA types in mEVs and sEVs. Slices of piecharts represent average values. Boxplot shows the distribution of miRNA percentages in all the samples. (**b**) Relative distribution of miRNA species in mEVs and sEVs. Colored slices of piecharts represent the amount of the 15 most enriched miRNAs in the samples. (**c**) Percentage of total miRNA content covered in each sample by its 15 most enriched miRNA species. (**d**) Upset plot shows miRNA species which are enriched regardless of treatment conditions and EV sub-fractioning.

We asked wether a global miRNome analysis could unveil any modulation of miRNA signatures, likely belonging to the lowly enriched ones. Most of the differences were observed comparing mEVs derived from differently conditioned MSCs, while sEVs presented few differentially enriched miRNAs (Fig. 3.7a). Of note, the differentially enriched (DE) miRNAs didn't correspond to the top expressed ones (Supplementary Fig. 3.7). Addition of inflammatory stimuli, regardless of oxygen level, induced a characteristic signature in both m- and sEVs, when compared to non-inflamed counterparts (Supplementary Fig. 3.7). The most significant outlier miRNA present in both EV subtypes upon inflammation and hypoxia is miR-146a-5p, described to modulate the expression of pro-inflammatory genes, thus reducing or delaying inflammation and enhancing wound healing[117,118] (Supplementary Fig. 3.7). Given the lower number of DE miRNAs in sEVs, we hypothesized that their miRNA composition could be more homogeneous than mEVs among the culture conditions. To test this hypothesis, we evaluated whether the lower amount of DE miRNAs was due to lower inter-class heterogeneity or higher intra-class heterogeneity (noise). No significant differences in terms of intra-class heterogeneity were observed between sEVs and mEVs, while the inter-class heterogeneity was significantly lower among sEV classes (Fig. 3.7b). Consistently, correlation analysis provided further evidence that sEVs miRNome is globally less affected by environmental changes than the one of mEVs (Fig. 3.7c).

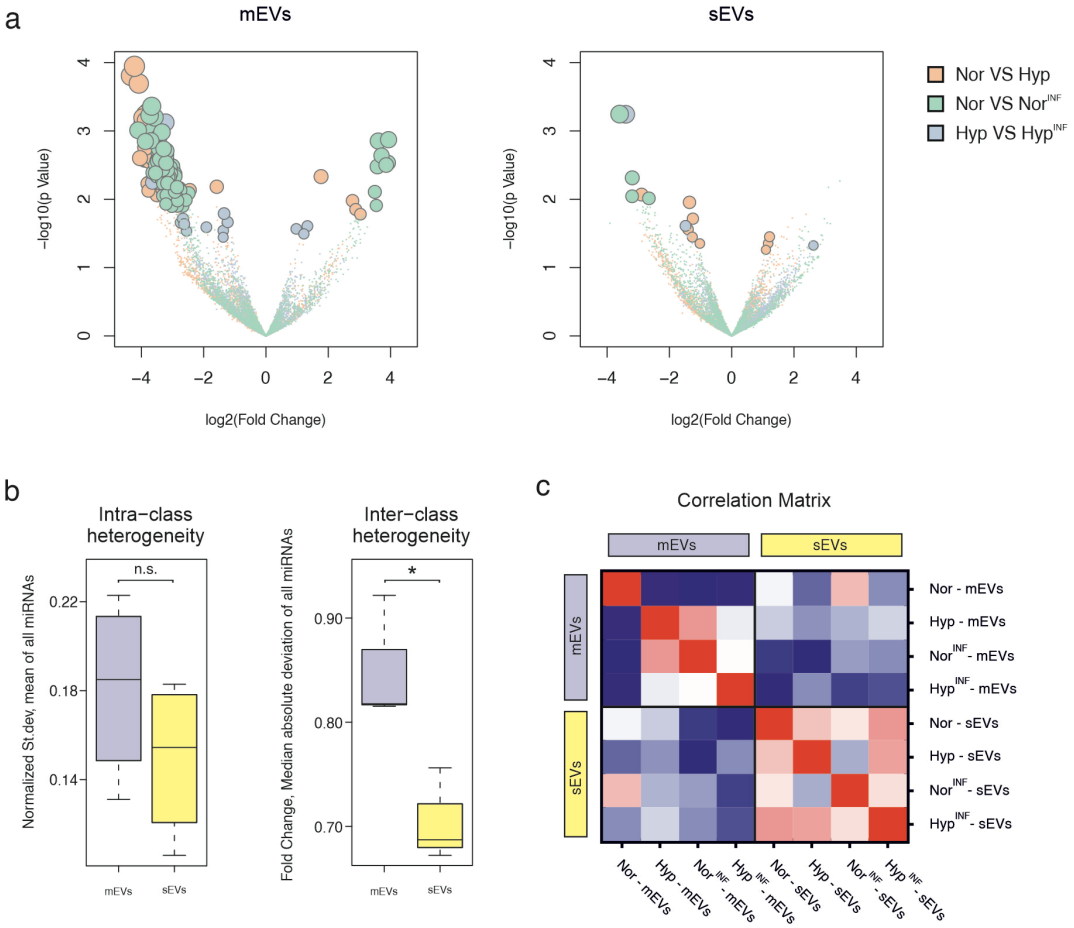

Figure 3.7: Differential expression analysis reveals sEVs are more homogeneous than mEVs in miRNA content. (a) Volcano plots show miRNAs enriched in EVs derived from differently treated cells. (**b**) Boxplots compare the intra-class and inter-class heterogeneity estimators of mEVs and sEVs. (**c**) Correlation matrix of EV groups, based on Spearman correlation of miRNA levels. *p<0.05 (Student's t test).

3.4 Discussion

MSC-sourced secretome consists of soluble and EV-encapsulated components, whose synergistic action is able to reduce cell injury and improve tissue repair capacity [119]. Indeed, cells release heterogeneous vesicles of different sizes and intracellular origins, including small EVs generated in the endosomal compartments (i.e., exosomes) and EVs of various sizes budding from the plasma membrane, generally referred to as microvesicles [120]. A large number of MSC-derived bioactive molecules containing genetic material (DNA, RNA fragments, miRNAs) are enveloped within extracellular vesicles [113]. It has been reported that the composition of the MSC secretome can be regulated by preconditioning strategies during the culture *in vitro*[79]. An appropriate preconditioning

may prepare the cells to release factors that could better respond to the harsh environment present at the site of injury, characterized by strong inflammation and low oxygen supply [121]. Several approaches have been investigated so far, and a variety of different factors has been proven to modulate the MSC therapeutic capacity, including 3D culture [122,123], pharmacological molecules [124,125], inflammatory cytokines [126,127], and hypoxia [79,128]. This study shows for the first time the effects of a simultaneous stimulation with pro-inflammatory cytokines (TNF-α and IL-1α) and hypoxia (1% O_2) on the different components of the MSC secretome. These cytokines were selected being able to induce endothelial cells to express adhesion molecules and chemokines that attract white cells from the blood to the site of injury [129]. Thus, four different culture conditions were considered: the normoxic environment (20% O_2) (Nor) was regarded as the control condition and compared to a hypoxic one (Hyp), with or without the simultaneous stimulation with the inflammatory cytokines (Nor^{INF} and Hyp^{INF}, respectively). We observed that the environmental variations strongly influenced the angiogenic potential of the MSC secretomes. Several literature reports indicate that MSC secretome can exert different effects in the context of angiogenesis, and many of these differences largely depends upon the various culture conditions [85,86]. Although MSCs have historically been reported to be an interesting source of pro-angiogenic factors, recent studies indicate that MSCs can also exert detrimental effects on endothelial cell function. These discrepancies could be ascribed to a multitude of reasons, ranging from the isolation techniques, the species from which MSC populations have originated, the cell source (bone marrow, adipose tissue, umbilical cord), the passage number, and, last but not least, the adopted preconditioning strategy. In particular, the activation of MSCs with inflammatory cytokines have been reported to induce opposite effects in the context of angiogenesis. Adipose tissue-derived MSCs stimulated with 10 ng/mL TNF-α produced a conditioned medium (CM) able to stimulate the homing and engraftment of endothelial progenitors in a hindlimb ischemia mouse model [90]. Moreover, treatments with CM derived from TNF-α preconditioned MSCs have been described to accelerate cutaneous wound healing and angiogenesis *in vivo* [130]. On the contrary, recent literature reports have demonstrated that, once activated by a pro-inflammatory environment (given by a cocktail composed by 25 ng/mL IL1b, 20 ng/mL IL6, 25 ng/mL TNF-α), the total conditioned medium derived from both human and mouse bone marrow-MSCs exerted strong anti-angiogenic effects [91,131]. The same group has recently demonstrated that the extracellular vesicles produced by MSCs activated by the same cocktail of inflammatory cytokines inhibited angiogenesis

targeting both ECM remodeling and endothelial cell migration [92]. Here, we demonstrated that when human adipose tissue-derived MSCs were licensed by hypoxia and by 50 ng/mL TNF-α and 50 ng/mL IL-1α, they produced a total CM that significantly inhibited the proliferation, migration and tubulogenesis of responder endothelial cells, as well as the sprouting capacity of CD31+ cells in an *ex vivo* fetal mouse metatarsal sprouting assay. Surprisingly, when we deeply investigated these effects in the secretome fractions composing the total CM, namely EVs and soluble proteins, interesting differences emerged. Indeed, the pro-angiogenic capacity of the soluble component of the MSC secretome was significantly inhibited, regardless of the oxygen level, if compared to the non-inflamed counterparts. On the contrary, the EV-encapsulated component was not strongly affected by the inflammatory stimuli, suggesting a different capacity of the secretome fractions to sense the environmental variations. When MSCs were licensed by inflammation, they reacted increasing significantly the release of proteins such as GM-CSF, MCP-1, MMP-8, MMP-9, and HB-EGF, involved mainly in the interaction with the innate immune system, as well as in tissue remodeling and repair [132]. MSCs exposed to hypoxia modulated the expression of proteins (Endoglin, HGF, VEGF, and uPA) implicated, to different extents, in the angiogenic process, confirming previously reported data [93,133,134]. A great part of the EV effects is due to their miRNA content [135–137]. Interestingly, miRNA profiling of both medium- and small-EVs released by preconditioned MSCs revealed that the relative distribution of miRNA species was unbalanced, with few (15) miRNAs accounting for almost two-thirds of the total miRNA content. More importantly, the top enriched miRNAs were shared not only by the small and medium vesicles belonging to the same experimental group, but also by the different preconditioning strategies. We also observed that the differentially enriched miRNAs did not correspond to the top expressed ones, and the most significant outlier present in both EV subtypes upon inflammation and hypoxia was miR-146a-5p, described to modulate the expression of pro-inflammatory genes, thus reducing or delaying inflammation and enhance wound healing [117,138].

3.5 Conclusion

In conclusion, this study provides insight into the capacity of the different MSC secretome fractions to respond to the different environmental variations. Our results highlight the importance of not only selecting the appropriate preconditioning strategy to alter properly the release of paracrine factors, but also the relevance of considering separately the effects that such approaches could induce on either the soluble or EV-encapsulated components of the cell secretome. Future studies will need to focus on developing standardize protocols among the scientific community to establish preconditioning regimes useful to enhance the regenerative capacities of MSC therapies.

3.6 Supplementary Information

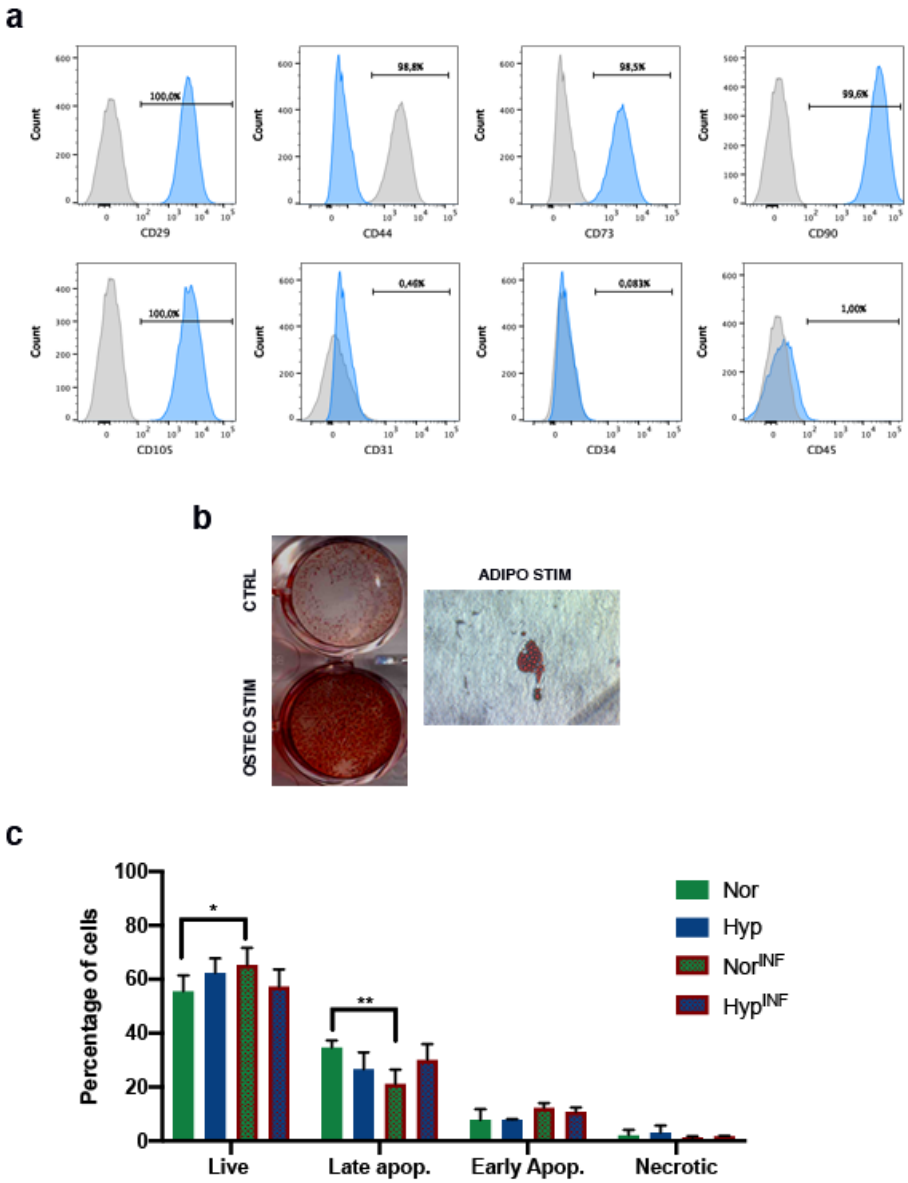

Supplementary Figure 3.1: Characterization of isolated MSCs and cell viability in experimental conditions after serum deprivation. (a) Representative histograms of phenotypic characterization of MSCs following the isolation, cultured in standard medium. CD29, CD44, CD73, CD90, CD105 were selected as markers for mesenchymal lineage, while CD31, CD34 and CD45 were indicating the absence of contaminating cells. (**b**) *In vitro* osteogenic (left panels) and adipogenic (right panel) differentiation potential of MSCs. (**c**) Quantification of Annexin V/PI-stained MSCs exposed to serum deprivation for 24 hours. N=3, **** p<0.0001, *** p<0.001, ** p <0.01, * p <0.05 (two-way ANOVA and Tukey multiple comparison).

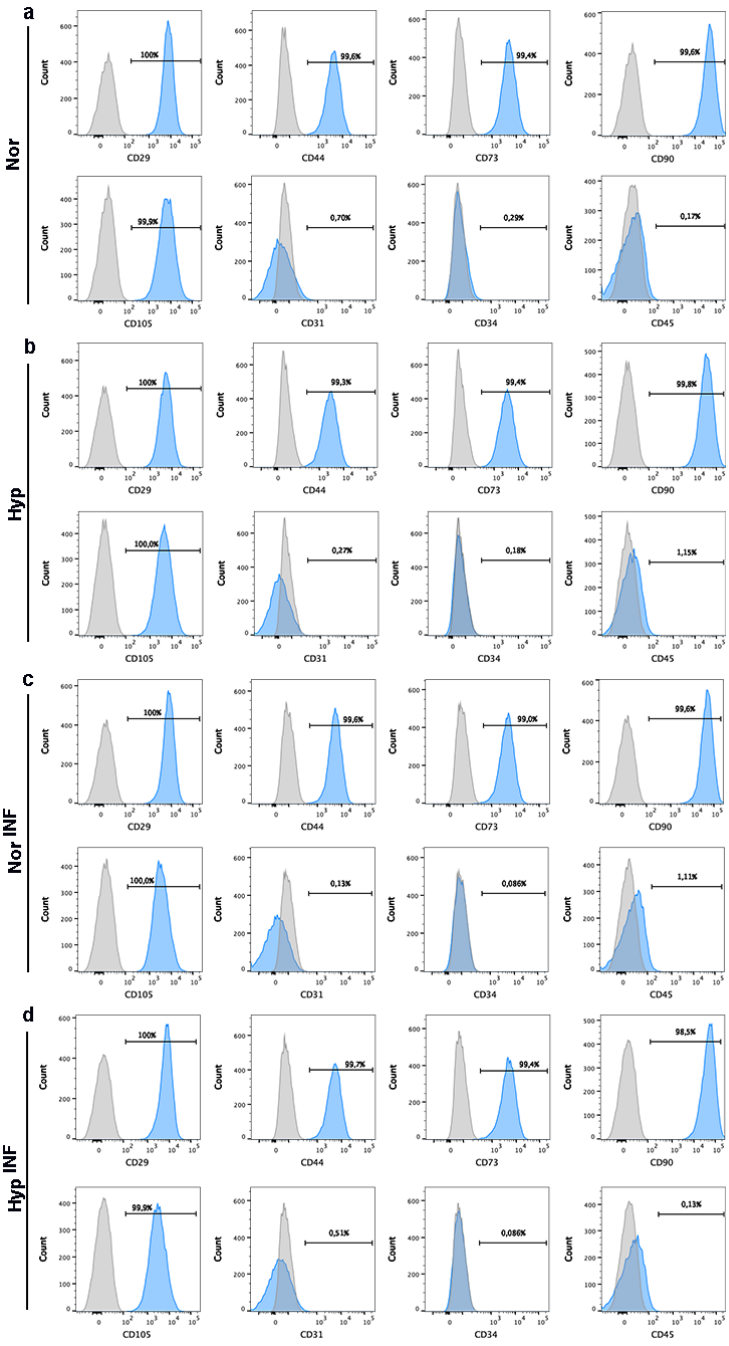

Supplementary Figure 3.2: Phenotypic characterization of preconditioned MSCs. Representative flowcytometry analysis of MSCs exposed to serum deprivation for 24 hours. CD29, CD44, CD73, CD90, CD105 were selected as markers for mesenchymal lineage, while CD31, CD34 and CD45 were indicating the absence of contaminating cells. MSCs were cultured in Hyp (**a**), Nor (**b**), Hyp^{INF} (**c**), and Nor^{INF} (**d**) conditions.

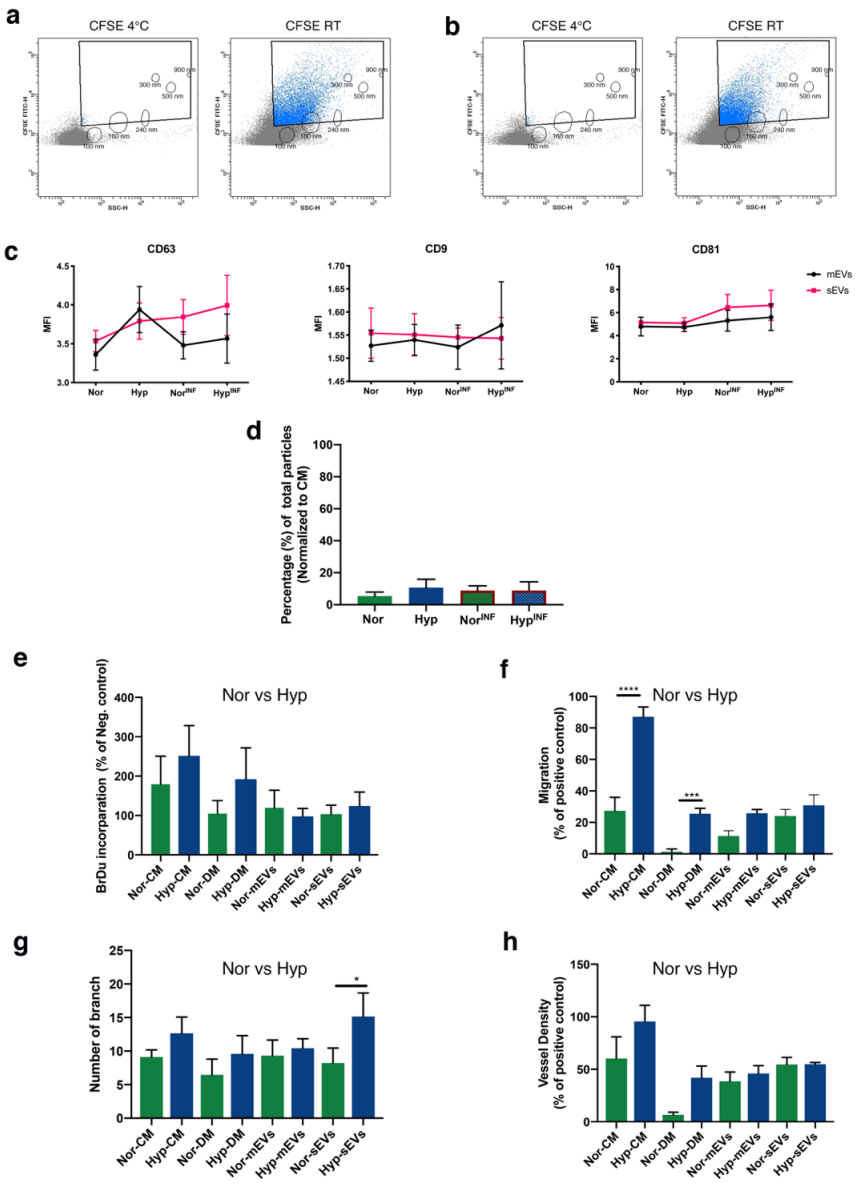

Supplementary Figure 3.3: (**a, b**) Flowcytometry strategy used to characterize mEVs (**a**) and sEVs (**b**). Blue areas identify CFDA-SE positive events. EVs were stained with CFSE at 4°C as "blank tube", useful to define the appropriate dimensional gate when considering EVs stained with CFSE at room temperature. (**c**) Quantification of CD9-, CD63- and CD81-positive events falling within the CFDA-SE gate by mEVs and sEVs. Data are expressed as percentages of positive cells and as ratio between mean fluorescence intensity (MFI) of cells stained with a specific antibody and MFI of correspondent isotype control (relative MFI). **(d)** Histograms representing the percentage of particle numbers in DMs relative to their corresponding CMs derived from the 4 preconditioning treatments (Nor, Hyp, Nor^{INF}, Hyp^{INF}). (**e**) Comparison of normoxic vs hypoxic secretome fractions in HUVEC proliferation, (**f**) HUVEC migration, (**g**) tube formation capacity, and (**h**) metatarsal sprouting assay. Error bars in the graphs represent mean ± SD. N=3, (*) presents the statistical differences between the groups, **** p<0.0001, *** p<0.001, ** p <0.01, * p <0.05. ##p<0.01, #p<0.05 (one-way ANOVA and Tukey multiple comparison).

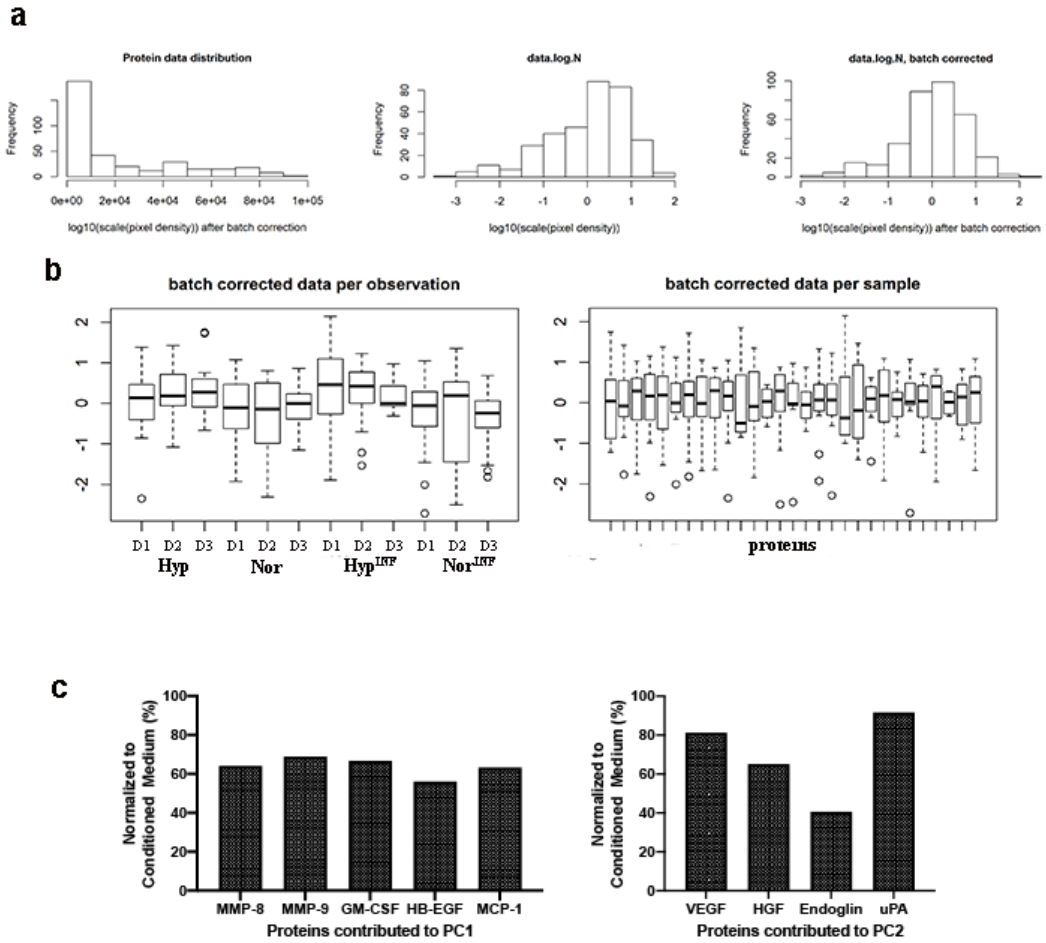

Supplementary Figure 3.4: Proteomic data distribution. (a) Histograms of pixel density frequency across the raw (left panel), standardized and log scaled (data.log.N) (middle panel) or standardize, log scaled and batch corrected (data. log.N batch corrected) (right panel) dataset. **(b)** Boxplot of pixel densities for standardize, log10 scaled and batch corrected data, gathered by observation (distribution of protein expression for a given sample) (left panel) or by protein type (distribution of expression for a given protein across all samples) (right panel). (**c**) Histograms refer to the Depleted Media (DM) expression of those proteins that are significantly expressed in the corresponding total conditioned media (CM) along the first component (PC1) (left panel) and second component (PC2) (right panel) of the Principal Component Analysis. Data are presented as percentages normalized to the corresponding CM.

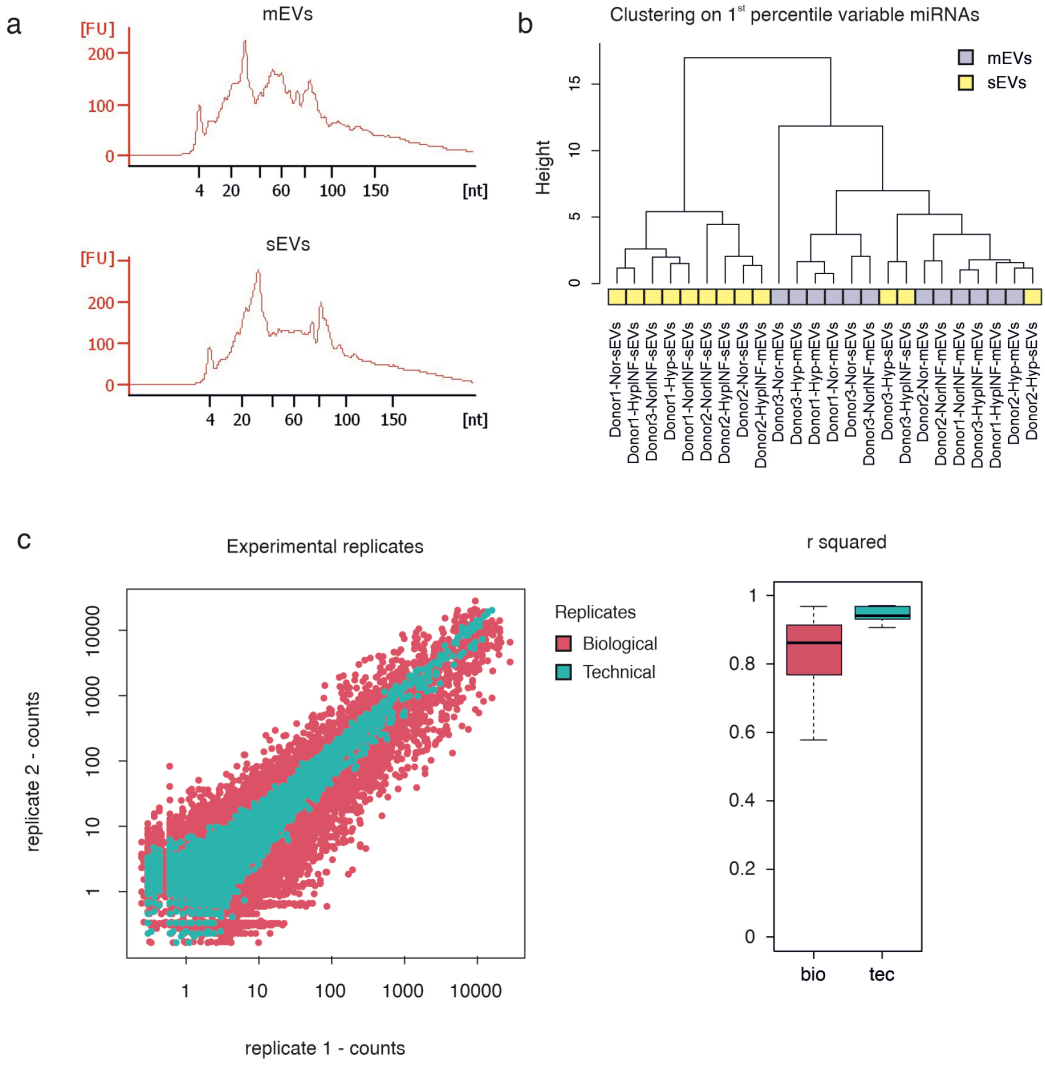

Supplementary Figure 3.5: miRNAseq quality control. (a) Representative electropherograms of mEVs and sEVs small RNA used in the RNAseq library production. (**b**) Unsupervised clustering analysis. Levels of the most variable miRNAs across all samples were used to perform a hierarchical clustering. The two generated main clusters separate mEV and sEV subfractions. **(c)** Analysis of correlation between technical replicates, and comparison with correlation of biological replicates. Scatterplot coordinates show miRNA counts correlation in all the replicates couples. Boxplot shows the higher correlation of technical over biological replicates (r squared of 0.94 and 0.84 respectively).

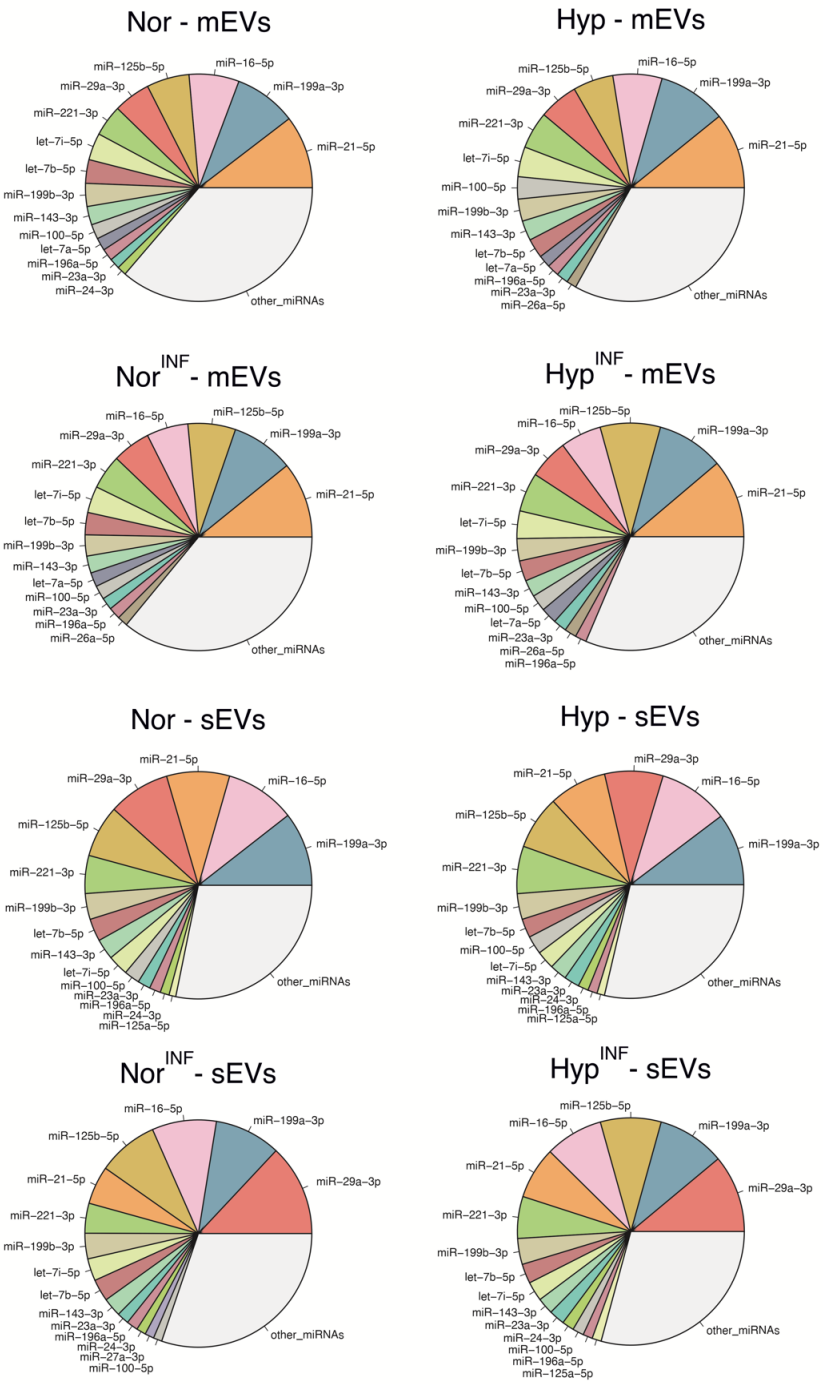

Supplementary Figure 3.6: Relative distribution of miRNA species in all different culture conditions and EVs subfractions. Colored slices of pie-charts represent the amount of the 15 most enriched miRNAs in each group.

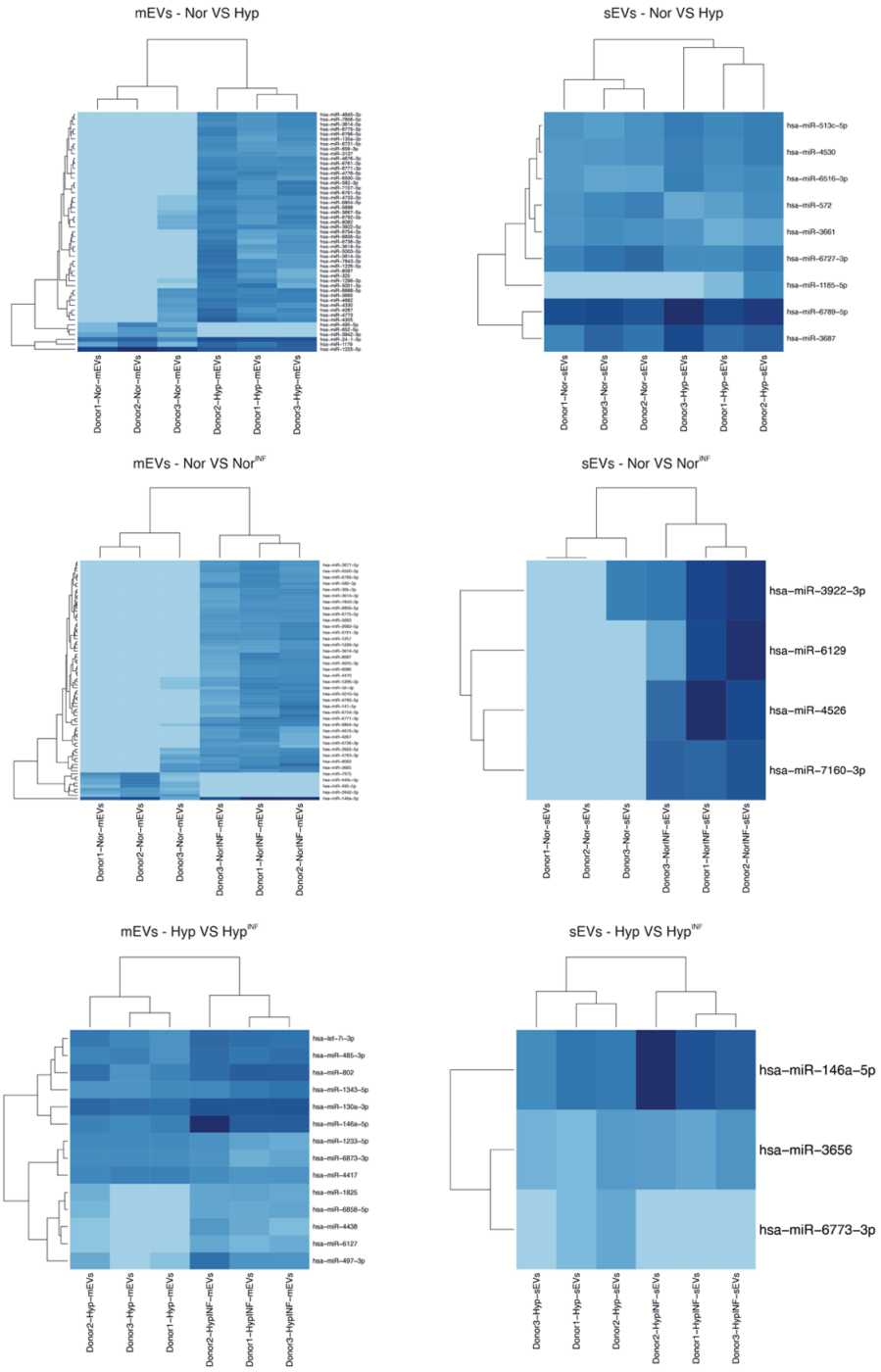

Supplementary Figure 3.7: Heatmap of differentially enriched EV miRNAs derived from differently treated cells. Each set of miRNAs correctly classifies the compared sample groups in hierarchical clustering.

CHAPTER

4

Extracellular Vesicles from adipose tissue- and bone marrow-mesenchymal stromal cells play different roles in the endochondral ossification process

Gorgun C[§], Palama MEF[§], Reverberi D, Gagliani MC, Cortese K, Tasso R[§], Gentili C[§]. Extracellular Vesicles from adipose tissue- and bone marrow-mesenchymal stromal cells play different roles in the endochondral ossification process. *Under review.*

[§] These authors contributed equally.

4.1 Introduction

A combination of regenerative and trophic properties has prompted exploration of the therapeutic use of Mesenchymal Stromal Cells (MSCs) over the last decades [139]. MSCs virtually reside in all tissues, where part of them localize near the microvasculature walls, stabilizing endothelial networks [140,141]. Thanks to manifold mechanisms through which MSCs act, they are considered a powerful tool for the treatment of various diseases [142]. Although bone marrow (BM) has been regarded as the gold standard source, it presents significant drawbacks, such as low cell yield and invasive and painful procedure for BM collection [143]. These issues induced the scientific community to analyze and characterize MSCs from alternative sources [144]. Among the others, adipose tissue (AD) represents a promising source for its abundance, accessibility and less invasive collection [145]. Although MSCs from different tissues share many biological features, some differences exist in the immunophenotype, proliferative capacity, differentiation potential, gene expression profile and immunomodulatory activity [146,147]. Altogether, these putative disparities can lead to different efficacies. For example, it has been reported that ADSCs possess a higher angiogenic potential in comparison to bone marrow-MSCs (BMSCs) [148]. Therefore, there may be the advantage of using a cell population over another for specific clinical applications.

Apart from differentiation potential, it is now accepted that MSCs exert their beneficial effects promoting cytoprotection and tissue repair through their paracrine activity [149]. Among the components responsible for the paracrine effects, extracellular vesicles (EVs) have been recently described as new players in cell-cell communication and tissue homeostasis [150]. EVs are a heterogeneous group of cell-derived membranous structures comprising small-sized vesicles (exosomes) originating from the endosomal compartment and middle-sized vesicles (microvesicles) directly budding from the cell plasma membrane [151]. MSC-derived EVs are involved in a wide spread of processes, including angiogenesis, senescence, proliferation, and differentiation, beside strong immunomodulatory properties [152]. Since EVs trigger specific cellular responses, reflecting the status and composition of the parental cell, we here aimed to identify morphological and functional differences between BMSC- and ADSC-derived EV subpopulations. EVs were isolated from the cell conditioned media by serial differential centrifugations, to collect both medium-sized and small-sized vesicles. The role of EVs in the different phases of the endochondral ossification process, namely

angiogenesis, chondrogenic and osteogenic differentiation, was evaluated taking advantage of fetal mouse metatarsal bone explants.

Just as in some pathologies there may be the advantage of using one cell population over another, in the same way it may be important to know in depth the functional differences between the corresponding EVs to be used in cell-free therapeutic approaches.

4.2 Materials and Methods

4.2.1 Isolation and culture of Mesenchymal Stromal Cells (MSCs)

Human ADSCs were obtained from subcutaneous adipose tissue, isolated and cultured, as previously described [153], and in compliance to Regione Liguria Ethical Committee authorization (P.R. 23571). Human BMSCs were obtained from femoral condyles of patients undergoing knee arthroplasty, after informed consent and according to the guidelines of the Ethics Committee of IRCCS Policlinico San Martino Hospital (Genova, Italy), N. Registro CER Liguria: 372/2019. Liposuction aspirates obtained from human healthy donors during routine lipoaspiration after informed consent was used. Adipose tissue was washed with cold phosphate-buffered saline (PBS) and digested in 0.1% type I Collagenase (Gibco, MI, Italy) in PBS at 37°C for 60 min. Following, stromal vascular fraction (SVF) pellet was rinsed and cultured in Dulbecco's MEM (D-MEM) (Biochrome GmbH, Berlin, Germany) supplemented with 10% Fetal Bovine Serum (FBS) (Gibco, Milan, Italy), 2 mM of l-glutamine, and 50 mg/ml penicillin/streptomycin. The cultures were performed in the presence of 1 ng/ml of fibroblast growth factor-2 (FGF-2; Peprotech, Milan, Italy) (standard condition).

Bone marrow fraction was washed from the subchondral bone and centrifuged at 300 xg for 10 min. Cell nucleated fraction was cultured in α-MEM-Glutamax medium (Gibco, Waltham, MA, USA), supplemented with 10% FBS (FBS, Gibco), 1 ng/ml Fibroblast Growth Factor-2 (FGF-2, Peprotech, London, UK) and 50 mg/ml penicillin/streptomycin. Both ADSCs and BMSCs cultures were maintained in a humidified incubator at 37°C with 5% CO2. Only cells that were in passage 2 were used for all the experiments. MSCs immunophenotype in standard condition was also evaluated by flow cytometry using following monoclonal antibodies to: CD31-FITC (390), CD34-FITC (4H11), CD45-PE (2D1), CD73-FITC (AD2), mouse IgG1 kappa Isotype Control-FITC (P3.6.2.8.1), mouse IgG1 kappa Isotype Control-PE (P3.6.2.8.1) (eBioscience), and CD90-PE (5E10), CD29-PE (MAR4), CD105-PE (266), CD44-FITC (L178), mouse IgG1 kappa Isotype Control-FITC (MOPC-

21), mouse IgG1 kappa Isotype Control-PE (MOPC-21) (BD Biosciences). Cells were analyzed using a flow cytometer (FACSCanto, BD Biosciences) and data were analyzed using FlowJo software.

4.2.2 Extracellular Vesicles (EVs) separation and characterization

We have submitted all relevant data of our experiments to the EV-TRACK knowledgebase (EV-TRACK ID: EV210113) [38]. When ADSCs and BMSCs reached 70% confluence, they were rinsed twice with PBS and maintained for 20 min in culture medium without FBS (serum-free medium). Medium was then replaced with fresh serum-free medium, and cells were maintained for 24 h in starvation. Cell conditioned media (CM) were collected and centrifuged at 300 xg for 10 min and at 2000 xg for 20 min to remove cells/cell debris and apoptotic bodies. Supernatants were transferred into ultracentrifugation tubes (Beckman-Coulter, USA) and subjected to a first centrifugation at 10.000 xg for 40 min to obtain an EV pellet (10K pellet) enriched in medium sized-vesicles (mEVs). Resulting supernatants were then centrifuged at 100.000 xg for 120 min in order to obtain a pellet (100K pellet) enriched in small sized-vesicles (sEVs) [154]. Both EV pellets were washed in PBS and centrifuged at 100.000 xg. A Beckman Coulter ultracentrifuge (Beckman Coulter Optima XPN-100 ultracentrifuge; Beckman Coulter, USA) was used with the swinging bucket rotors SW28 and SW55Ti. After the last washing step, EVs were resuspended in sterile filtered (0.22 μm) PBS for further analysis. The concentration of membrane-bound proteins on the surface of freshly isolated EVs was measured by BCA (BicinChoninic Acid) Protein Assay Kit (Thermo Fisher Scientific, Massachusetts, USA).

4.2.3 Tunable Resistive Pulse Sensing (TRPS)

EV concentrations and size distribution were analyzed by Tunable Resistive Pulse Sensing (TRPS)[155]. Analysis was performed on ADSC and BMSC-derived EVs from three different primary cultures using qNano (Izon Science Ltd, Burnside, Christchurch, New Zealand).

4.2.4 Transmission Electron Microscopy (TEM)

ADSCs and BMSCs were washed out in PBS and fixed with 3.7% paraformaldehyde (PFA), for 10 min at room temperature. They were then washed again with PBS, scraped and collected in a tube. Post-fixation was performed in osmium tetroxide for 2 h and 1% uranyl acetate for 1 h. Subsequently,

sample of cells were dehydrated through a graded ethanol series and embedded in epoxy resin (Poly-Bed; Polysciences, Inc., Warrington, PA) for 24 h at 60°C. Ultrathin sections (50 nm) were cut and stained with 5% uranyl acetate in 50% ethanol and observed with Hitachi TEM microscope (HT7800 series, Tokyo, Japan). For the imaging of EVs, after washing step with ultracentrifugation, EV pellets were resuspended in 20 µl PBS (pH 7.4) and fixed by adding an equal volume of 2% paraformaldehyde in 0.1 mol/l phosphate buffer (pH 7.4). EVs were then adsorbed for 10 min to formvar-carbon coated copper grids by floating the grids on 5 µl drops on parafilm. Subsequently, grids with adhered vesicles were rinsed in PBS and negatively stained with 2% uranyl acetate for 5 min at room temperature. Stained grids were embedded in 2.5% methylcellulose for improved preservation and air dried before examination. Electron micrographs were taken at Hitachi TEM microscope (HT7800 series, Tokyo, Japan) equipped with Megaview 3 digital camera and Radius software (EMSIS, Germany).

4.2.5 Western Blot Analysis

Isolated mEVs and sEVs from ADSCs and BMSCs were resuspended in RIPA buffer (1% NONIDET p-40, 0.1% SDS, 0.1% Sodium deoxycholate, protease inhibitor cocktail 1x, in PBS pH 7.5) and protein content was quantified by BCA assay. Blot membranes were incubated with the following specific antibodies: anti-CD63 (1:1000 dilution, 10628D, Invitrogen), anti- CD81 (1:5000 dilution, 555675, BD Biosciences), anti-syntenin (1:1000 dilution, ab133267, Abcam, USA), anti- Grp94 (1:1000 dilution, ab238126, Abcam, USA), anti-flotillin-1 (1:10000 dilution, ab133497, Abcam, USA).

A specific HRP-conjugated goat anti-rabbit/mouse secondary antibody (1:2000 dilution, Cell Signaling Technology, Danvers, Massachusetts, USA) was used for the detection. Positivity was highlighted by providing the substrates for the chemiluminescence reaction of HRP (Amersham ECL Prime Western Blotting Detection Reagent, GE Healthcare, Chicago, Illinois, USA) and impressing a photographic sheet by autoradiography (GE Healthcare). Images were scanned using the Epson perfection 1260 scanner.

4.2.6 Flow cytometry characterization of EVs

Each EV preparation was suspended in filtered PBS/EDTA and distributed in flow cytometry tubes (100 µl/tube). EVs were stained with 1 µM CFDA-SE at 4°C (VybrantTM CFDA SE Cell Tracer Kit,

Thermo Fisher Scientific) to visualize intact vesicles. A mixture of fluorescent beads of varying diameters (Megamix-Plus FSC and Megamix-Plus SSC, Biocytex) suspended in filtered PBS was used following the manufacturer's instructions to discriminate EV size. Expression of typical vesicle markers CD9 (APC Mouse Anti-Human CD9, Biolegend, 312108), CD63 (PE-CyTM7 Mouse Anti-Human CD63, BD Biosciences, 561982) and CD81 (BV421 Mouse Anti-Human CD81, BD Biosciences, 740079) was evaluated within the CFDA-SE positive events using the BD FACSAria II (BD Biosciences).

4.2.7 Proteome profiling of EVs

For the analysis of cytokine and chemokine content of EVs, 10 μg of proteins were analyzed with a Proteome Profiler Human XL Cytokine Array Kit (R&D, Minneapolis, Toll Free USA, Canada), according to the manufacturer's instructions. Images were scanned using the Epson perfection 1260 scanner and spot densities were quantified using the ImageJ software. Gene Ontology (GO) was also carried out using DAVID.

4.2.8 *Ex vivo* metatarsal sprouting assay

All animal procedures were approved by the Italian Ministry of Health, by the IRCCS Ospedale Policlinico San Martino Ethical Committee (Authorization n. 55/2020-PR) and performed in accordance with the national current regulations regarding the protection of animals used for scientific purpose.

E17.5 fetuses were removed from pregnant C57BL/6 wild-type mice and metatarsals were dissected under stereomicroscope. The isolated metatarsals were cultured in 24-well plates in 300 μL of α-MEM-GlutaMAX medium (Gibco, Waltham, MA, United States), supplemented with 10% FBS (Gibco, Milan, Italy) and 50 mg/ml penicillin/streptomycin for 96 h. After 96 h, attached bones covered with fibroblasts were selected and medium was replaced with α-MEM-GlutaMAX supplemented with 2% FBS. For each experiment, 0.5 μg mEVs and sEVs were added. After 7 days, bones were fixed and stained with rat anti-Mouse CD31 (clone SZ31) (Dianova, Hamburg, Germany). Images were captured by transmitted light microscopy using a Zeiss Axiovert 200M microscope. CD31-positive pixels were analyzed with Image J software with vessel density plugin.

4.2.9 *Ex vivo* metatarsal bone growth assay

E15.5 fetuses were removed from pregnant C57BL/6 wild-type mice and metatarsals were dissected under stereomicroscope. The isolated metatarsals were cultured in 24-well plates in 300 µL of α-MEM-GlutaMAX medium, supplemented with 0.2% w/v bovine serum albumin (BSA), 50 mg/ml penicillin/streptomycin and 1x Amphotericin B (basal medium). After 24h, 0.5 µg mEVs and sEVs were added. A positive control was used to trigger the bone growth/differentiation by adding 50 µg/mL ascorbic acid, 10 mM β-glycerophosphate and 10^{-7} M dexamethasone (all of them from Sigma-Aldrich, St. Louis, Missouri, USA) to the medium (osteogenic medium). Fresh EVs were added every 3 days, while osteogenic medium was changed every other day in positive controls. Metatarsal cultured in serum-free (basal medium) were used as negative controls. Bone growth was monitored daily and analyzed by Image J software.

4.2.10 Histological and immunohistochemical analysis

After 10 days of culture, E15.5 metatarsals were washed with PBS and fixed in 3.7% paraformaldehyde (PFA), then dehydrated and paraffin embedded. Sections of 5 µm were cut, dewaxed and stained with hematoxylin and eosin (H&E) and Safranin-O/Fast-Green. Sections of 5 µm were blocked over night at 4°C in Normal Goat Serum (NGS) and specific binding was allowed using rabbit anti-mouse type X collagen (1:300 dilution, in NGS 10%, ab58632, Abcam, USA) for 90 min at RT. Negative controls with pre-immune serum and positive controls were run in parallel. Images were captured using an AxioPhot microscope (Carl Zeiss, Jena, Germany). Captured images of Safranin-O/Fast-Green staining were used for calculating the hypertrophic, proliferative and resting zones with Image J software. Measurements were performed considering area of each zone and normalizing it to the whole area of the region of interest (ROI).

4.2.11 Statistical analysis

Statistical analysis of differences between multiple groups were performed applying Two-way ANOVA and Tukey's multiple comparisons test. For the analysis of protein arrays, multiple t test was performed. Data are presented as mean ± SD considering at least three independent replicates for each assay and analyzed by GraphPad Prism (Graph Pad Software, Inc.). For all analyses $p< 0.05$ was considered statistically significant. In all cases: **** $p<0.0001$, *** $p<0.001$, ** $p <0.01$, * $p <0.05$.

4.3 Results

4.3.1 ADSCs and BMSCs release EVs with similar characteristics

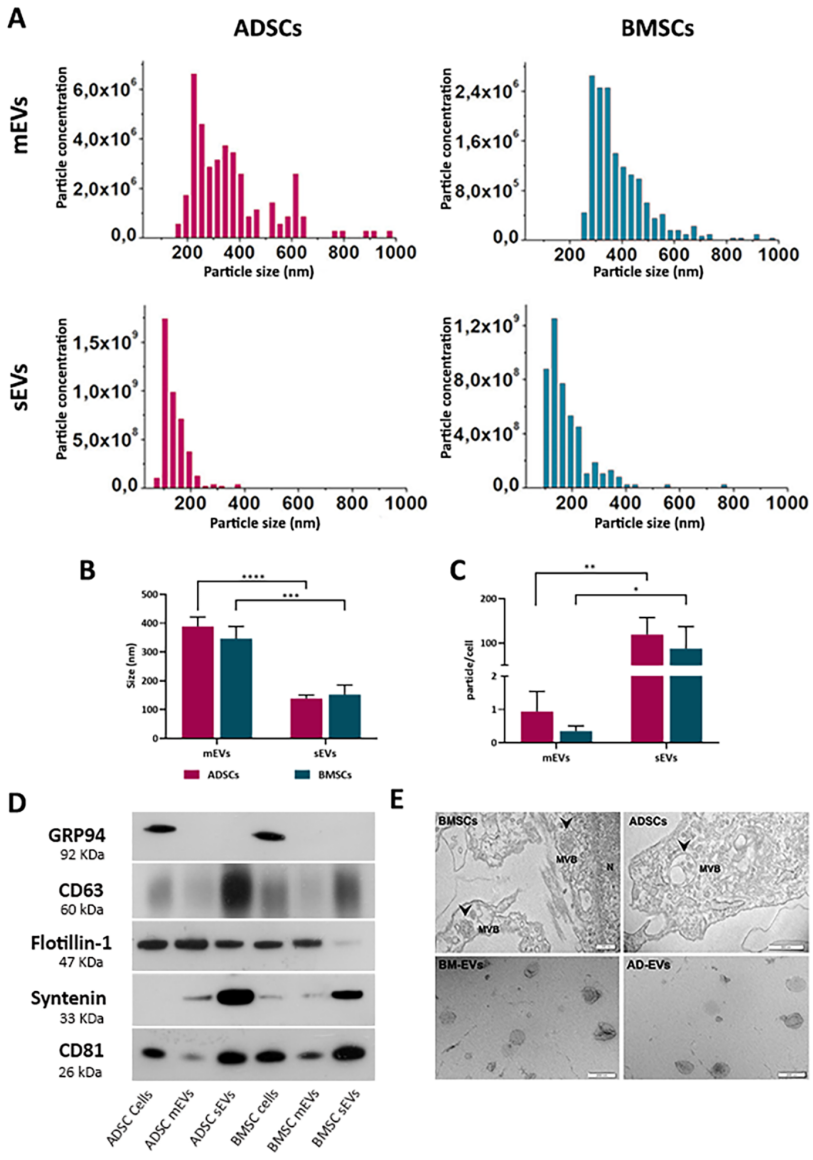

Figure 4.1: ADSCs- and BMSCs-derived EVs have common characteristics. (A) Tunable Resistive Pulse Sensing (TRPS) analysis measuring size distribution of ADSC-derived mEVs and sEVs (pink) and BMSC-derived mEVs and sEVs (green). Comparison of size distribution **(B)**, particle counting intended as particle/cell**. (C)**. Data are presented ad mean ± SD. N=3, **** p<0.0001, *** p<0.001, ** p <0.01, * p <0.05, (Two-way ANOVA and Tukey multiple comparison). **(D)** Western blot analysis on ADSCs and BMSCs-derived mEVs and sEVs. Control cell lysates were also loaded. Specific expressions of CD63, CD81, flotillin, syntenin and GRP94 were investigated. **(E)** TEM images of pre-conditioned ADSCs and BMSCs (top panel) and isolated EVs (bottom panel). Scale: 200 nm.

Primary cultures of MSCs isolated from either AD or BM have been investigated for their typical mesenchymal phenotype by flow cytometry. According to International Society for Cell Therapy (ISCT) indications [156], both ADSCs and BMSCs constitutively expressed the cell surface antigens CD29, CD44, CD73, CD90 and CD105. The expression of CD31, CD34 and CD45 was less than 1%, indicating the absence of contaminating endothelial, myeloid, and hematopoietic cells (Supplementary Fig. 4.1A). Cell conditioned medium (CM) was collected from either ADSCs or BMSCs maintained for 24 hours in serum free medium. Flow cytometry of Annexin V/PI-stained cells was used to quantify the apoptotic rate of cells exposed to serum deprivation for 24 hours. Less than 1% of both ADSCs and BMSCs underwent apoptosis or necrosis (Supplementary Fig. 4.1B). For EV separation, CM were subjected to differential ultracentrifugation (UC), using an intermediate speed (10K) prior to a high-speed step (100K), in order to obtain intermediate recovery and specificity [157]. Material pelleted at 10K, enriched in medium-sized vesicles (mEVs), was compared with the 100K pelleted one, considered to be enriched in small-sized EVs (sEVs). Both mEVs and sEVs separated from the two cell sources were firstly characterized by TRPS to check their size and concentration. No significant differences were observed in EV size among the two cell sources (Fig. 4.1A and 4.1B). mEVs released by ADSCs and BMSCs exhibited a mean size of 388±32.7 nm and 346±42.1 nm, respectively. sEVs isolated from ADSCs and BMSCs presented a mean size of 138±12 nm and 152±33.2 nm, respectively, indicating that the separation method here adopted allowed the effective and significant separation of two different EV subpopulations (ADSCs: mEVs vs sEVs, $p \leq 0.0001$; BMSCs: mEVs vs sEVs, $p \leq 0.001$) (Fig. 4.1A and 4.1B). Both cell types released a significantly higher amount of sEVs than mEVs (ADSCs: sEVs vs mEVs, $p < 0.01$; BMSCs: sEVs vs mEVs, $p < 0.05$) and with no significant differences between the two cell sources (Fig. 4.1C).

In order to evaluate whether mEVs and sEVs were successfully purified from cells, immunoblotting was performed. Both EV subpopulations, and in particular sEVs isolated from ADSCs and BMSCs expressed the vesicle-associated proteins CD81 and CD63 (Fig. 4.1D). To note, the expression of the tetraspanin CD9 was not detected in any MSC-derived EV. Syntenin, a specific marker for sEVs [158], was strongly expressed by ADSC- and BMSC-derived sEVs, poorly detected in mEVs and BMSC lysates, and not detected in ADSC lysates (Fig. 4.1D). Interestingly, flotillin-1 was expressed by cell lysates, both mEVs, and by sEVs released only by ADSCs (Fig. 4.1D). As expected, GRP94, a protein of the endoplasmic reticulum used as EV negative marker, was strongly detected only in the cell lysates

(Fig. 4.1D). After 24 hours of medium conditioning, isolated EVs, as well as the corresponding MSC monolayers, were analyzed by TEM. Ultrastructural analysis of both cell types revealed the presence of many multivesicular bodies (MVBs) containing several intraluminal vesicles within the cytoplasm, confirming the discharge of a prevalent population of sEVs (Fig. 4.1E, upper panels). The corresponding EV fractions showed the typical round or cup-shaped morphology surrounded by a bilayer membrane, with sizes ranging from 30 to 200 nm (Fig. 4.1E, bottom panels), confirming that the separation procedure picked out a mixed population of vesicles, enriched mostly in sEVs.

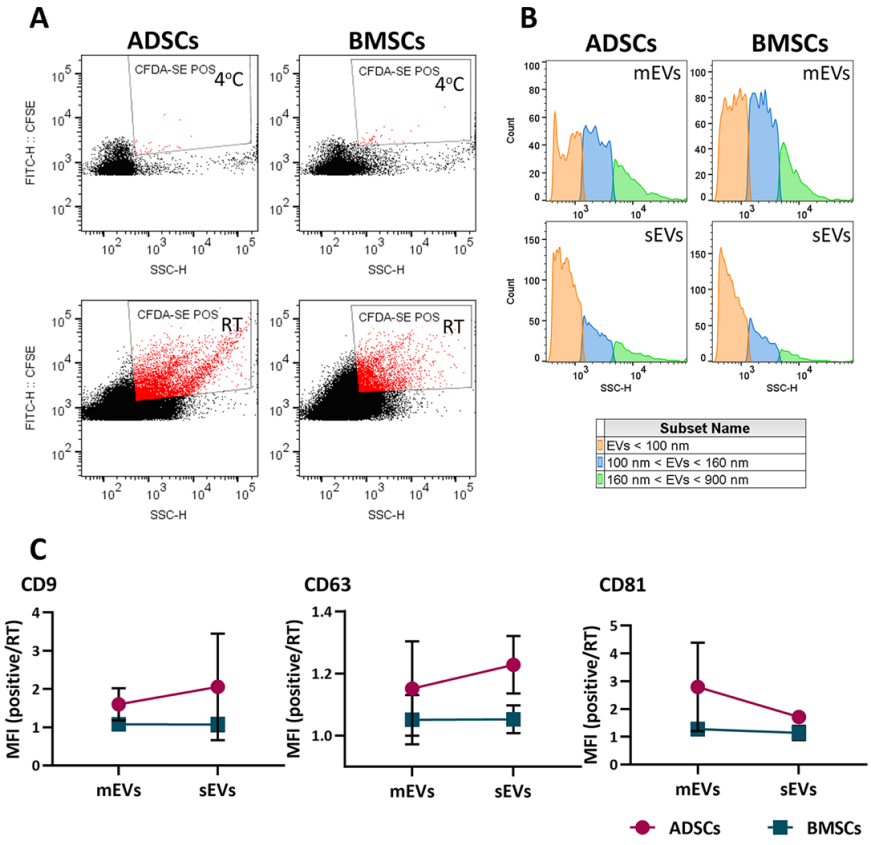

Figure 4.2: Non-conventional flow cytometry strategy used to characterize mEVs and sEVs. (A) Red areas identify CFDA-SE positive events. EVs were stained with CFDA-SE at 4°C as "blank tube" (top), useful to define the appropriate dimensional gate when considering EVs stained with CFDA-SE at room temperature (bottom). **(B)** Size distribution of EV subtypes. Three dimensional gates were considered: EVs ≤100nm (orange), 100nm ≤ EVs ≤ 160nm (blue) and 160nm ≤ EVs ≤ 900nm (green). **(C)** Quantification of CD9-, CD63- and CD81- positive events falling within the CFDA-SE gate by mEVs and sEVs. Data are presented as ratio between mean fluorescence intensity (MFI) of cells stained with a specific antibody and MFI of correspondent isotype control (relative MFI). Data are representative of at least three independent experiments.

ADSC- and BMSC-derived EVs were further characterized for size and marker expression by non-conventional flow cytometry [159]. Both mEVs and sEVs were stained with the cell-permeant, fluorescein-based CFDA-SE tracer, useful to discriminate intact vesicles from debris and membrane fragments. Since CFDA-SE passively diffuses within vesicles and interacts with intra-vesicular enzymes at room temperature (RT) (Fig. 4.2A, bottom panels), 4°C samples were used as controls (Fig. 4.2A, upper panels). Taking advantage of fluorescent dimensional beads (Supplementary Fig. 4.2A), specific size gates were considered (≤100nm, from 100 to 160nm and from 160 to 900nm) (Fig. 4.2B).

Table 4.1: Flow cytometry quantitative analysis. Table shows the size distribution of ADSCs- and BMSCs-derived EVs. Statistical analysis was performed with unpaired Student's t test, considering EVs derived from three independent MSC primary cultures for each condition.

	Size	mEVs % (*AVG* ± *S.D*)	sEVs % (*AVG* ± *S.D*)	*P value* (unpaired t-test)	*P value* (unpaired t-test) *ADSCs vs. BMSCs*
ADSCs	**EVs≤100nm**	40.1 ± 6.16	50.53 ± 12.94	0.276 (*ns*)	0.1569 (*ns*)
	100nm≤EVs≤160nm	40.36 ± 4.86	32.13 ± 9.7	0.2594 (*ns*)	0.064 (*ns*)
	160nm≤EVs≤900nm	20.73 ± 1.36	18.43 ± 5.85	0.5434 (*ns*)	0.0095 (**)
BMSCs	**EVs≤100nm**	48.1 ± 5.04	63.5 ±5.56	0.0238 (*)	0.1862 (*ns*)
	100nm≤EVs≤160nm	38.56 ± 3.35	28.3 ± 4.3	0.0314 (*)	0.5689 (*ns*)
	160nm≤EVs≤900nm	14.6 ± 1.82	9.44 ± 1.87	0.0269 (*)	0.0643 (*ns*)

The percentage of events falling within each dimensional gate was calculated (Table 4.1). While the percentage of vesicles smaller than 100 nm was significantly higher in sEVs released by BMSCs if compared to the mEV counterpart, the percentage of events ranging from 100 and 160 nm, as well as 160 and 900 nm, was significantly higher in BMSC-mEVs compared to sEVs (Table 4.1). A similar trend was also observed in the vesicles released by ADSCs, but no statistically significant differences were detected (Table 4.1). Moreover, no differences were noticed between EVs released by ADSCs and BMSCs, except for the bigger vesicles, ranging from 160 to 900 nm, whose percentage was significantly higher in ADSCs (Table 4.1). Upon accurate titration of antibodies and the use of related isotype controls [159], the expression of CD81, CD63, and CD9 was evaluated in both mEVs and sEVs

(Supplementary Fig. 4.2B and Fig. 4.2C). All vesicle subpopulations derived from both cell types expressed, at different extent, the three markers. The expression of CD9 was the lowest among the tetraspanins, confirming the western blot analysis. Taken together, these data indicate that MSCs release EV subtypes with similar characteristics, independent of the cell source.

Table 4.2: Flow cytometry quantitative analysis. Table shows the size distribution of ADSCs- and BMSCs-derived EVs. Statistical analysis was performed with unpaired Student's t test, considering EVs derived from three independent MSC primary cultures for each condition.

	Size	mEVs % (*AVG* ± *S.D*)	sEVs % (*AVG* ± *S.D*)	*P value* (unpaired t-test)	*P value* (unpaired t-test) *ADSCs vs. BMSCs*
ADSCs	**EVs≤100nm**	40.1 ± 6.16	50.53 ± 12.94	0.276 (*ns*)	0.1569 (*ns*)
	100nm≤EVs≤160nm	40.36 ± 4.86	32.13 ± 9.7	0.2594 (*ns*)	0.064 (*ns*)
	160nm≤EVs≤900nm	20.73 ± 1.36	18.43 ± 5.85	0.5434 (*ns*)	0.0095 (**)
BMSCs	**EVs≤100nm**	48.1 ± 5.04	63.5 ±5.56	0.0238 (*)	0.1862 (*ns*)
	100nm≤EVs≤160nm	38.56 ± 3.35	28.3 ± 4.3	0.0314 (*)	0.5689 (*ns*)
	160nm≤EVs≤900nm	14.6 ± 1.82	9.44 ± 1.87	0.0269 (*)	0.0643 (*ns*)

4.3.2 Differentially expressed proteins in BMSC- and ADSC-EVs

Although ADSCs and BMSCs share many biological features, little is known about differences in their secreted factors, and in particular EV subtypes. In order to evaluate the protein cargo of both mEVs and sEVs released by ADSCs and BMSCs, vesicle lysates were analyzed using a Proteome Profiler optimized to detect cytokines and chemokines (Fig. 4.3). Significant differences were detected not only between mEVs and sEVs derived from the same cell source, but also between the two different cell sources. Gene Ontology (GO) analysis was applied to identify key pathways characterizing EV subtypes and the relative frequency of ontology terms (i.e. biological functions) was considered. The main biological processes characterizing ADSC- and BMSC-sEVs and mEVs were related to "cell proliferation", "angiogenesis", "regulation of cellular communication", "defense response", "chemotaxis", "response to external stimulation", and "cell migration", with no significant differences among them (Fig. 4.3A). Table 4.2 resumes the more relevant biological functions and factors involved, with frequency and p value.

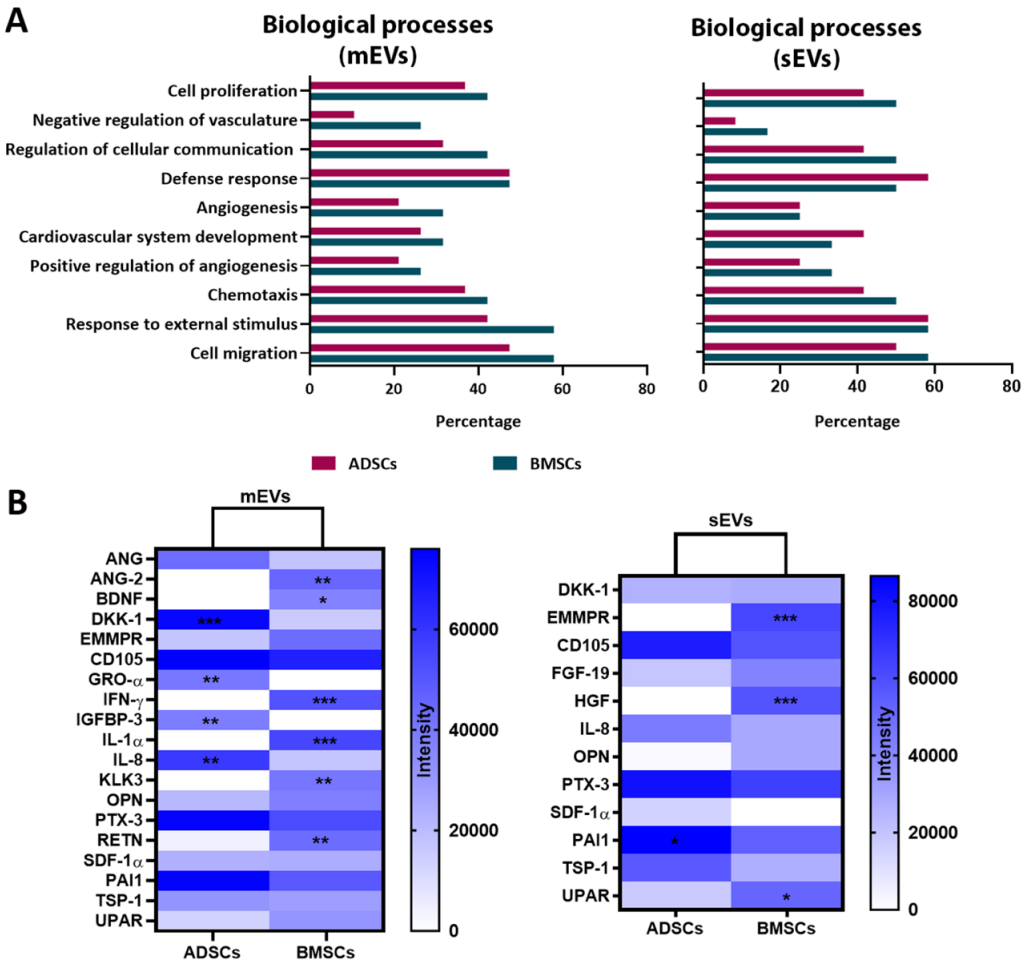

Figure 4.1: Proteome profiler analysis of ADSC- and BMSC-derived EVs. (A) Gene ontology analysis of biological functions in mEVs and sEVs. **(B)** Heatmaps of expressed proteins by mEVs and sEVs. N=3, (*) presents the statistical differences between the groups. *** p<0.001, ** p <0.01, * p <0.05 (Multiple t-test comparison). ANG: Angiogenin, ANG-2: Angiopoietin-2, BDNF: Brain-Derived Neurotrophic Factor, DKK1: Dickkopf-1, EMMPRIN: Extracellular Matrix Metalloproteinase inducer, CD105: Endoglin, FGF19: Fibroblast Growth Factor 19, GROα: Growth-regulated oncogene-alpha, HGF: Hepatocyte Growth Factor, IFNγ: Interferon γ, IGFBP3: Insulin-like growth factor-binding protein 3, IL1α: Interleukin 1 alpha, IL8: Interleukin-8, KLK3: Kallikrein-3; OPN: Osteopontin, PTX3: Pentraxin-3, RETN: Resistin, SDF1α: Stromal cell Derived Factor 1 alpha, PAI1: Plasminogen activator inhibitor-1, TSP1: Thrombospondin-1, uPAR: urokinase-type Plasminogen Activator Receptor.

Compared to the BMSC-counterpart, ADSC-mEVs presented a significant up-regulation of 4 different proteins, involved, at different extents, in injury environment modulation: DKK-1 (Dickkopf-related protein 1), GRO-a (Growth-Regulated Oncogene-a), IL-8 (Interleukin-8), and IGFBP-3 (Insulin-like Growth Factor Binding Protein-3) (Fig. 4.3B, left panel). On the contrary, BMSC-derived mEVs

exhibited a significant overexpression of proteins involved in the modulation of angiogenic and osteogenic responses (Angiotensin-2 [ANG-2] and Brain Derived Growth Factor [BDNF], respectively), as well as in the crosstalk with immune cells (Interferon-γ [IFN-γ Interleukin-1α [IL-1α], Kallikrein-3 [KLK-3], and Resistin [RETN]) (Fig. 4.3B, left panel). Regarding sEVs, only one protein, Plasminogen Activator Inhibitor-1 (PAI-1), was significantly overexpressed by ADSC-derived vesicles (Fig. 4.3B, right panel), while three proteins were significantly up-regulated in BMSC-sEVs: EMMPRIN (CD147), Hepatocyte Growth Factor (HGF), and Urokinase-type Plasminogen Activator Receptor (uPAR) (Fig. 4.3B, right panel).

Table 4.3: Gene Ontology term frequency. ANG: Angiogenin, ANG-2: Angiopoietin-2, BDNF: Brain-Derived Neurotrophic Factor, DKK1: Dickkopf-1, EMMPRIN: Extracellular Matrix Metalloproteinase inducer, CD105: Endoglin, FGF19: Fibroblast Growth Factor 19, GROα: Growth-regulated oncogene-alpha, HGF: Hepatocyte Growth Factor, IFNγ: Interferon γ, IGFBP3: Insulin-like growth factor-binding protein 3, IL1α: Interleukin 1 alpha, IL8: Interleukin-8, KLK3: Kallikrein-3; OPN: Osteopontin, PTX3: Pentraxin-3, RETN: Resistin, SDF1α: Stromal cell Derived Factor 1 alpha, PAI1: Plasminogen activator inhibitor-1, TSP1: Thrombospondin-1, uPAR: urokinase-type Plasminogen Activator Receptor.

	Cell migration	Response to external stimulus	Chemotaxis	Positive regulation of angiogenesis	Cardiovascular system development	Angiogenesis	Defense response	Regulation of cellular communication	Negative regulation of vasculature	Cell proliferation
IL1α	*			*	*	*	*	*		*
ANG	*				*	*	*			*
ANG-2	*	*	*	*	*	*			*	*
BDNF	*	*	*					*		
EMPPRIN	*									
CD105	*	*	*	*	*	*		*		*
FGF19	*				*			*		*
GROα	*	*	*				*			*
HGF	*	*	*	*	*	*	*	*		*
IFNγ	*	*	*		*		*	*	*	*
IGFBP3	*							*		*
IL1α	*			*	*	*	*	*		*
IL8	*	*	*	*	*	*	*	*		*
KLK3		*			*	*	*		*	
OPN		*					*			
PTX3		*					*			
RETN	*	*						*		*
SDF1α	*	*	*				*			*
PAI1	*	*	*	*	*	*	*	*	*	
TSP1	*	*	*				*	*	*	*
uPAR			*	*				*		
Count	15	10	11	7	12	9	12	14	5	12
P	2E-12	2.1E-10	2E-10	6.2E-9	1.9E-9	1.3E-8	2-7E-7	4.8E-6	2.6E-6	2.1E-6

4.3.3 ADSC-sEVs promote vessel outgrowth from fetal metatarsal explants more efficiently than BMSC-sEVs

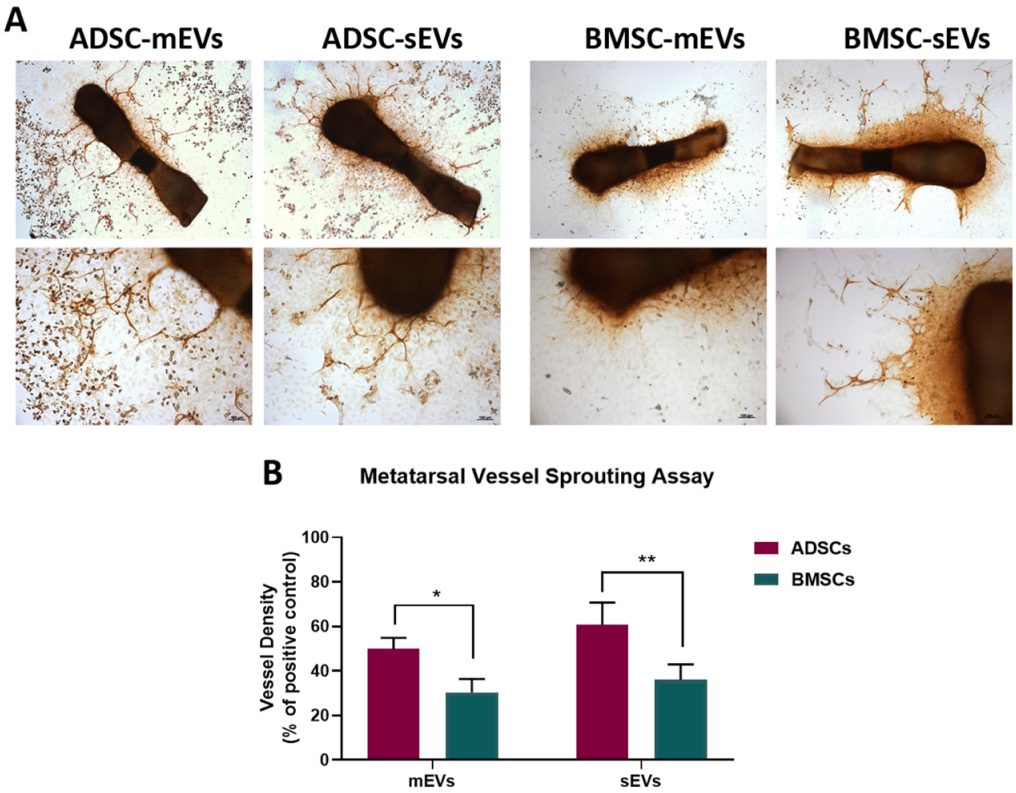

Figure 4.2: Ex vivo metatarsal sprouting assay. (A) Representative image of $CD31^+$ vessel structures, scale bar: 100 µm. (**B**) Quantitative analysis of vessel density, CD31-positive cells were considered for the analysis. Data are presented as mean ± SD. N=3, ** p <0.01, * p <0.05, (Two-way ANOVA and Tukey multiple comparison).

We studied the effects of EVs secreted by ADSCs and BMSCs on two different aspects of the endochondral ossification process. Taking advantage of mouse metatarsal organ explant cultures, E17.5 and E15.5 mice metatarsal were exploited as models of angiogenesis and osteogenesis, respectively [160,161].

In comparison with other commonly used *in vitro* or *ex vivo* angiogenesis assays, vessel outgrowth from mouse fetal metatarsals is more representative of sprouting angiogenesis *in vivo* [161]. The assay performed on E17.5 metatarsals revealed that ADSC-derived mEVs and sEVs were able to induce the outgrowth of a significant higher number of CD31+ vessels in comparison to BMSC-derived counterparts ($p \leq 0.05$ and $p \leq 0.01$, respectively) (Fig. 4.4A and B).

Blood vessel formation from metatarsals is the result of complex interactions between various cell types, overall contributing to the development of an intricate vascular network on the top of a fibroblast sheet [161]. Although BMSC-sEVs possessed a lower ability to induce vessel sprouting than ADSC-counterparts, interestingly we noticed a strong induction of fibroblast proliferation by this experimental group (Fig. 4.4A). This evidence corroborates our gene ontology results, in which the biological process "cell proliferation" was mostly associated to BMSC-EVs.

4.3.4 Metatarsal bone explants exposed to BMSC-sEVs exhibit more organized growth plate areas compared to ADSC-sEVs

The culture of E15.5 mouse metatarsals is a highly physiological *ex vivo* model for studying endochondral ossification and bone growth. Since ADSCs and BMSCs release a significant larger amount of sEVs compared to mEVs (Fig. 4.1C), we focused on the effects induced by sEVs. E15.5 metatarsals were cultured in the following conditions: (i) basal medium (negative control), (ii) osteogenic medium (positive control), (iii) basal medium supplemented with 0.5 μg ADSC-sEVs or (iv) BMSC-sEVs. As shown in figure 4.5A, at day 9 a mineralization center was observed only in the positive control. Bone growth was significantly higher in positive control compared to the other experimental groups ($p \leq 0.0001$) (Fig. 4.5B). Although ADSC-sEVs seemed to promote metatarsal growth during the first 7 days in culture compared to both negative controls ($p=0.0114$) and BMSC-counterparts ($p= 0{,}0220$) (Fig. 4.5B), their effect appears to reach a *plateau* between day 7 and 9. This evidence suggests that, at macroscopic level, both ADSC- and BMSC-sEVs did not elicit drastic effects on metatarsal bone growth.

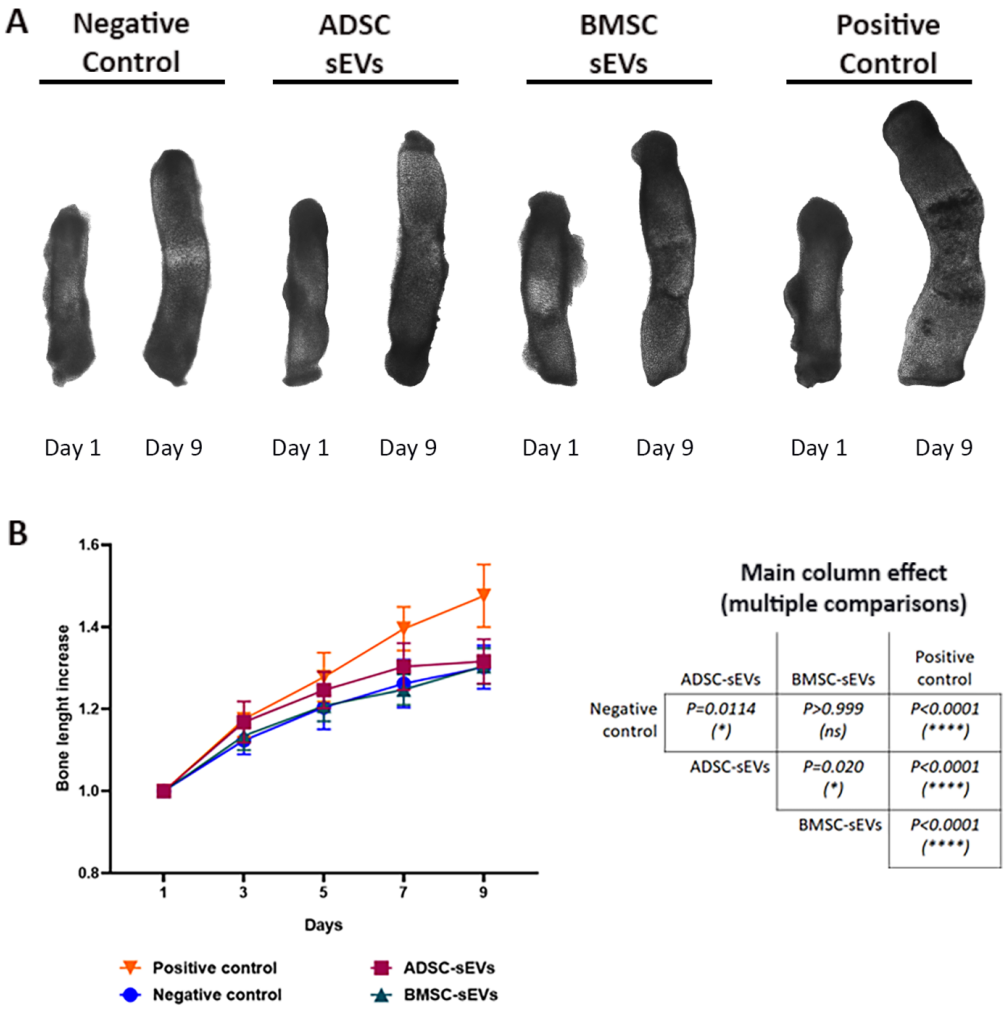

Figure 4.3: Effect of ADSC- and BMSC-derived sEVs on longitudinal bone growth. (A) Representative images of mouse metatarsals at day 1 and day 9 of culture, in different culture conditions. **(B)** Quantification of bone length increase during the time in different experimental groups. Each bone length was normalized on its day 1 value. Data are presented as mean ± S.D. Table shows statistical significance between experimental groups. N=10, **** p<0.0001, * p <0.05 (one-way ANOVA and Tukey multiple comparison).

For this reason, the pro-differentiative effect of EVs was further investigated at microscopic level, evaluating possible differences in the growth plate dynamics. Longitudinal bone growth occurs in the growth plate, in which chondrocytes are finely organized in resting, proliferative and hypertrophic zone [162]. As reported in figure 4.6A, the resting zone (RZ) is characterized by single or paired chondrocytes, irregularly dispersed and embedded in a cartilage matrix. Adjacent to the RZ, chondrocytes are flattened and arranged in columns parallel to the long bone axis. This proliferative zone (PZ) is the area of active cell replication, while the hypertrophic zone (HZ) is featured by enlarged,

terminally differentiated cells and it initiates ossification by attracting vasculature [162,163]. We examined the morphology of chondrocytes within the growth plate and measured the extension of each zone, to understand the potential of MSC-sEVs in supporting endochondral ossification (EO). Negative controls exhibited a predominance of RZ (about 80% of total bone area), while PZ represented a restricted flap, with a not well-organized structure, and HZ was just sketchy (Fig. 4.6B and 4.6C). Conversely, in positive controls all zones were clearly detectable (Fig. 4.6C). RZ resulted strongly restricted compared to negative control ($p<0.0001$), while PZ was abundant (about 40% of total bone area, $p>0.0001$) (Fig. 4.6A and 4.6B). No statistical differences were found in the extension of HZ, even if positive control presented a more defined organization of the cells composing this area (Fig. 4.6A and 4.6B). Similarly, both ADSC- and BMSC-sEVs induced a significant reduction of RZ compared to negative controls ($p<0.01$ and $p<0.0001$, respectively), but no statistical differences were observed between the two cell sources (Fig. 4.6B). Interestingly, BMSC-sEVs triggered a significant increase in the PZ area in comparison to both ADSC-sEVs and negative controls ($p<0.01$ and $p<0.001$, respectively). Accordingly, an initial columnar cell organization similar to positive control can be detected in the samples treated with BMSC-sEVs (Fig. 4.6C).

No significant differences were noticed among ADSC- and BMSC-sEVs in HZ area (Fig. 4.6B). Type X-Collagen (Coll-X) is the main marker of hypertrophic chondrocytes [164,165]. Both EV-treated groups and positive controls expressed Coll-X in their HZ, localized near the center, suggesting the establishment of a differentiation stage close to mineralization (Fig. 4.6C). On the contrary, no Coll-X expression was detected in negative controls, confirming that in basal conditions bone metatarsal were stuck in a very early differentiation stage (Fig. 4.6C).

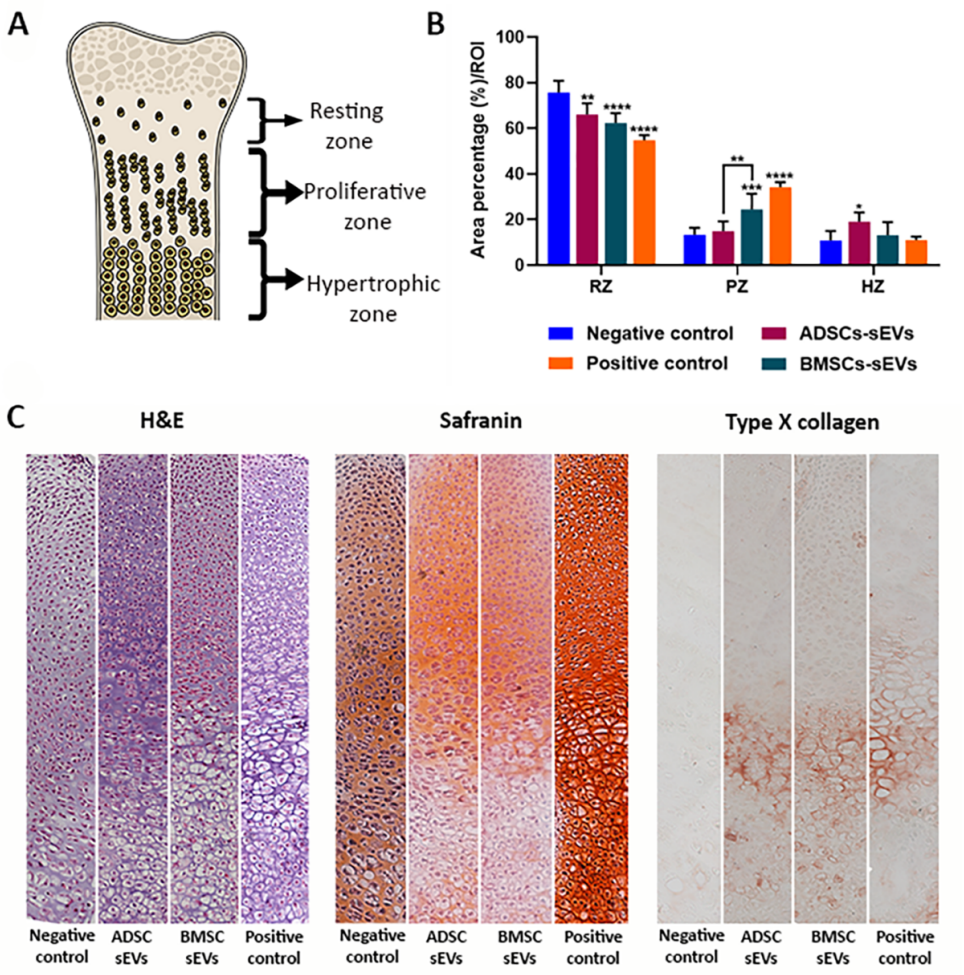

Figure 4.6: Effect of ADSC- and BMSC-derived EVs on metatarsal growth plate organization. (A) Schematic representation of growth plate morphology. **(B)** Quantification of growth plate zones in different experimental groups. Area of the zone is calculated and reported as percentage of area/ROI (ROI= total bone area). Data are presented as mean ± S.D. N=5, (*) represent statistical significance compared to negative control. Statistics between ADSC- and BMSC-sEVs are also reported. **** p<0.0001, *** p<0.001, ** p <0.01, * p <0.05 (Two-way ANOVA and Tukey multiple comparison). **(C)** Representative H&E, Safranin and type-X collagen staining images of different groups.

Apart from the extension, also the morphology and spatial orientation of the cells composing each zone are responsible for the correct organization of the growth plate [162]. RZ was well distinguishable in all experimental groups and, as expected, it was characterized by single or paired chondrocytes immersed in a dense matrix (Fig. 4.7). In positive controls, PZ-chondrocytes were arranged in columns parallel to the long axis of the bone (Fig. 4.7), and HZ were characterized by enlarged cells, with a matrix relegated to some portions surrounding the hypertrophic cells (Fig. 4.7). Close to the

perichondrium, flattened and elongated cells with an osteoblast-like morphology were progressively incorporated in a bone-like matrix in the area straddling PZ and HZ (Fig. 4.7). On the contrary, in negative controls, PZ-chondrocytes started to show their flattened morphology, but they were not able to self-orientate and arrange into columnar structures (Fig. 4.7). These cells enlarged in HZ, but they were still scattered, and portions of dense cartilaginous matrix were still visible. No osteoblast-like cells were detectable, and perichondrium was not organized (Fig. 4.7).

Similarly, to positive controls, the proliferative zone of BMSC-sEV-treated groups presented flattened and self-orientated chondrocytes starting to arrange into columns parallel to bone growth axis (Fig. 4.7). A different outcome was observed in ADSC-sEV groups, where proliferating chondrocytes were not able to organize in columns and remained chondron-like entities (Fig. 4.7). In both EV groups, hypertrophic chondrocytes of HZ were enlarged and compacted, like positive controls. Close to perichondrium, few osteoblast-like cells were detectable in BMSC-sEV-treated metatarsals. Taken together, these observations suggest that BMSC-sEVs possess a more pronounced differentiation potential, promoting the correct spatial organization of the different growth plate area, particularly the proliferative zone.

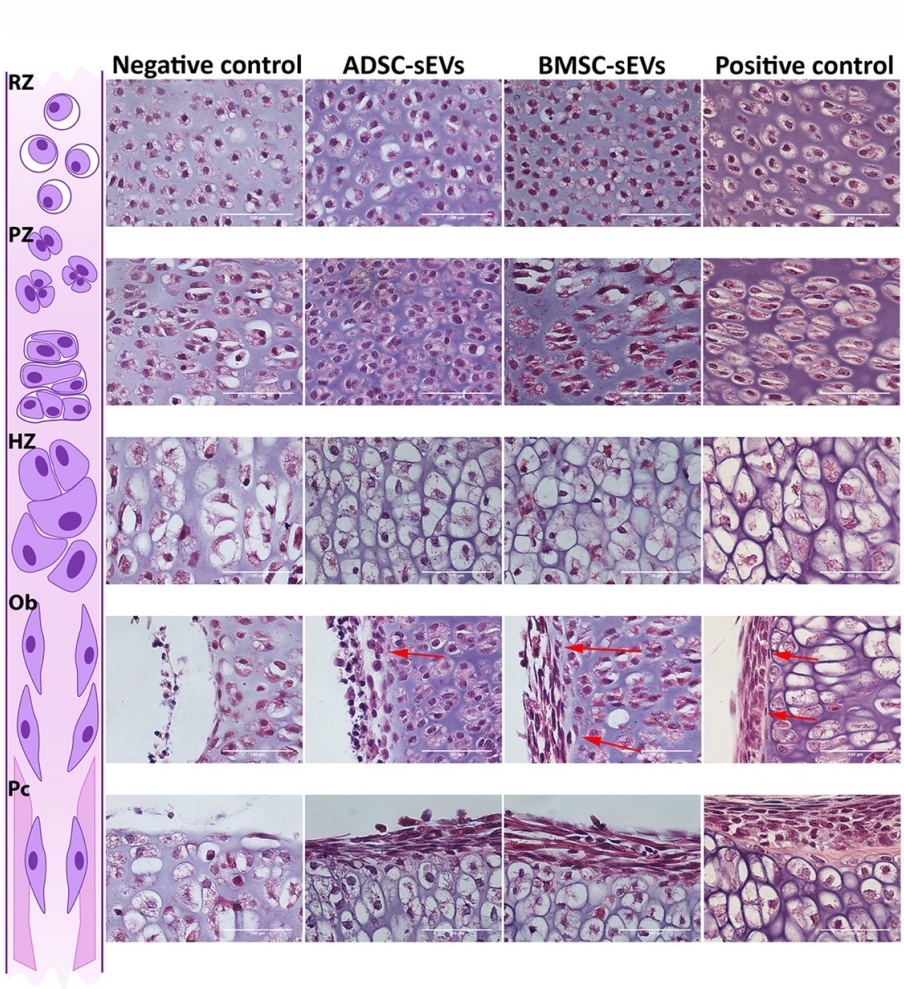

Figure 4.7: High magnification images of metatarsal bones. Representative H&E images of different zones at high magnification, to show details and chondrocytes morphology in different experimental groups. Scale bar: 100 µm. RZ: Resting zone, PZ: Proliferative zone, HZ: Hypertrophic zone, Ob: osteoblast-like cells, Pc: perichondrium.

4.4 Discussion

MSC-EVs have gained significant interest as cell-free regenerative therapies [166]. EVs are heterogeneous cell-derived membranous structures, originating from the endosomal compartment or shedding from plasma membrane [151]. Due to their biogenesis, the biological message transferred by EVs reflects the information carried by parental cells [167]. Indeed, MSC-EVs have been reported to be effective in numerous preclinical models, recapping the cell-mediated effects [168]. EVs can be easily isolated from MSCs of various origins, including adipose tissue and bone marrow. Although both ADSC- and BMSC-derived EVs are indifferently used in many studies [169], it is not yet clear

whether and how the MSC source can affect EV structure and content and consequent biological function.

In this study, we isolated mEVs and sEVs from ADSCs and BMSCs and we compared their activity in a highly physiological *ex vivo* model of endochondral ossification. Most of the vesicles released by both cell types were enriched in sEVs (100K pellet). This could have a functional reason, since it has been reported that MSC-derived sEVs are therapeutically effective in different preclinical models [170]. However, once isolated, EV subpopulations from both cell sources exhibited similar characteristics. According to MISEV 2018 guidelines, ADSC- and BMSC-sEVs were enriched in syntenin, a cytosolic protein described to be segregated mostly in small vesicles, being involved in exosome biogenesis [171]. As expected, tetraspanins CD81 and CD63 were highly abundant in both sEVs, but CD81 was also present, to various degrees, in mEVs and in the corresponding cell lysates. CD9 was not detected in any of the EV populations analyzed, confirming its absence in MSC-derived vesicles [157]. Interestingly, flotillin-1, a caveolae associated factor, was the only protein whose expression differentiated EVs released by ADSCs and BMSCs, being expressed by both mEVs and sEVs secreted by ADSCs, but only by BMSC-mEVs.

A better understanding of how specific factors are sorted into EV subpopulations could help to elucidate their biological role. ADSC-mEVs were mainly enriched in factors involved in the response to damage, such as GRO-α and IL-8, two structurally related proteins with a potent neutrophil-stimulating activity [172,173], IGFBP3, that modulates endothelial cell behavior and mediates cytoprotection following vascular injury [174], and DKK-1, an antagonist of the Wnt/ -catenin signaling involved in tissue homeostasis and repair, whose expression is induced by inflammatory cytokines [175]. Conversely, biological factors involved in the modulation of angiogenic and osteogenic responses (ANG-2 and BDNF), as well as in the crosstalk with immune cells (IFN- , IL-1 , and KLK-3) were upregulated in BMSC-mEVs. Indeed, ANG-2 is a well-known growth factor belonging to the angiopoietin/TIE pro-angiogenic signaling pathway [176]. BDNF is a growth factor described to play a role in the modulation of bone repair increasing the expression of the osteogenic markers [177]. IFN- γ and IL-1α are two important immunomodulators that trigger MSCs towards an anti-inflammatory and pro-trophic phenotype [178–180]. KLK3 is an angiogenesis suppressor [181]. Surprisingly, the pro-inflammatory adipokine RETN, described to regulate MSC proliferation and homing [182,183], was significantly up-regulated in BMSC-mEVs. PAI-1 was the only up-regulated protein in ADSC-sEVs. PAI-1 exerts both pro- and anti-angiogenic properties, with the

concentration of PAI-1 being an important determinant of which effect is observed [184]. On the other side, three proteins associated with MSC osteogenic differentiation (EMMPRin, uPAR and HGF) were overexpressed by BMSC-sEVs. The glycoprotein EMMPRin (CD147), has been found to be up-regulated in MSCs, and in particular in osteogenically-differentiated MSCs [185]. The multifunctional receptor uPAR mediates mobilization, migration and differentiation of MSCs, controlling their trafficking to the vascular wall in response to injury [186]. Finally, HGF promotes osteogenic differentiation through the expression of key osteogenic markers in human MSCs and it's a necessary component for the establishment of osteoblast mineralization [187]. The results described above suggest that EVs, and in particular sEVs, are enriched in proteins that could play a key role in angiogenesis and osteogenic differentiation, two fundamental phases of the endochondral ossification (EO) process. For this reason, the fetal metatarsal bone explant model has been selected, since it recapitulates these phases, providing conditions closer to the *in vivo* situation than cells grown in monolayer or 3D culture [160,161]. Indeed, EO acts on three different levels: the differentiation of chondrocytes and their maturation, the establishment of a vascularized network that supports the ossification process, and the bone remodeling. Different studies demonstrated functional differences between BMSCs and ADSCs in this regard. BMSCs appear to be more osteoinductive than ADSCs *in vivo*. On the other hand, ADSCs contain vasculogenic subpopulations, which could be effective for bone repair, by promoting neovascularization. Accordingly, also their secretory profile can undergo variations dependent on the cell source. Hsiao and colleagues have already shown that ADSC total secretome exerts enhanced pro-angiogenic activities than BMSC-derived one [188]. In our study, we showed that the EV-encapsulated components of the ADSC secretome exhibit greater angiogenic capabilities compared to BMSC-counterparts, confirming that ADSCs could be preferred over other MSC populations in therapeutic approaches dependent upon angiogenesis. Nevertheless, the ability of EVs released by either ADSCs or BMSCs to interfere with the subsequent phases of EO is still unclear. Long bone growth occurs in the growth plate, a structure in which cartilage is clearly organized in three different horizontal layers: resting, proliferative and hypertrophic zone (RZ, PZ, HZ), and the chondrocyte cell fate is recapitulated along the different areas. In RZ, chondrocytes start to replicate, and the daughter cells flatten and arrange themselves in columnar structures, orientated parallel to the growth axis. When chondrocytes stop replicating, they enlarge, reaching a terminally differentiated state. This peculiar organization and spatial orientation guides EO, leading to the maturation of cartilage and its remodeling into bone [162,163]. The *ex vivo* E15.5 bone explant model allowed us to

evaluate the role played by ADSC- and BMSC-EVs on growth plate morphology. Although neither type of vesicle can induce significant macroscopic differences in terms of bone growth, BMSC-sEVs induced a more defined spatial organization of the growth plate, compared to ADSC-sEVs. The substantial difference lied in the organization of chondrocytes within the PZ, which is known to play a crucial role in EO, being the region of active cell replication. Columns in PZ are formed by four to eight flattened chondrocytes, longitudinally oriented. This orientation is related to a well-defined cartilage matrix composition, whose maturation determines an increase in matrix stiffness and drives the transition from round to flat chondrocytes [189]. The morphometric analysis of E15.5 metatarsals revealed that the percentage of PZ-area/total area was significantly increased in the BMSC-sEV treated groups compared to ADSC counterparts. The latter did not induce any change in PZ area compared to negative control. More importantly, PZ-chondrocytes of BMSC-sEV-treated groups maintained the flat columnar arrangement embedded in the extracellular matrix, which is not detected in ADSC-sEV and negative control groups. It is well known that the mechanisms of chondrocyte mediolateral elongation involve, among the others, several morphogenetic signals that modulate chondrocyte orientation [189]. Contrary to ADSC, BMSC-sEVs release signals that guide the spatial organization of chondrocytes in this specific and fundamental area of the growth plate that will dictate bone growth. Moreover, we provided evidence that initial perichondral formation occurred in positive controls, where a *vis a vis* cell pattern between elongated osteoblast-like cells and hypertrophic chondrocytes was detected. Only in BMSC-sEV-treated metatarsals we could appreciate an initial collar organization with elongated cells placed in front of the hypertrophic chondrocytes as described by Riminucci and colleagues [190]. Despite our *ex vivo* E15.5 explant model is a powerful tool that closely mimics the *in vivo* process, it presents some drawbacks, such as limited lifespan and absence of a vascular network that could lead to a complete ossification of HZ-chondrocytes. This could partially explain the poor differences observed in HZ of treated metatarsals, in the organization of perichondrium and the total bone length. Further investigations using *ex vivo* bone cultures derived from different developmental stages could help to better discriminate the EV-mediated effects and understand the priming of bone formation.

Various reports indicate that, regardless of the cell source, MSC-derived EVs possess immunomodulatory, pro-regenerative, pro-angiogenic and anti-apoptotic properties. Nevertheless, few of them focus on the mechanism of action of MSC-EVs during embryonic tissue development, a key point to better understand tissue regeneration. This study shows how the differences among MSC

sources are reflected in the corresponding EVs, highlighting the importance of selecting the appropriate cell source for the development of innovative cell-free therapeutic strategies.

4.5 Conclusion

This work explores the role of MSC-EVs during the differentiation and maturation of cartilage and points out how EVs from different origins can modulate early endochondral bone formation process in a different manner. Therefore, despite apparently few differences were found between EVs derived from ADSCs and BMSCs, a deeply investigation of their biological effects is crucial, before selecting the optimal EV-cell source.

4.6 Supplementary Information

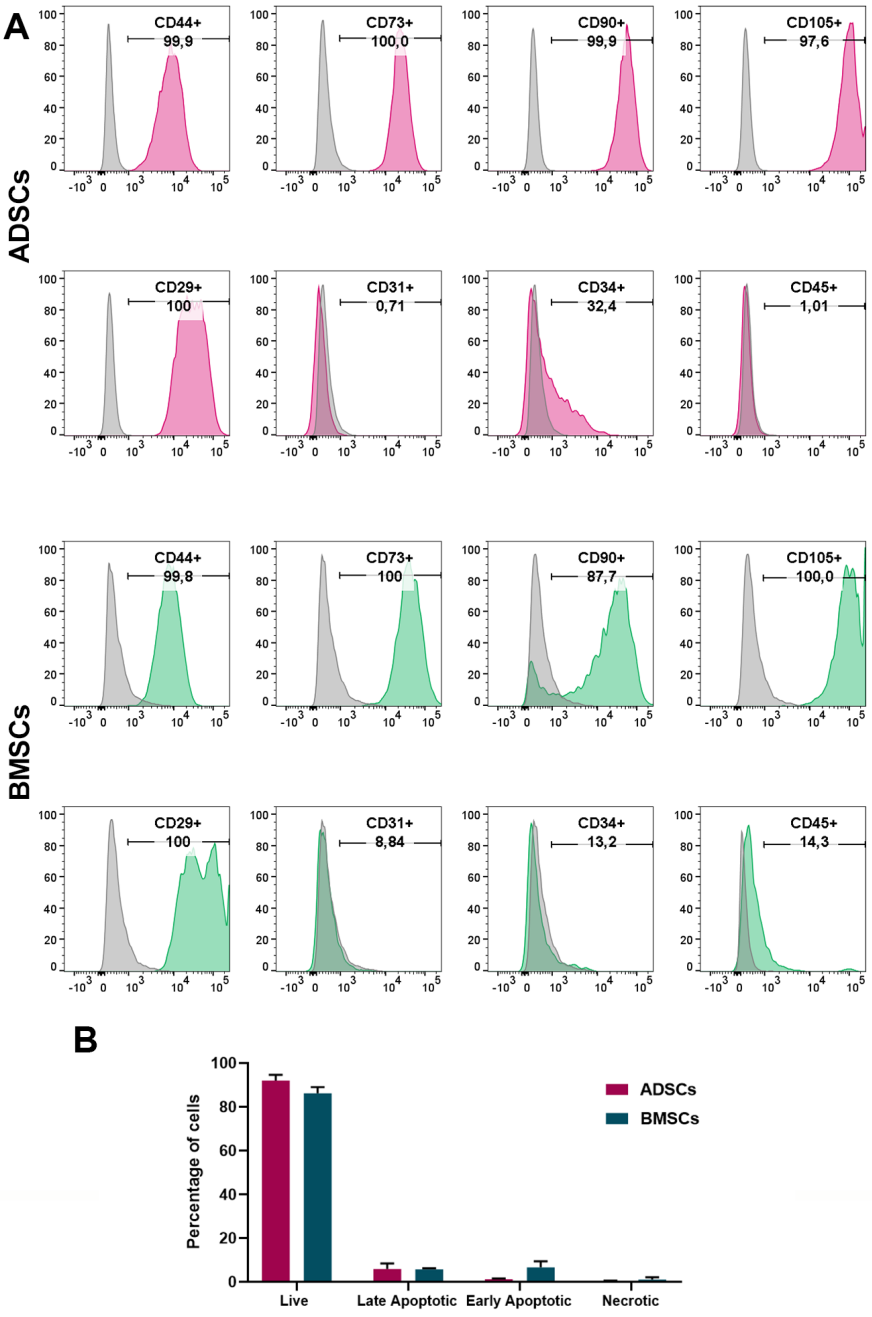

Supplementary Figure 4.1: Characterization of secreting cells. (A) Phenotypic characterization of MSCs by flow cytometry **(B)** Apoptotic cells detection. Detection of apoptosis by concurrent staining with FITC-anti-annexin V and PI of ADSCs and BMSCs after 24h of pre-conditioning. Data are reported as mean ± S.D. N=3, t-test.

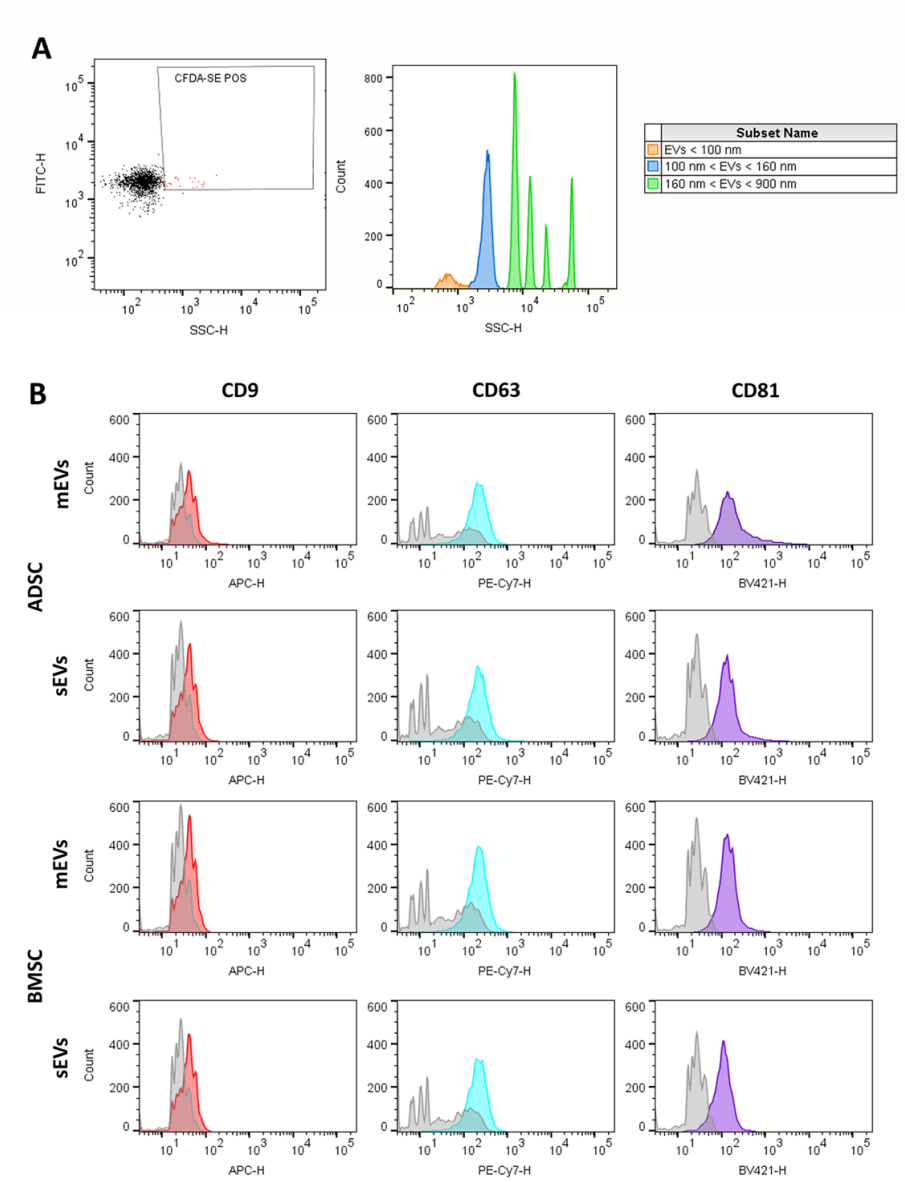

Supplementary Figure 4.2: Non-conventional flow cytometry approach used to characterize MSC-EVs. (A) Representative dot blot of PBS-EDTA (left) and histogram of fluorescent beads (right). **(B)** Flow cytometry analysis of ADSC- and BMSC-derived mEVs and sEVs. The presented data are from one representative experiment. The areas under the orange (CD9), green (CD63) and purple (CD81) lines identify EVs reacting with specific antibodies. The areas under the gray lines indicate the interactions of EVs with corresponding nonreactive immunoglobulin of the same isotype.

CHAPTER

5

General Discussion

EVs have great interest in regenerative medicine. Research on EVs is increasing exponentially due to large appreciation of EVs as therapeutics and an expanding number of EV-containing materials are under study with the new preparation, detection, and cargo analysis methods [191]. The development of improved approaches to EV detection and characterization is critical to further understanding their roles in physiology and disease [192]. While reference guidelines and minimal requirements for EV research have achieved the important objective of assembling community consensus, it is also essential to understand which methodologies and quality controls are currently being applied, and how usage trends are evolving. Several position papers were published by International Society of Extracellular Vesicles (ISEV) aiming at setting minimal rules for the EV research and providing researchers a guideline [193–196]. However, the complexity of biochemical properties of EVs leads to many additional concerns, such as standard isolation and purification method and functional characterization. Recent efforts to standardize procedures and document the effects of different methodologies such as the EV-Track platform [38] have helped to address this shortcoming, but much work remains.

Since it is important to report the challenges on the comparison of measurements and results between studies and laboratories on EV research, within **Chapter 2**, we have reported an innovative method to characterize adipose-tissue derived MSC-EVs by FCM was reported. Recently, several groups described novel strategies to stain EVs and characterize them with their well-defined markers [60,63,197]. However, when analyzing very small particles, accuracy depends on the proper discrimination of EVs from other non-cell-derived particles and on thorough removal of background noise [198]. Here, we have taken the advantage of commercial beads in order to determine the size distribution of EVs with FCM. Moreover, since it is important to distinguish the EVs from background, such as cell-membrane contaminants and small particles, we have used CFSE-DA in order to select the intact vesicles. With the tetraspanin markers which have been accepted as a gold standard [199] for the characterization, we were able to distinguish both expression levels of CD9, CD63 and CD81 within the size distribution of EVs. Thus, recent ongoing studies from our department are also demonstrating that it is possible to adapt the same protocol for other cell derived EVs with selected markers.

Recent efforts were made to characterize EVs deeply in order to understand the purity and avoid the contaminants [200]. Because for functional studies, it is important to examine that observed functions

are associated with EVs and not with other co-isolated materials [37]. Protein secreted by MSCs can be found either as free-form (soluble) in the conditioned medium or they can be found also in EV-encapsulated form. On the other hand, MSC-derived EVs (MSC-EVs) could mimic the therapeutic function of parental MSCs by transferring their components such as in particularly microRNAs to recipient cells [201].

MSC has a regulatory phenotype, their paracrine activity can be mediated by different pre-conditioning strategies. Several theories have been proposed to explain the effect of pre-conditioning strategies on MSCs [22]. In **Chapter 3**, the consequences of pre-conditioning strategies on different secretome fractions were considered. To our knowledge, this is the first study that investigates the effects of simultaneous stimulation with pro-inflammatory cytokines (TNF-α and IL-1α) and hypoxia (1% O_2) on different secretome fractions such as conditioned medium, EV-depleted medium, middle-sized EVs and small-sized EVs. Extensive *in vitro* and *ex vivo* data, supported by a specific proteome array and by microRNA sequencing, demonstrated that the synergistic action of hypoxia and inflammation affected the MSC secretome fractions at different extents. In response to inflammatory cytokines, cells released soluble factors with a strong anti-angiogenic effect. On the contrary, the corresponding MSC-EV fractions were less sensitive to the influence of external stimuli. An important implication of these findings is that the choice of preconditioning strategy can affect the functions of MSC paracrine factors components distinctly.

These results prompted further investigation into the application of same preconditioning strategy for MSCs derived from different sources, focusing on EVs. In the context of soluble factors, MSCs isolated from different tissue origins already present variations in their secretory profile. While the secretome of MSCs from adipose tissue consists of a broader range of angiogenic factors and thus may be preferred over the secretome of bone marrow MSCs for angiogenesis-mediated tissue regeneration [202–204], bone marrow MSC secretomes are widely used in bone regeneration field [155,205,206]. Since EVs from different origin contain diverse contents and exert different functions, some studies have come up with the comparison of exosomes from adipose tissue- and bone marrow derived MSCs [207,208]. Yet, these studies were limited for considering only one type of EV subpopulation. Considering whether an EV-dependent function is specific to a given EV subtype, **in Chapter 4**, we carried out a detailed and comparative characterization of middle-sized and small-sized EVs released by both

adipose-tissue and bone marrow MSCs to investigate their involvement as modulators of MSC paracrine effects. Although EVs derived from adipose tissue- and bone marrow derived MSCs present similar characteristics in terms of size, concentration and marker expression, they possess significant differences in their protein content that are reflected in their functional effects. The comparison of proteins with a wide range protein array showed that EVs derived from adipose tissue contained pro-angiogenic factors in comparison to the bone marrow counterpart. As a consequence, they were able to induce a significant increase in vessel sprouting. On the other hand, EVs derived from the bone marrow contained a higher amount of pro-differentiation and chemotactic proteins in comparison to the adipose tissue MSC-EVs, and they were able to prompt growth plate morphology. Interesting, during these comparisons of functional effects, even though that same concentration of EVs applied, small sized EVs had a significant effect in comparison with their counterpart middle-sized EVs. However, further experimental investigations are needed to understand the mechanism of action behind the EV functions.

From the research that has been carried out during this thesis, it is possible to conclude that the functional benefits of MSC paracrine activity could be used to develop promising alternative strategies to cell-based therapies.

The studies presented in this thesis demonstrate that in the presence of appropriate stimuli and correct MSC-source, MSC-EVs are able to further promote their efficiency for innovative clinical applications in the regenerative medicine field.

REFERENCES

1 Hoogduijn MJ, Betjes MGH, Baan CC. Mesenchymal stromal cells for organ transplantation: different sources and unique characteristics? Curr Opin Organ Transplant 2014;19:41–46.

2 Han Y, Li X, Zhang Y, et al. Mesenchymal stem cells for regenerative medicine. Cells 2019;8:886.

3 Friedenstein AJ, Petrakova KV, Kurolesova AI, et al. Heterotopic transplants of bone marrow. Transplantation 1968;6:230–247.

4 Friedenstein AJ, Chailakhjan RK, Lalykina K. The development of fibroblast colonies in monolayer cultures of guinea-pig bone marrow and spleen cells. Cell Prolif 1970;3:393–403.

5 Caplan AI. Mesenchymal stem cells. J Orthop Res 1991;9:641–650.

6 Dennis JE, Merriam A, Awadallah A, et al. A quadripotential mesenchymal progenitor cell isolated from the marrow of an adult mouse. J Bone Miner Res 1999;14:700–709.

7 Kuznetsov SA, Mankani MH, Gronthos S, et al. Circulating skeletal stem cells. J Cell Biol 2001;153:1133–1140.

8 Zuk PA, Zhu M, Ashjian P, et al. Human adipose tissue is a source of multipotent stem cells. Mol Biol Cell 2002;13:4279–4295.

9 Dominici M, Le Blanc K, Mueller I, et al. Minimal criteria for defining multipotent mesenchymal stromal cells. The International Society for Cellular Therapy position statement. Cytotherapy 2006;8:315–317.

10 Caplan AI. Mesenchymal stem cells: time to change the name! Stem Cells Transl Med 2017;6:1445–1451.

11 Quarto R, Mastrogiacomo M, Cancedda R, et al. Repair of large bone defects with the use of autologous bone marrow stromal cells. N Engl J Med 2001;344:385–386.

12 Marcacci M, Kon E, Moukhachev V, et al. Stem cells associated with macroporous bioceramics for long bone repair: 6-to 7-year outcome of a pilot clinical study. Tissue Eng 2007;13:947–955.

13 Davatchi F, Abdollahi BS, Mohyeddin M, et al. Mesenchymal stem cell therapy for knee osteoarthritis. Preliminary report of four patients. Int J Rheum Dis 2011;14:211–215.

14 Liu J, Hu Q, Wang Z, et al. Autologous stem cell transplantation for myocardial repair. Am J Physiol Circ Physiol 2004;287:H501–H511.

15 Satija NK, Singh VK, Verma YK, et al. Mesenchymal stem cell-based therapy: a new paradigm

in regenerative medicine. J Cell Mol Med 2009;13:4385–4402.

16 Prockop DJ. Repair of tissues by adult stem/progenitor cells (MSCs): controversies, myths, and changing paradigms. Mol Ther 2009;17:939–946.

17 Tjalsma H, Bolhuis A, Jongbloed JDH, et al. Signal peptide-dependent protein transport inBacillus subtilis: a genome-based survey of the secretome. Microbiol Mol Biol Rev 2000;64:515–547.

18 Tjalsma H, Antelmann H, Jongbloed JDH, et al. Proteomics of protein secretion by Bacillus subtilis: separating the "secrets" of the secretome. Microbiol Mol Biol Rev 2004;68:207–233.

19 Cantinieaux D, Quertainmont R, Blacher S, et al. Conditioned medium from bone marrow-derived mesenchymal stem cells improves recovery after spinal cord injury in rats: an original strategy to avoid cell transplantation. PLoS One 2013;8:e69515.

20 Sun J, Zhang Y, Song X, et al. The healing effects of conditioned medium derived from mesenchymal stem cells on radiation-induced skin wounds in rats. Cell Transplant 2019;28:105–115.

21 Hu C, Li L. Preconditioning influences mesenchymal stem cell properties *in vitro* and *in vivo*. J Cell Mol Med 2018;22:1428–1442.

22 Saparov A, Ogay V, Nurgozhin T, et al. Preconditioning of human mesenchymal stem cells to enhance their regulation of the immune response. Stem Cells Int 2016;2016.

23 Fujio M, Xing Z, Sharabi N, et al. Conditioned media from hypoxic-cultured human dental pulp cells promotes bone healing during distraction osteogenesis. J Tissue Eng Regen Med 2017;11:2116–2126.

24 Chang C-P, Chio C-C, Cheong C-U, et al. Hypoxic preconditioning enhances the therapeutic potential of the secretome from cultured human mesenchymal stem cells in experimental traumatic brain injury. Clin Sci 2013;124:165–176.

25 Yu Y, Yoo SM, Park HH, et al. Preconditioning with interleukin-1 beta and interferon-gamma enhances the efficacy of human umbilical cord blood-derived mesenchymal stem cells-based therapy via enhancing prostaglandin E2 secretion and indoleamine 2, 3-dioxygenase activity in dextran sul. J Tissue Eng Regen Med 2019;13:1792–1804.

26 Carter K, Lee HJ, Na K-S, et al. Characterizing the impact of 2D and 3D culture conditions on the therapeutic effects of human mesenchymal stem cell secretome on corneal wound healing in vitro and ex vivo. Acta Biomater 2019;99:247–257.

27 Follin B, Juhl M, Cohen S, et al. Increased paracrine immunomodulatory potential of mesenchymal stromal cells in three-dimensional culture. Tissue Eng Part B Rev 2016;22:322–329.

28 Jahandideh S, Maghsood F, Ghahhari NM, et al. The effect of Trimetazidine and Diazoxide on immunomodulatory activity of human embryonic stem cell-derived mesenchymal stem cell secretome. Tissue Cell 2017;49:597–602.

29 Jahandideh S, Khatami S, Eslami Far A, et al. Anti-inflammatory effects of human embryonic stem cell-derived mesenchymal stem cells secretome preconditioned with diazoxide, trimetazidine and MG-132 on LPS-induced systemic inflammation mouse model. Artif Cells, Nanomedicine, Biotechnol 2018;46:1178–1187.

30 Anderson HC. Vesicles associated with calcification in the matrix of epiphyseal cartilage. J Cell Biol 1969;41:59–72.

31 Gould SJ, Raposo G. As we wait: coping with an imperfect nomenclature for extracellular vesicles. J Extracell Vesicles 2013;2:20389.

32 Van Niel G, d'Angelo G, Raposo G. Shedding light on the cell biology of extracellular vesicles. Nat Rev Mol Cell Biol 2018;19:213.

33 Li Y, Yin P, Guo Z, et al. Bone derived extracellular vesicles: novel players of interorgan crosstalk. Front Endocrinol (Lausanne) 2019;10:846.

34 Kowal J, Arras G, Colombo M, et al. Proteomic comparison defines novel markers to characterize heterogeneous populations of extracellular vesicle subtypes. Proc Natl Acad Sci U S A 2016;113:E968–E977.

35 Hartjes TA, Mytnyk S, Jenster GW, et al. Extracellular vesicle quantification and characterization: common methods and emerging approaches. Bioengineering 2019;6:7.

36 Lötvall J, Hill AF, Hochberg F, et al. Minimal experimental requirements for definition of extracellular vesicles and their functions: a position statement from the International Society for Extracellular Vesicles 2014.

37 Théry C, Witwer KW, Aikawa E, et al. Minimal information for studies of extracellular vesicles 2018 (MISEV2018): a position statement of the International Society for Extracellular Vesicles and update of the MISEV2014 guidelines. J Extracell Vesicles 2018;7:1535750.

38 Van Deun J, Mestdagh P, Agostinis P, et al. EV-TRACK: Transparent reporting and centralizing knowledge in extracellular vesicle research. Nat Methods 2017;14.

39 Furi I, Momen-Heravi F, Szabo G. Extracellular vesicle isolation: present and future. Ann Transl Med 2017;5.

40 Sidhom K, Obi PO, Saleem A. A review of exosomal isolation methods: is size exclusion chromatography the best option? Int J Mol Sci 2020;21:6466.

41 Buschmann D, Kirchner B, Hermann S, et al. Evaluation of serum extracellular vesicle isolation methods for profiling miRNAs by next-generation sequencing. J Extracell Vesicles 2018;7:1481321.

42 Yang D, Zhang W, Zhang H, et al. Progress, opportunity, and perspective on exosome isolation-efforts for efficient exosome-based theranostics. Theranostics 2020;10:3684.

43 Konoshenko MY, Lekchnov EA, Vlassov A V, et al. Isolation of extracellular vesicles: general methodologies and latest trends. Biomed Res Int 2018;2018.

44 Martin-Rufino JD, Espinosa-Lara N, Osugui L, et al. Targeting the immune system with mesenchymal stromal cell-derived extracellular vesicles: what is the cargo's mechanism of action? Front Bioeng Biotechnol 2019;7:308.

45 Bruno S, Tapparo M, Collino F, et al. Renal regenerative potential of different extracellular vesicle populations derived from bone marrow mesenchymal stromal cells. Tissue Eng Part A 2017;23:1262–1273.

46 Park K-S, Bandeira E, Shelke G V, et al. Enhancement of therapeutic potential of mesenchymal stem cell-derived extracellular vesicles. Stem Cell Res Ther 2019;10:288.

47 Baek G, Choi H, Kim Y, et al. Mesenchymal stem cell-derived extracellular vesicles as therapeutics and as a drug delivery platform. Stem Cells Transl Med 2019;8:880–886.

48 Zhang B, Yeo RWY, Tan KH, et al. Focus on extracellular vesicles: therapeutic potential of stem cell-derived extracellular vesicles. Int J Mol Sci 2016;17:174.

49 Harting MT, Srivastava AK, Zhaorigetu S, et al. Inflammation-stimulated mesenchymal stromal cell-derived extracellular vesicles attenuate inflammation. Stem Cells 2018;36:79–90.

50 Almeria C, Weiss R, Roy M, et al. Hypoxia conditioned mesenchymal stem cell-derived extracellular vesicles induce increased vascular tube formation in vitro. Front Bioeng Biotechnol 2019;7:292.

51 Adlerz K, Patel D, Rowley J, et al. Strategies for scalable manufacturing and translation of MSC-derived extracellular vesicles. Stem Cell Res 2020;48:101978.

52 Lelek J, Zuba-Surma EK. Perspectives for Future Use of Extracellular Vesicles from Umbilical

Cord-and Adipose Tissue-Derived Mesenchymal Stem/Stromal Cells in Regenerative Therapies—Synthetic Review. Int J Mol Sci 2020;21:799.

53 Chance TC, Rathbone CR, Kamucheka RM, et al. The effects of cell type and culture condition on the procoagulant activity of human mesenchymal stromal cell-derived extracellular vesicles. J Trauma Acute Care Surg 2019;87:S74–S82.

54 Caplan AI, Dennis JE. Mesenchymal stem cells as trophic mediators. J Cell Biochem 2006;98:1076–1084.

55 Sicco C Lo, Reverberi D, Balbi C, et al. Mesenchymal stem cell-derived extracellular vesicles as mediators of anti-inflammatory effects: Endorsement of macrophage polarization. Stem Cells Transl Med 2017;6:1018–1028.

56 Rani S, Ryan AE, Griffin MD, et al. Mesenchymal stem cell-derived extracellular vesicles: toward cell-free therapeutic applications. Mol Ther 2015;23:812–823.

57 Willms E, Johansson HJ, Mäger I, et al. Cells release subpopulations of exosomes with distinct molecular and biological properties. Sci Rep 2016;6:1–12.

58 Tkach M, Kowal J, Théry C. Why the need and how to approach the functional diversity of extracellular vesicles. Philos Trans R Soc B Biol Sci 2018;373:20160479.

59 Lässer C, Jang SC, Lötvall J. Subpopulations of extracellular vesicles and their therapeutic potential. Mol Aspects Med 2018;60:1–14.

60 Van Der Vlist EJ, Nolte ENM, Stoorvogel W, et al. Fluorescent labeling of nano-sized vesicles released by cells and subsequent quantitative and qualitative analysis by high-resolution flow cytometry. Nat Protoc 2012;7:1311–1326.

61 Welsh JA, Holloway JA, Wilkinson JS, et al. Extracellular vesicle flow cytometry analysis and standardization. Front Cell Dev Biol 2017;5:78.

62 Lo Sicco C, Reverberi D, Pascucci L, et al. A Method for Isolating and Characterizing Mesenchymal Stromal Cell-derived Extracellular Vesicles. Curr Protoc Stem Cell Biol 2018;46:e55.

63 Arraud N, Gounou C, Turpin D, et al. Fluorescence triggering: A general strategy for enumerating and phenotyping extracellular vesicles by flow cytometry. Cytom Part A 2016;89:184–195.

64 Van der Pol E, Coumans FAW, Grootemaat AE, et al. Particle size distribution of exosomes and microvesicles determined by transmission electron microscopy, flow cytometry,

nanoparticle tracking analysis, and resistive pulse sensing. J Thromb Haemost 2014;12:1182–1192.

65 Poncelet P, Robert S, Bailly N, et al. Tips and tricks for flow cytometry-based analysis and counting of microparticles. Transfus Apher Sci 2015;53:110–126.

66 Shapiro HM. Practical flow cytometry. John Wiley & Sons, 2005.

67 Kormelink TG, Arkesteijn GJA, Nauwelaers FA, et al. Prerequisites for the analysis and sorting of extracellular vesicle subpopulations by high-resolution flow cytometry. Cytom Part A 2016;89:135–147.

68 Caplan AI. Why are MSCs therapeutic? New data: new insight. J Pathol A J Pathol Soc Gt Britain Irel 2009;217:318–324.

69 da Silva Meirelles L, Fontes AM, Covas DT, et al. Mechanisms involved in the therapeutic properties of mesenchymal stem cells. Cytokine Growth Factor Rev 2009;20:419–427.

70 Ulivi V, Tasso R, Cancedda R, et al. Mesenchymal stem cell paracrine activity is modulated by platelet lysate: induction of an inflammatory response and secretion of factors maintaining macrophages in a proinflammatory phenotype. Stem Cells Dev 2014;23:1858–1869.

71 Konala VBR, Mamidi MK, Bhonde R, et al. The current landscape of the mesenchymal stromal cell secretome: a new paradigm for cell-free regeneration. Cytotherapy 2016;18:13–24.

72 Willms E, Cabañas C, Mäger I, et al. Extracellular vesicle heterogeneity: subpopulations, isolation techniques, and diverse functions in cancer progression. Front Immunol 2018;9:738.

73 Erdbrügger U, Lannigan J. Analytical challenges of extracellular vesicle detection: A comparison of different techniques. Cytom Part A 2016;89:123–134.

74 Wallace H. Preparation of polyallomer centrifuge tubes for density gradients. Anal Biochem 1969;32:334–339.

75 DiMarino AM, Caplan AI, Bonfield TL. Mesenchymal Stem Cells in Tissue Repair. Front Immunol 2013;4:201.

76 Eleuteri S, Fierabracci A. Insights into the Secretome of Mesenchymal Stem Cells and Its Potential Applications. Int J Mol Sci 2019;20:4597.

77 Pittenger MF, Discher DE, Péault BM, et al. Mesenchymal stem cell perspective: cell biology to clinical progress. Npj Regen Med 2019;4:1–15.

78 A S, V O, T N, et al. Preconditioning of Human Mesenchymal Stem Cells to Enhance Their Regulation of the Immune Response. Stem Cells Int 2016;2016.

79 Noronha Nc NDC, Mizukami A, Caliári-Oliveira C, et al. Priming approaches to improve the efficacy of mesenchymal stromal cell-based therapies. Stem Cell Res Ther 2019;10.

80 Hong WX, Hu MS, Esquivel M, et al. The Role of Hypoxia-Inducible Factor in Wound Healing. Adv Wound Care 2014;3:390–399.

81 Ruthenborg RJ, Ban JJ, Wazir A, et al. Regulation of wound healing and fibrosis by hypoxia and hypoxia-inducible factor-1. Mol Cells 2014;37:637–643.

82 MacLeod AS, Mansbridge JN. The Innate Immune System in Acute and Chronic Wounds. Adv Wound Care 2016;5:65–78.

83 Fan XL, Zhang Y, Li X, et al. Mechanisms underlying the protective effects of mesenchymal stem cell-based therapy. Cell Mol Life Sci 2020.

84 Gianni-Barrera R, Di Maggio N, Melly L, et al. Therapeutic vascularization in regenerative medicine. Stem Cells Transl Med 2020;9:433–444.

85 Kwon HM, Hur SM, Park KY, et al. Multiple paracrine factors secreted by mesenchymal stem cells contribute to angiogenesis. Vascul Pharmacol 2014;63:19–28.

86 Marfy-Smith SJ, Clarkin CE. Are Mesenchymal Stem Cells So Bloody Great After All? Stem Cells Transl Med 2017;6:3–6.

87 Liu L, Gao J, Yuan Y, et al. Hypoxia preconditioned human adipose derived mesenchymal stem cells enhance angiogenic potential via secretion of increased VEGF and bFGF. Cell Biol Int 2013;37:551–560.

88 Ferreira JR, Teixeira GQ, Santos SG, et al. Mesenchymal stromal cell secretome: Influencing therapeutic potential by cellular pre-conditioning. Front Immunol 2018;9.

89 Zhao L, Hu C, Zhang P, et al. Preconditioning strategies for improving the survival rate and paracrine ability of mesenchymal stem cells in acute kidney injury. J Cell Mol Med 2019;23:720–730.

90 Kwon YW, Heo SC, Jeong GO, et al. Tumor necrosis factor-α-activated mesenchymal stem cells promote endothelial progenitor cell homing and angiogenesis. Biochim Biophys Acta - Mol Basis Dis 2013;1832:2136–2144.

91 Maffioli E, Nonnis S, Angioni R, et al. Proteomic analysis of the secretome of human bone marrow-derived mesenchymal stem cells primed by pro-inflammatory cytokines. J Proteomics 2017;166:115–126.

92 Angioni R, Liboni C, Herkenne S, et al. CD73+ extracellular vesicles inhibit angiogenesis

through adenosine A2B receptor signalling. J Extracell Vesicles 2020;9.

93 Sicco C Lo, Reverberi D, Balbi C, et al. Mesenchymal stem cell-derived extracellular vesicles as mediators of anti-inflammatory effects: Endorsement of macrophage polarization. Stem Cells Transl Med 2017;6:1018–1028.

94 Kowal J, Arras G, Colombo M, et al. Proteomic comparison defines novel markers to characterize heterogeneous populations of extracellular vesicle subtypes. Proc Natl Acad Sci U S A 2016;113:E968–E977.

95 Gorgun C, Reverberi D, Rotta G, et al. Isolation and Flow Cytometry Characterization of Extracellular-Vesicle Subpopulations Derived from Human Mesenchymal Stromal Cells. Curr Protoc Stem Cell Biol 2019;48:e76.

96 Song W, Fhu CW, Ang KH, et al. The fetal mouse metatarsal bone explant as a model of angiogenesis. Nat Protoc 2015;10:1459–1473.

97 Ritchie M, Phipson undefined, Wu D, et al. limma powers differential expression analyses for RNA-sequencing and microarray studies | Nucleic Acids Research | Oxford Academic 2015;43:undefined-undefined.

98 Robinson MD, McCarthy DJ, Smyth GK. edgeR: a Bioconductor package for differential expression analysis of digital gene expression data | Bioinformatics | Oxford Academic. Bioinformatics 2010;26:139–140.

99 Law CW, Chen Y, Shi W, et al. Voom: Precision weights unlock linear model analysis tools for RNA-seq read counts. Genome Biol 2014;15:R29.

100 Qiu G, Zheng G, Ge M, et al. Mesenchymal stem cell-derived extracellular vesicles affect disease outcomes via transfer of microRNAs. Stem Cell Res Ther 2018;9:1–9.

101 Mitchell R, Mellows B, Sheard J, et al. Secretome of adipose-derived mesenchymal stem cells promotes skeletal muscle regeneration through synergistic action of extracellular vesicle cargo and soluble proteins.

102 Zijlstra A, Di Vizio D. Size matters in nanoscale communication. Nat Cell Biol 2018;20:228–230.

103 Théry C, Witwer KW, Aikawa E, et al. Minimal information for studies of extracellular vesicles 2018 (MISEV2018): a position statement of the International Society for Extracellular Vesicles and update of the MISEV2014 guidelines. J Extracell Vesicles 2018;7.

104 Mann A, Niekisch K, Schirmacher P, et al. Granulocyte-macrophage colony-stimulating factor

is essential for normal wound healing. J. Investig. Dermatology Symp. Proc., vol. 11, Elsevier, 2006:87–92.

105 Wood S, Jayaraman V, Huelsmann EJ, et al. Pro-Inflammatory Chemokine CCL2 (MCP-1) Promotes Healing in Diabetic Wounds by Restoring the Macrophage Response. PLoS One 2014;9:e91574.

106 Dao DT, Anez-Bustillos L, Adam RM, et al. Heparin-Binding Epidermal Growth Factor–Like Growth Factor as a Critical Mediator of Tissue Repair and Regeneration. Am J Pathol 2018;188:2446–2456.

107 Corbel M, Boichot E, Lagente V. Role of gelatinases MMP-2 and MMP-9 in tissue remodeling following acute lung injury. Brazilian J Med Biol Res 2000;33:749–754.

108 López-Novoa JM, Bernabeu C. The physiological role of endoglin in the cardiovascular system. Am J Physiol - Hear Circ Physiol 2010;299:959–974.

109 J. Braga Osorio Gomes Salgado A, L. Goncalves Reis R, Jorge Carvalho Sousa N, et al. Adipose Tissue Derived Stem Cells Secretome: Soluble Factors and Their Roles in Regenerative Medicine. Curr Stem Cell Res Ther 2010;5:103–110.

110 Shibuya M. Vascular Endothelial Growth Factor (VEGF) and Its Receptor (VEGFR) Signaling in Angiogenesis: A Crucial Target for Anti- and Pro-Angiogenic Therapies. Genes and Cancer 2011;2:1097–1105.

111 Stepanova V, Jayaraman PS, Zaitsev S V., et al. Urokinase-type plasminogen activator (upa) promotes angiogenesis by attenuating proline-rich homeodomain protein (prh) transcription factor activity and de-repressing vascular endothelial growth factor (vegf) receptor expression. J Biol Chem 2016;291:15029–15045.

112 Turchinovich A, Drapkina O, Tonevitsky A. Transcriptome of Extracellular Vesicles: State-of-the-Art. Front Immunol 2019;10:202.

113 O'Brien K, Breyne K, Ughetto S, et al. RNA delivery by extracellular vesicles in mammalian cells and its applications. Nat Rev Mol Cell Biol 2020:1–22.

114 Chen X, Liang H, Zhang J, et al. Secreted microRNAs: A new form of intercellular communication. Trends Cell Biol 2012;22:125–132.

115 Valadi H, Ekström K, Bossios A, et al. Exosome-mediated transfer of mRNAs and microRNAs is a novel mechanism of genetic exchange between cells. Nat Cell Biol 2007;9:654–659.

116 Kosaka N, Iguchi H, Yoshioka Y, et al. Secretory mechanisms and intercellular transfer of

microRNAs in living cells. J Biol Chem 2010;285:17442–17452.

117 Ti D, Hao H, Fu X, et al. Mesenchymal stem cells-derived exosomal microRNAs contribute to wound inflammation. Sci China Life Sci 2016;59:1305–1312.

118 Hamanishi J, Mandai M, Matsumura N, et al. Activated local immunity by CC chemokine ligand 19-transduced embryonic endothelial progenitor cells suppresses metastasis of murine ovarian cancer. Stem Cells 2010;28:164–173.

119 Harrell C, Fellabaum C, Jovicic N, et al. Molecular Mechanisms Responsible for Therapeutic Potential of Mesenchymal Stem Cell-Derived Secretome. Cells 2019;8:467.

120 Raposo G, Stoorvogel W. Extracellular vesicles: Exosomes, microvesicles, and friends. J Cell Biol 2013;200:373–383.

121 Chen L, Deng H, Cui H, et al. Inflammatory responses and inflammation-associated diseases in organs. Oncotarget 2018;9:7204–7218.

122 Bartosh TJ, Ylöstalo JH, Mohammadipoor A, et al. Aggregation of human mesenchymal stromal cells (MSCs) into 3D spheroids enhances their antiinflammatory properties. Proc Natl Acad Sci U S A 2010;107:13724–13729.

123 Follin B, Juhl M, Cohen S, et al. Increased Paracrine Immunomodulatory Potential of Mesenchymal Stromal Cells in Three-Dimensional Culture. Tissue Eng - Part B Rev 2016;22:322–329.

124 Cui X, Wang H, Guo H, et al. Transplantation of mesenchymal stem cells preconditioned with diazoxide, a mitochondrial ATP-sensitive potassium channel opener, promotes repair of myocardial infarction in rats. Tohoku J Exp Med 2010;220:139–147.

125 Pessina A, Coccè V, Pascucci L, et al. Mesenchymal stromal cells primed with Paclitaxel attract and kill leukaemia cells, inhibit angiogenesis and improve survival of leukaemia-bearing mice. Br J Haematol 2013;160:766–778.

126 K M, X W, S D, et al. Adiponectin Inhibits Vascular Endothelial Growth Factor-Induced Migration of Human Coronary Artery Endothelial Cells. Cardiovasc Res 2008;78:376–384.

127 Prasanna SJ, Gopalakrishnan D, Shankar SR, et al. Pro-Inflammatory Cytokines, IFNγ and TNFα, Influence Immune Properties of Human Bone Marrow and Wharton Jelly Mesenchymal Stem Cells Differentially. PLoS One 2010;5:e9016.

128 Leroux L, Descamps B, Tojais NF, et al. Hypoxia preconditioned mesenchymal stem cells improve vascular and skeletal muscle fiber regeneration after ischemia through a wnt4-

dependent pathway. Mol Ther 2010;18:1545–1552.

129 Ray A. Cytokines and their Role in Health and Disease: A Brief Overview. MOJ Immunol 2016;4.

130 Heo SC, Jeon ES, Lee IH, et al. Tumor necrosis factor-α-activated human adipose tissue-derived mesenchymal stem cells accelerate cutaneous wound healing through paracrine mechanisms. J Invest Dermatol 2011;131:1559–1567.

131 Zanotti L, Angioni R, Calì B, et al. Mouse mesenchymal stem cells inhibit high endothelial cell activation and lymphocyte homing to lymph nodes by releasing TIMP-1. Leukemia 2016;30:1143–1154.

132 Rodríguez D, Morrison CJ, Overall CM. Matrix metalloproteinases: What do they not do? New substrates and biological roles identified by murine models and proteomics. Biochim Biophys Acta - Mol Cell Res 2010;1803:39–54.

133 Schäfer R, Spohn G, Baer PC. Mesenchymal stem/stromal cells in regenerative medicine: Can preconditioning strategies improve therapeutic efficacy? Transfus Med Hemotherapy 2016;43:256–267.

134 Bader AM, Klose K, Bieback K, et al. Hypoxic Preconditioning Increases Survival and Pro-Angiogenic Capacity of Human Cord Blood Mesenchymal Stromal Cells In Vitro. PLoS One 2015;10:e0138477.

135 Kinoshita T, Yip KW, Spence T, et al. MicroRNAs in extracellular vesicles: Potential cancer biomarkers. J Hum Genet 2017;62:67–74.

136 Lindoso RS, Collino F, Bruno S, et al. Extracellular vesicles released from mesenchymal stromal cells modulate miRNA in renal tubular cells and inhibit ATP depletion injury. Stem Cells Dev 2014;23:1809–1819.

137 Zhang J, Li S, Li L, et al. Exosome and exosomal microRNA: Trafficking, sorting, and function. Genomics, Proteomics Bioinforma 2015;13:17–24.

138 Song Y, Dou H, Li X, et al. Exosomal miR-146a Contributes to the Enhanced Therapeutic Efficacy of Interleukin-1β-Primed Mesenchymal Stem Cells Against Sepsis. Stem Cells 2017;35:1208–1221.

139 Hoogduijn MJ, Lombardo E. Mesenchymal Stromal Cells Anno 2019: Dawn of the Therapeutic Era? Concise Review. Stem Cells Transl Med 2019;8:1126–1134.

140 da Silva Meirelles L, Chagastelles PC, Nardi NB. Mesenchymal stem cells reside in virtually all

post-natal organs and tissues. J Cell Sci 2006;119:2204–2213.

141 Nombela-Arrieta C, Ritz J, Silberstein LE. The elusive nature and function of mesenchymal stem cells. Nat Rev Mol Cell Biol 2011;12:126–131.

142 Glenn JD. Mesenchymal stem cells: Emerging mechanisms of immunomodulation and therapy. World J Stem Cells 2014;6:526.

143 Laroye C, Gauthier M, Antonot H, et al. Mesenchymal Stem/Stromal Cell Production Compliant with Good Manufacturing Practice: Comparison between Bone Marrow, the Gold Standard Adult Source, and Wharton's Jelly, an Extraembryonic Source. J Clin Med 2019;8:2207.

144 Mastrolia I, Foppiani EM, Murgia A, et al. Challenges in Clinical Development of Mesenchymal Stromal/Stem Cells: Concise Review. Stem Cells Transl Med 2019;8:1135–1148.

145 Mazini L, Rochette L, Amine M, et al. Regenerative capacity of adipose derived stem cells (ADSCs), comparison with mesenchymal stem cells (MSCs). Int J Mol Sci 2019;20.

146 Heo JS, Choi Y, Kim HS, et al. Comparison of molecular profiles of human mesenchymal stem cells derived from bone marrow, umbilical cord blood, placenta and adipose tissue. Int J Mol Med 2016;37:115–125.

147 Fan XL, Zhang Y, Li X, et al. Mechanisms underlying the protective effects of mesenchymal stem cell-based therapy. Cell Mol Life Sci 2020;77:2771–2794.

148 Lu H, Wang F, Mei H, et al. Human adipose mesenchymal stem cells show more efficient angiogenesis promotion on endothelial colony-forming cells than umbilical cord and endometrium. Stem Cells Int 2018;2018.

149 Baraniak PR, McDevitt TC. Stem cell paracrine actions and tissue regeneration. Regen Med 2010;5:121–143.

150 Tetta C, Ghigo E, Silengo L, et al. Extracellular vesicles as an emerging mechanism of cell-to-cell communication. Endocrine 2013;44:11–19.

151 Yáñez-Mó M, Siljander PRM, Andreu Z, et al. Biological properties of extracellular vesicles and their physiological functions. J Extracell Vesicles 2015;4:1–60.

152 Rani S, Ryan AE, Griffin MD, et al. Mesenchymal stem cell-derived extracellular vesicles: Toward cell-free therapeutic applications. Mol Ther 2015;23:812–823.

153 Lo Sicco C, Reverberi D, Balbi C, et al. Mesenchymal Stem Cell-Derived Extracellular Vesicles

as Mediators of Anti-Inflammatory Effects: Endorsement of Macrophage Polarization. Stem Cells Transl Med 2017;6:1018–1028.

154 Gorgun C, Ceresa D, Lesage R, et al. Dissecting the effects of preconditioning with inflammatory cytokines and hypoxia on the angiogenic potential of mesenchymal stromal cell (MSC)-derived soluble proteins and extracellular vesicles (EVs). Biomaterials 2021;269:120633.

155 Palamà MEF, Shaw GM, Carluccio S, et al. The secretome derived from mesenchymal stromal cells cultured in a xeno-free medium promotes human cartilage recovery in vitro. Front Bioeng Biotechnol 2020;8.

156 Dominici M, Le Blanc K, Mueller I, et al. Minimal criteria for defining multipotent mesenchymal stromal cells. The International Society for Cellular Therapy position statement. Cytotherapy 2006;8:315–317.

157 Théry C, Witwer KW, Aikawa E, et al. Minimal information for studies of extracellular vesicles 2018 (MISEV2018): a position statement of the International Society for Extracellular Vesicles and update of the MISEV2014 guidelines. J Extracell Vesicles 2018;7:1535750.

158 Kowal J, Arras G, Colombo M, et al. Proteomic comparison defines novel markers to characterize heterogeneous populations of extracellular vesicle subtypes. Proc Natl Acad Sci U S A 2016;113:E968–E977.

159 Gorgun C, Reverberi D, Rotta G, et al. Isolation and Flow Cytometry Characterization of Extracellular-Vesicle Subpopulations Derived from Human Mesenchymal Stromal Cells. Curr Protoc Stem Cell Biol 2019;48.

160 Houston DA, Staines KA, Macrae VE, et al. Culture of murine embryonic metatarsals: A physiological model of endochondral ossification. J Vis Exp 2016;2016.

161 Song W, Fhu CW, Ang KH, et al. The fetal mouse metatarsal bone explant as a model of angiogenesis. Nat Protoc 2015;10:1459–1473.

162 Abad V, Meyers JL, Weise M, et al. The role of the resting zone in growth plate chondrogenesis. Endocrinology 2002;143:1851–1857.

163 Hunziker EB. Mechanism of longitudinal bone growth and its regulation by growth plate chondrocytes. Microsc Res Tech 1994;28:505–519.

164 Reno PL, McBurney DL, Lovejoy CO, et al. Ossification of the mouse metatarsal: Differentiation and proliferation in the presence/absence of a defined growth plate. Anat Rec -

Part A Discov Mol Cell Evol Biol 2006;288:104–118.

165 Shen G. The role of type X collagen in facilitating and regulating endochondral ossification of articular cartilage. Orthod Craniofacial Res 2005;8:11–17.

166 Keshtkar S, Azarpira N, Ghahremani MH. Mesenchymal stem cell-derived extracellular vesicles: Novel frontiers in regenerative medicine. Stem Cell Res Ther 2018;9:63.

167 Zaborowski MP, Balaj L, Breakefield XO, et al. Extracellular Vesicles: Composition, Biological Relevance, and Methods of Study. Bioscience 2015;65:783–797.

168 Maumus M, Rozier P, Boulestreau J, et al. Mesenchymal Stem Cell-Derived Extracellular Vesicles: Opportunities and Challenges for Clinical Translation. Front Bioeng Biotechnol 2020;8:997.

169 Martin-Rufino JD, Espinosa-Lara N, Osugui L, et al. Targeting the Immune System With Mesenchymal Stromal Cell-Derived Extracellular Vesicles: What Is the Cargo's Mechanism of Action? Front Bioeng Biotechnol 2019;7.

170 Witwer KW, Van Balkom BWM, Bruno S, et al. Defining mesenchymal stromal cell (MSC)-derived small extracellular vesicles for therapeutic applications. J Extracell Vesicles 2019;8:1609206.

171 Théry C, Witwer KW, Aikawa E, et al. Minimal information for studies of extracellular vesicles 2018 (MISEV2018): a position statement of the International Society for Extracellular Vesicles and update of the MISEV2014 guidelines. J Extracell Vesicles 2018;7.

172 Geiser T, Dewald B, Ehrengruber MU, et al. The interleukin-8-related chemotactic cytokines GROα, GROβ, and GROγ activate human neutrophil and basophil leukocytes. J Biol Chem 1993;268:15419–15424.

173 Fujiwara K, Matsukawa A, Ohkawara S, et al. Functional distinction between CXC chemokines, interleukin-8 (IL-8), and growth related oncogene (GRO)α in neutrophil infiltration. Lab Investig 2002;82:15–23.

174 Kielczewski JL, Jarajapu YPR, McFarland EL, et al. Insulin-like growth factor binding protein-3 mediates vascular repair by enhancing nitric oxide generation. Circ Res 2009;105:897–905.

175 Koch S, Nava P, Addis C, et al. The Wnt antagonist Dkk1 regulates intestinal epithelial homeostasis and wound repair. Gastroenterology 2011;141.

176 Maisonpierre PC, Suri C, Jones PF, et al. Angiopoietin-2, a natural antagonist for Tie2 that disrupts in vivo angiogenesis. Science (80-) 1997;277:55–60.

177 Loy TL, Vehlow D, Kauschke V, et al. Effects of BDNF and PEC Nanoparticles on Osteocytes. Molecules 2020;25:4151.

178 Krampera M, Cosmi L, Angeli R, et al. Role for Interferon-γ in the Immunomodulatory Activity of Human Bone Marrow Mesenchymal Stem Cells. Stem Cells 2006;24:386–398.

179 Bodo M, Venti G, Pezzetti F, et al. Interleukin-1 alpha: regulation of cellular proliferation and collagen synthesis in cultured human osteoblast-like cells. Cell Mol Biol (Noisy-Le-Grand) 1992;38:679–686.

180 Redondo-Castro E, Cunningham C, Miller J, et al. Interleukin-1 primes human mesenchymal stem cells towards an anti-inflammatory and pro-trophic phenotype in vitro. Stem Cell Res Ther 2017;8:79.

181 Fortier AH, Holaday JW, Liang H, et al. Recombinant prostate specific antigen inhibits angiogenesis in vitro and in vivo. Prostate 2003;56:212–219.

182 Acquarone E, Monacelli F, Borghi R, et al. Resistin: A reappraisal. Mech Ageing Dev 2019;178:46–63.

183 He Y, Guo Y, Xia Y, et al. Resistin promotes cardiac homing of mesenchymal stem cells and functional recovery after myocardial ischemia-reperfusion via the ERK1/2-MMP-9 pathway. Am J Physiol - Hear Circ Physiol 2019;316:H233–H244.

184 Wu J, Strawn TL, Luo M, et al. Plasminogen activator inhibitor-1 inhibits angiogenic signaling by uncoupling vascular endothelial growth factor receptor-2-αVβ3 integrin cross talk. Arterioscler Thromb Vasc Biol 2015;35:111–120.

185 Chen J, Shi ZD, Ji X, et al. Enhanced osteogenesis of human mesenchymal stem cells by periodic heat shock in self-assembling peptide hydrogel. Tissue Eng - Part A 2013;19:716–728.

186 Vallabhaneni KC, Tkachuk S, Kiyan Y, et al. Urokinase receptor mediates mobilization, migration, and differentiation of mesenchymal stem cells. Cardiovasc Res 2011;90:113–121.

187 Aenlle KK, Curtis KM, Roos BA, et al. Hepatocyte growth factor and p38 promote osteogenic differentiation of human mesenchymal stem cells. Mol Endocrinol 2014;28:722–730.

188 Hsiao ST-F, Asgari A, Lokmic Z, et al. Comparative analysis of paracrine factor expression in human adult mesenchymal stem cells derived from bone marrow, adipose, and dermal tissue. Stem Cells Dev 2012;21:2189–2203.

189 Prein C, Warmbold N, Farkas Z, et al. Structural and mechanical properties of the proliferative zone of the developing murine growth plate cartilage assessed by atomic force microscopy.

Matrix Biol 2016;50:1–15.

190 Riminucci M, Bradbeer JN, Corsi A, et al. Vis-a-vis cells and the priming of bone formation. J Bone Miner Res 1998;13:1852–1861.

191 Royo F, Théry C, Falcón-Pérez JM, et al. Methods for separation and characterization of extracellular vesicles: Results of a worldwide survey performed by the ISEV rigor and standardization subcommittee. Cells 2020;9:1955.

192 Nolan JP. Flow cytometry of extracellular vesicles: potential, pitfalls, and prospects. Curr Protoc Cytom 2015;73:13–14.

193 Lener T, Gimona M, Aigner L, et al. Applying extracellular vesicles based therapeutics in clinical trials–an ISEV position paper. J Extracell Vesicles 2015;4:30087.

194 Hill AF, Pegtel DM, Lambertz U, et al. ISEV position paper: extracellular vesicle RNA analysis and bioinformatics. J Extracell Vesicles 2013;2:22859.

195 Russell AE, Sneider A, Witwer KW, et al. Biological membranes in EV biogenesis, stability, uptake, and cargo transfer: an ISEV position paper arising from the ISEV membranes and EVs workshop. J Extracell Vesicles 2019;8:1684862.

196 Mateescu B, Kowal EJK, van Balkom BWM, et al. Obstacles and opportunities in the functional analysis of extracellular vesicle RNA–an ISEV position paper. J Extracell Vesicles 2017;6:1286095.

197 Kormelink TG, Arkesteijn GJA, Nauwelaers FA, et al. Prerequisites for the analysis and sorting of extracellular vesicle subpopulations by high-resolution flow cytometry. Cytom Part A 2016;89:135–147.

198 Inglis HC, Danesh A, Shah A, et al. Techniques to improve detection and analysis of extracellular vesicles using flow cytometry. Cytom Part A 2015;87:1052–1063.

199 Andreu Z, Yáñez-Mó M. Tetraspanins in extracellular vesicle formation and function. Front Immunol 2014;5:442.

200 Gardiner C, Vizio D Di, Sahoo S, et al. Techniques used for the isolation and characterization of extracellular vesicles: results of a worldwide survey. J Extracell Vesicles 2016;5:32945.

201 Qiu G, Zheng G, Ge M, et al. Mesenchymal stem cell-derived extracellular vesicles affect disease outcomes via transfer of microRNAs. Stem Cell Res Ther 2018;9:320.

202 Zou X, Gu D, Xing X, et al. Human mesenchymal stromal cell-derived extracellular vesicles alleviate renal ischemic reperfusion injury and enhance angiogenesis in rats. Am J Transl Res

2016;8:4289.

203 Mou S, Zhou M, Li Y, et al. Extracellular vesicles from human adipose-derived stem cells for the improvement of angiogenesis and fat-grafting application. Plast Reconstr Surg 2019;144:869–880.

204 Lopatina T, Mazzeo A, Bruno S, et al. The angiogenic potential of adipose mesenchymal stem cell-derived extracellular vesicles is modulated by basic fibroblast growth factor 2014.

205 Qin Y, Wang L, Gao Z, et al. Bone marrow stromal/stem cell-derived extracellular vesicles regulate osteoblast activity and differentiation in vitro and promote bone regeneration in vivo. Sci Rep 2016;6:1–11.

206 Vonk LA, van Dooremalen SFJ, Liv N, et al. Mesenchymal stromal/stem cell-derived extracellular vesicles promote human cartilage regeneration in vitro. Theranostics 2018;8:906.

207 Del Fattore A, Luciano R, Saracino R, et al. Differential effects of extracellular vesicles secreted by mesenchymal stem cells from different sources on glioblastoma cells. Expert Opin Biol Ther 2015;15:495–504.

208 Baglio SR, Rooijers K, Koppers-Lalic D, et al. Human bone marrow-and adipose-mesenchymal stem cells secrete exosomes enriched in distinctive miRNA and tRNA species. Stem Cell Res Ther 2015;6:127.

PhD Portfolio

Personal Details

Name	Cansu Gorgun
Department	Department of Experimental Medicine
PhD Period	November 2017- November 2020
Tutor	Dr. Roberta Tasso
PhD Fund	CarBon- Controlling Cartilage to Bone Transitions for Improved Treatment of Osteoarthritis and Bone Defects (Marie Sklodowska-Curie ITN Project, Funded by European Union's Horizon 2020)

Publications

Gorgun C, Reverberi D, Rotta G, Villa F, Quarto R, Tasso R. Isolation and Flow Cytometry Characterization of Extracellular-Vesicle Subpopulations Derived from Human Mesenchymal Stromal Cells. Curr Protoc Stem Cell Biol. 2019 Feb;48(1):e76. doi: 10.1002/cpsc.76. Epub 2019 Jan 9. PMID: 30624011.

Gorgun C, Ceresa D, Lesage R, Villa F, Reverberi D, Balbi C, Santamaria S, Cortese K, Malatesta P, Geris L, Quarto R, Tasso R. Dissecting the effects of preconditioning with inflammatory cytokines and hypoxia on the angiogenic potential of mesenchymal stromal cell (MSC)-derived soluble proteins and extracellular vesicles (EVs). Biomaterials. 2021 Feb;269:120633. doi: 10.1016/j.biomaterials.2020.120633. Epub 2020 Dec 28. PMID: 33453634.

Gorgun C, Palama MEF, Reverberi D, Gagliani MC, Cortese K, Tasso R, Gentili C. Extracellular Vesicles from adipose tissue- and bone marrow-mesenchymal stromal cells play different roles in the endochondral ossification process. *Under review.*

Courses and Training Activities

2017	Animal Handling Course (Ospedale Policlinico San Martino), Genova, Italy
2017	Comprehensive Summer School on Tissue Engineering: From Biology To Materials And Products Validation, University of Trento, Trento, Italy
2018	"Animal models for perinatal stress and metabolism", Genova, Italy
2018	Training on "Nanoparticle Tracking Analysis" Cardiocentro Ticino Lugano, Switzerland
2018	"Animal models for perinatal stress and metabolism", Genova, Italy
2019	Training course on specific risks in the environment – CISEF, Gaslini (Virtual course)
2020	EMBL Technology Day: Technologies for Extracellular Vesicles Research (Virtual Event)

(Inter)National Conferences and Symposiums

2017	TERMIS-EU 2017, Davos, Svitzerland
2018	TERMIS World Congress 2018, Kyoto, Japan (poster presentation)
2019	N4M (Nanoengineering for Mechanobiology Symposium, Camogli, Italy
2019	2019 GISM Annual Meeting, Research challenges for clinical application of MSCs, Genova, Italy (Poster presentation)
2019	TERMIS-EU 2019 Rhodes, Greece (Oral Presentation)
2019	1st Lugano Exoday "Technical Challenges in Exosome Research), Lugano, Switzerland (Poster Presentation)
2019	1st EVIta (Italian Society of Extracellular Vesicles, Palermo, Italy (Oral Presentation)

Teaching and Student Mentoring

2019	Didactic support activities for laboratory lessons of "Stem Cell Biology and Regenerative Medicine,"Master course of Medical-Pharmaceutical Biotechnology" University of Genova, Italy (32 hours)
2019	Mentoring Master Thesis (Carolina Lampitelli) Master's in biology, University of Genova, Italy
2020	Mentoring Master Thesis (Chiara Africano) Master's in medical-Pharmaceutical Biotechnology, University of Genova, Italy

"CarBon" Project Meetings and Trainings

2017	CarBon Consortium Meeting and Training on" Computational models" Leuven, Belgium
2018	CarBon Consortium Meeting and Training on "Commercialization and IP rights" Dublin, Ireland
2018	CarBon Midterm Meeting and Training on "Translation of a discovery to a product", Genova, Italy
2019	CarBon Consortium Meeting and Training on "Communication to lay public" Frankfurt, Germany
2018	CarBon Consortium Meeting and Training on "Communication to lay public " Eindhoven, Netherlands
2019	CarBon online Consortium Meeting (Virtual Event)

Secondments

2017	Secondment "Training on *in vitro* angiogenesis assays" Depts. of Orthopaedics, Otorhinolaryngology Oral and Maxillofacial Surgery, Erasmus University Medical Centre, Supervisors: Prof. Dr. Gerjo van Osch, Dr. Eric Farrell.
2018	Secondment "Comprehensive analysis of secretomes by Mass Spectrophotometry" Centre for Biochemistry, Medical Faculty, Uniklinik Köln, Cologne, Germany. Supervisor: Prof. Dr. Bent Brachvogel.